Material design for impact-resistant nanocomposite plastics by embedding “plant cell wall”-like frameworks of amphiphilic cellulose nanofibrils

鴨川, 正人

Material design for impact-resistant nanocomposite plastics by embedding “plant cell wall”-like frameworks of amphiphilic cellulose nanofibrils

Masato Kamogawa

2024

Contents

List of Abbereviations

ACC	Aqueous counter collision
AFM	Atomic force microscopy
BBKP	Bamboo bleached kraft pulp
BNC	Bacterial nanocellulose
C.I.	Crystallinity index
CLSM	Confocal laser scanning microscopy
CNCs	Cellulose nanocrystals
CNFs	Cellulose nanofibrils
DIC-Pol	Differential interference contrast polarized
DSC	Differential scanning calorimetry
iPP	Isotactic polypropylene
LAS X	Leica application suite X
LLDPE	Linear low-density polyethylene
MCC	Microcrystalline cellulose
NCs	Nanocelluloses
PCW	Plant cell wall
PE	Polyethylene
PET	Polyethylene terephthalate
POM	Polarized optical microscopy
S-S curve	Stress-strain curve
Tc	Crystallization temperature
Tm	Melting temperature
WAXD	Wide angle X-ray diffraction
χ_c	Crystallinity
T_m^{eq}	Equilibrium melting points

General Introduction

1. Cellulose nanofibrils as an environment-friendly functional material

1.1. Cellulose fiber as a main component of tree contributing to its mechanical strength

Utilization of eco-friendly materials is an efficient way to minimize our environmental issues and encourage creation of decarbonized and sustainable society. Among such eco-friendly materials, cellulose, which is the most abundant as a main component of plant cell wall, is a promising material. Cellulose as a molecule is an extended homopolysaccharide that consists of anhydro-β-D-glucopyranose units connected by $\beta(1\rightarrow4)$ glycosidic bonds [1–3]. Cellulose glucan chains exhibit an amphiphilic nature attributed to equatorial hydroxy groups and axial C-H moieties that are bound chemically to a glucopyranose ring [2,4]. The glucan chain tends to engage intramolecular hydrogen bonding between hydroxy groups and oxygens of the adjacent ring molecules and stabilizes the linkage to result in the linear configuration of the cellulose chain [2]. The glucan chains readily form a glucan sheet by their individual hydrogen-bonded interactions, then the resultant glucan sheets are stacked themselves by van der Waals forces in the native aqueous system to form the highly crystalline cellulose fiber structure [3–5]. The higher-ordered cellulose fibers exhibit hydrophilic nature dominantly due to exposing hydroxy groups on the fiber surface.

In nature, plants, animals like tunicate and microorganisms produce the crystalline cellulose nanofibers that by the assembly of glucan sheets to containing cellulose I crystalline structure (= cellulose microfibril) [5]. In plants, the cellulose microfibrils, composed of 18 glucan chains [6–8] , with a 3 – 4 nm in width and in thickness as a structural unit form a bundle state, and deposit onto the surface of pre-formed cell

wall layers with hierarchical structure surrounding a plasma membrane, together with pectin, hemi-cellulose and lignin as shown in Fig. G-1 [4,5,9]. The cell walls with anisotropic structure are connected with each other to form three-dimensional structure as intercellular layers, assisting mechanical strength to support body of tree.

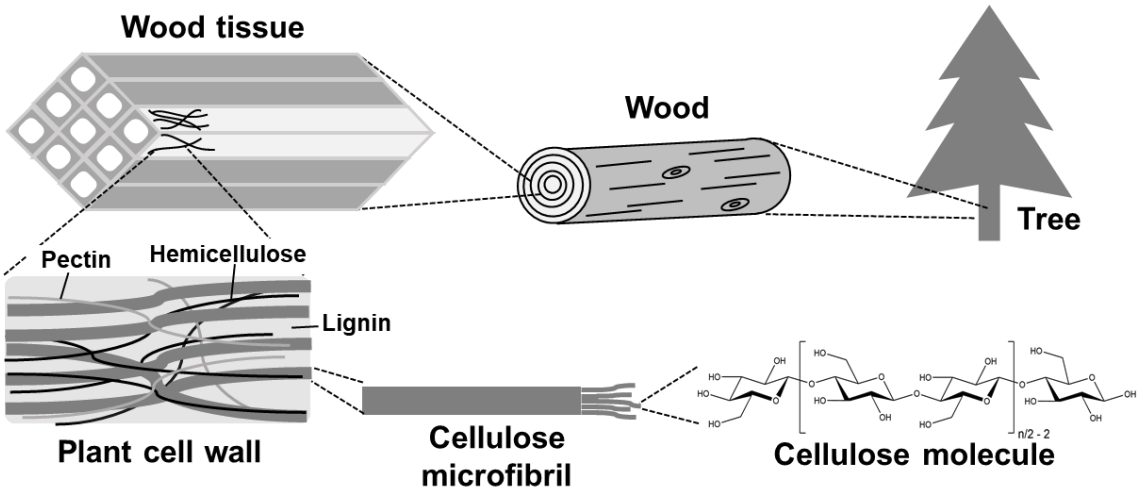

Fig. G-1 Hierarchical structure of wood cellulose [9].

1.2. Cellulose nanofibrils: its definition and mechanical properties

In the last two decades, nanocelluloses (= NCs) have attracted increasing interests due to their own excellent chemical/physical properties and sustainability of their raw materials [1,10]. NCs represent nanosized cellulose materials with a fiber width of 100 nm or less and they are typically distinguished into two categories: cellulose nanocrystals (= CNCs) with a low aspect ratio (< 100) [10], and cellulose nanofibrils (= CNFs) with a high aspect ratio (≥ 100) [10,11]. Most of NCs are fabricated by top-down processes while bacterial nanocellulose (= BNC) is produced by a bottom-up process by several bacteria. Although BNC is sometimes distinguished from other CNFs, it is

included as a type of CNF based on aspect ratio. Table G-1 summarizes morphology and physical properties in the three types of NCs.

Table G-1 Comparison among BNC, CNF, and CNC in that morphology, physical properties and production methods [3].

Nanocellulose type	Length	Diameter	Degree of polymerization	Crystallinity / crystal structure	Production method
Bacterial nanocellulose (BNC)	Different types of nanofiber network	20 – 100 nm	4000 – 10000	Mixture of Iα and Iβ Highest degree of crystallinity	Biological production by bacteria
Cellulose nanofibrils (CNF)	0.1 – 2 µm	5 – 60 nm	≥ 500	Primarily Iβ Lowest degree of crystallinity	Chemical pre-treatment and/or directly mechanical treatment
Cellulose nanocrystals (CNC)	100 – 250 nm (from plant) 100 nm to several µm (from tunicate, algae, bacteria)	5 – 70 nm	500 - 15000	Primarily Iβ, sometimes Iα Medium degree of crystallinity	Chemical hydrolysis or oxidation

CNFs are generally produced by downsizing of native cellulose pulp fibers with chemical pre-treatments [12–14] or directly by mechanical process [15–18] and physicochemical process [10,19–21] as an aqueous dispersion or water-containing state. The obtained CNFs have different surface characteristics attributed to their surface morphology depending on the preparation methods [1,3,10]. Commonly, CNFs have excellent materials properties including high mechanical strength (2 – 6 GPa [22]), high elastic modulus (160 GPa) [23], low thermal expansion (0.1 ppm/K) [24] in the range from – 200 °C to 200 °C, and large specific surface areas (≥ 250 m^2/g) [3].

1.3. Application of CNFs as reinforcing fillers with plastics: its potential and drawbacks

According to their advantages described in 1.2, CNFs have been extensively studied as eco-friendly functional materials. In particular, CNFs have been expected to be used as reinforcing fillers in polymer composites to replace inorganic fillers [1,5,25,26].

However, the dominant surface hydrophilicity in CNFs has been drawbacks to be utilized for mixing with hydrophobic commodity plastics such as polyethylene (PE) and polypropylene (PP) [27]. CNFs are readily aggregated during isolation or dehydration. The aggregation is difficult to be re-dispersed due to formation of hydrogen bonding among CNFs and what is worse, the aggregations in polymeric nanocomposite may act as a structural defect to decrease in mechanical properties. Homogeneous dispersion states of CNFs in the nanocomposite materials have been preferably required to date, for emergence of a reinforcement effect by addition of CNFs [27]. Therefore, compatibility between the components in a composite is considered to play a critical role to achieve emergence of superior properties. For emergence of a better reinforcement in a composite by addition of CNFs, it may be of necessity to achieve both a good dispersibility of CNFs and a compatible interface on base polymers.

For achievement of compatibility, addition of additives such as coupling agent [28,29] and compatibilizer [30] and/or chemical pre-modification [31] such as acetylation [32,33] and/or grafting [34] are listed, and in fact they have been extensively studied in CNFs nanocomposites. However, these treatments are likely to cause discoloration of the composite [35], and additonally chemical pre-treatments of CNFs may generate waste solvent. Note that CNFs are currently expensive materials and thus, further increase in the production cost due to additional treatments above described is not desirable. Therefore, the commercial viability of composites incorporating hydrophilic CNFs requires development of a simple and inexpensive process for composite production including manners for good compatibility between two components and/or good dispersion without aggregations. It should be noted here that it is difficult to prevent

decreasing impact resistance of the nanocomposites, together with emergence of reinforcement effects in mechanical properties of the products.

2. Aqueous counter collision (ACC) treatment as a physicochemical CNFs preparation method

2.1. Mechanism of ACC treatment and production of ACC-CNFs

Aqueous counter collision (ACC) as a physicochemical nano-pulverization method is able to produce more hydrophobic (= less hydrophilic) CNFs (= ACC-CNFs) [19–21]. The ACC method, developed by Kondo et al., relies on the impingement of two high-speed jets of aqueous suspension of raw materials ejected through a pair of opposing nozzles (Fig. G-2) [10]. The calculated kinetic energy generated by impingement of the water jets in the ACC method is up to 14.3 kJ/mol at an ejection pressure of 200 MPa [21]. The relationship between water ejection pressure and calculated kinetic energy of water molecules in the ACC process is shown in Table G-2, together with a summary of typical bonding energies. Regardless of dissipative energy loss during the ACC process, the kinetic energy, which can be converted into shockwaves, remains higher than the van der Waals force and weak hydrogen bonds at an ejection pressure of 200 MPa [10,21].

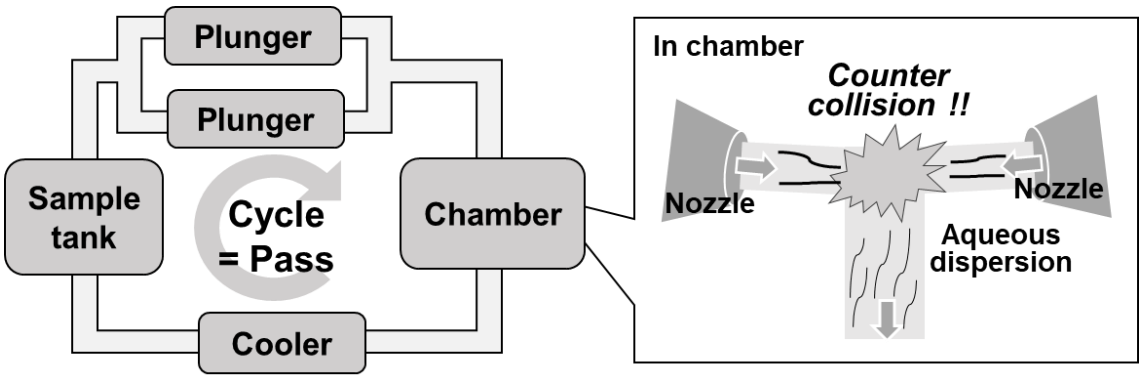

Fig. G-2 Schematic image showing ACC instruments [19,21].

Table G-2 (a) Relationship between water ejection pressure and calculated kinetic energy of water molecules. (b) Various bonding energies. Reprinted from [21] © from Elsevier.

(a)

Ejecting pressure / MPa	Kinetic energy / kJ·mol^{-1}
50	3.6
100	7.2
150	10.8
200	14.3

(b)

Type of bond	Bonding energy / kJ·mol^{-1}
H – OH (covalent bond)	499
H – H (covalent bond)	436
Ion – ion	250
Medium hydrogen bond	21 – 62
Weak hydrogen bond	$4.2 \cdot \times 10^{-1}$ – 4.2
London dispersion force	2
Dipole – dipole	0.6 – 2

In the case of cellulose raw materials, the energy propagation caused cleaving weak interaction such as van der Waals force between inner (200) planes in native I_β cellulose crystals to downsize micro-objects into ACC-CNFs without significantly decreasing in crystallinity inherent of raw materials [20,21]. According to the ACC nano-pulverization mechanism, two types of surface properties are exposed on a single fiber: hydrophilic faces due to hydroxy groups and hydrophobic faces due to C-H groups both of which appear along the fiber axis (Fig. G-3) [4,21,36–38]. Therefore, ACC-CNFs were proposed as an amphiphilic Janus-type nanofibrils [4]. The fiber morphologies and surface properties are dependent on their raw materials [20,21,36,39].

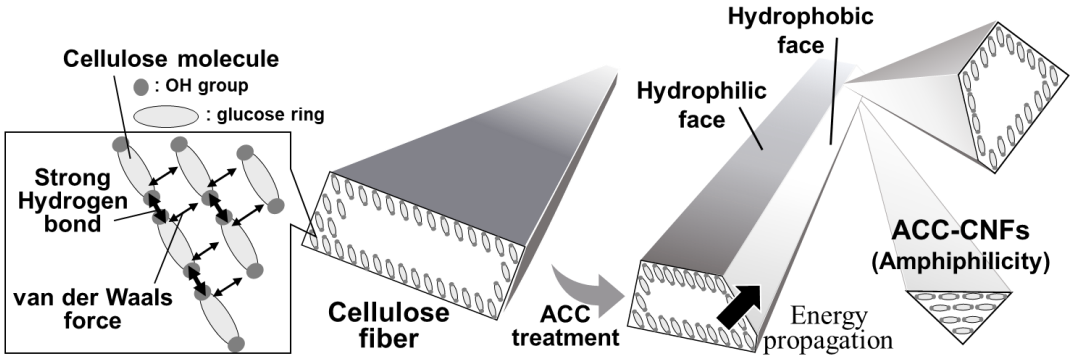

Fig. G-3 Schematic diagrams of the ACC process, which is likely to express hydrophobic van der Waals (200) face normally hidden inside the native crystalline cellulose fibers to the surface [10,19,21].

2.2. Affinity interaction with hydrophobic iPP due to its amphiphilic surface properties

The ACC-CNFs with the Janus-type fiber structure exhibit characteristic amphiphilic properties in addition to common properties in usual CNF. A mixture of ACC-CNFs aqueous dispersions and organic solvents forms stabilized Pickering emulsions simply by mixing, because ACC-CNFs cover entire surfaces of oil droplets in aqueous media [36,37] as shown in Fig. G-4. ACC-CNFs interacted with some hydrophilic polymers such as poly(lactic acid) and poly(vinyl alcohol) to act as a nucleating agent and/or diluent [40–42].

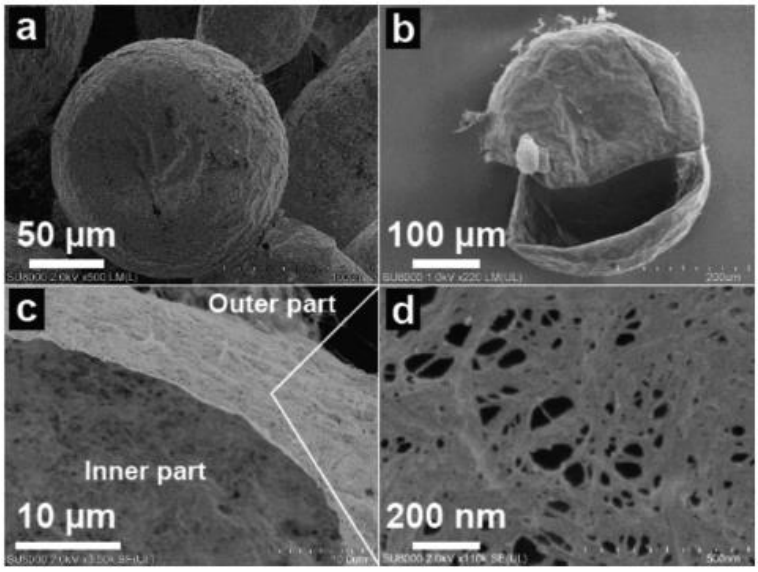

Fig. G-4 SEM images of bamboo nanocellulose hollow particles prepared from freeze-dried stable emulsion with (a) spherical and (b) cracked shapes; (c) fracture surface of hollow particle and (d) magnified image of skin area, indicating nanofibril network structure. Reprinted from [37] ©2019 from Elsevier.

Furthermore, the amphiphilic ACC-CNFs exhibit facile coating onto surfaces of commodity hydrophobic polymer substrates such as PE and iPP [43,44]. Note that the ACC-CNFs favorably adsorbed onto entire iPP microspheres, simply via mixing each other in aqueous media. In contrast, hydrophilic TEMPO-oxidized cellulose nanofibril (= TOCN) fabricated via pre-chemical treatments was not detected by the observations, it was suggested TOCN was hard to adsorb onto the microspheres (Fig. G-5) [43,44]. From the calculating work of adhesion, the adsorption of ACC-CNFs onto iPP surface contributed to stabilization of the whole system due to the replacement with iPP/water interface [45]. As shown in Fig. G-6 (a), the ACC-CNFs-coated iPP microspheres exhibited a small endothermic peak at 142.6 ºC, in addition to the microsphere's inherent melting endothermic peak around 162.3 ºC [43]. This indicates presence of thermodynamic affinity interaction between ACC-CNFs and iPP surface. Then, melting points without

morphologic effect (= equilibrium melting points; T_m^{eq}) of both the smaller and the inherent peaks which were 1st T_m^{eq} and 2nd T_m^{eq}, respectively, were estimated by Hoffman-Weeks plot (in Fig. G-6 (b) [43]). The difference value between both T_m^{eq} (=Δ T_m^{eq}) was used as an indicator for the strength of the affinity interaction. ACC-CNFs with different sources exhibited the different values and the values have positive correlation with the degree of hydrophobicity of ACC-CNFs [43].

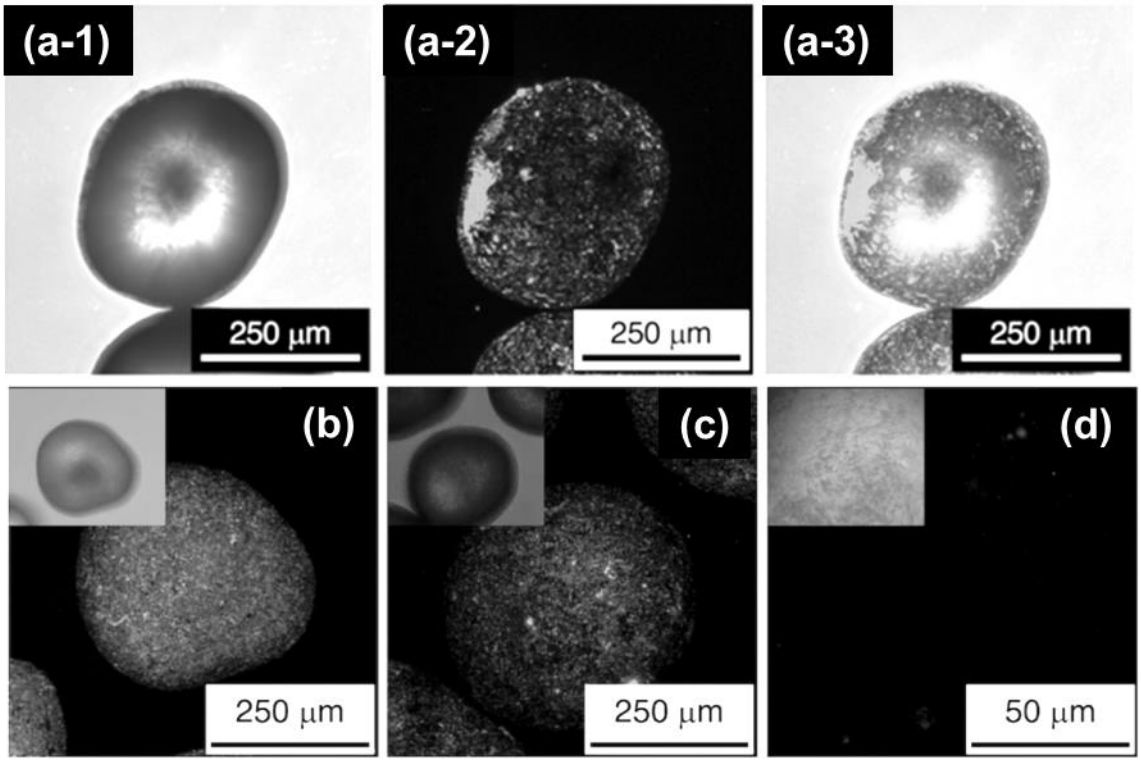

Fig. G-5 (a) Confocal laser scanning microscope (CLSM) images of iPP microparticle coated with ACC-CNFs derived from bamboo bleached kraft pulp (= ACC-BBKP) stained with cellulose specific dye; (1) bright-field image, (2) dark-field fluorescent image, and (c) their merged image. (b-d) CLSM images of iPP microparticles coated with various CNFs; (b) ACC-CNFs derived from BNC (= ACC-BNC), (c) ACC-CNFs derived from microcrystalline cellulose (= ACC-MCC), and (d) TOCN. Reprinted from [43] ©2019 from American Chemical Society.

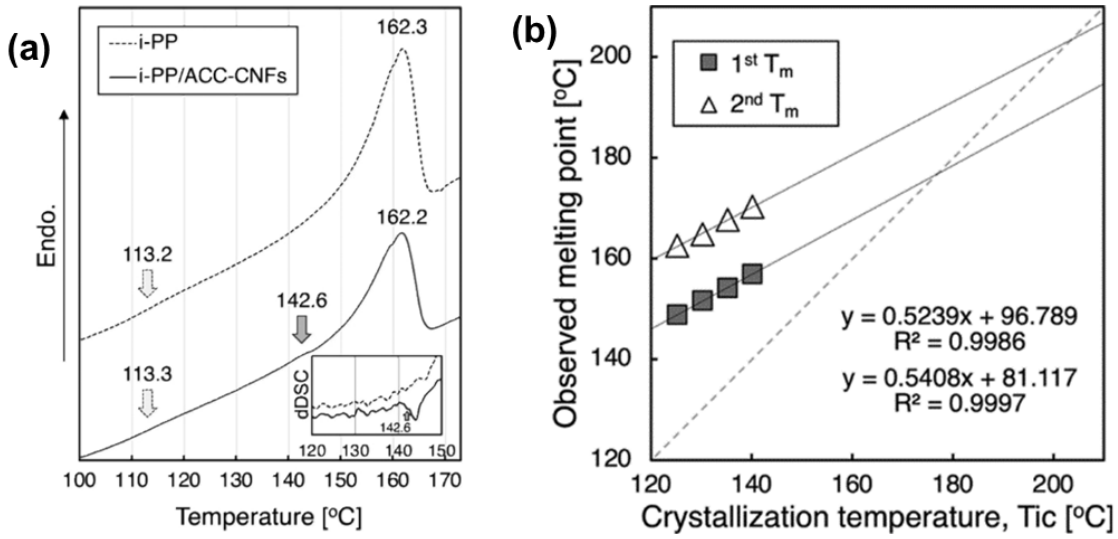

Fig. G-6 (a) Differential scanning calorimetry (DSC) endothermic curves of the first scan at 10 ºC/min. The inset indicates the seconds derivative (dDSC) in the range 120 – 150 ºC. (b) Hoffman-Weeks plots used to obtain the tentative T_m^{eq} values for the different T_m values. Reprinted from [43] ©2019 from American Chemical Society.

Table G-2 Two sets of tentative T_m^{eq} values for iPP microparticles coated with various CNFs [43]. ΔT_m^{eq} indicated the strength of affinity interaction between CNFs and iPP.

CNFs	1st T_m^{eq} / ºC	2nd T_m^{eq} / ºC	ΔT_m^{eq} / ºC
ACC-BBKP	175.65	203.30	27.65
ACC-BNC	163.68	188.23	24.55
ACC-MCC	191.36	204.17	12.81
TOCN	(not applicable)	(not applicable)	

3. Polymer based composite materials

Materials have their own inherent properties to be applied to various usages in a wide variety of fields. It is often designed to modify their properties by mixing with another components for composites. Composite materials are usually defined as the assembly of two or more materials, so that the final properties are superior to the properties of each constituent component [46]. They are commonly composed of a continuous phase called a matrix and dispersed fillers compatible with a matrix for additional reinforcements and/or functionalization [46].

Among materials, plastic materials have superior properties such as light weight, excellent molding processability, corrosion resistance, and good transparency, when compared with metals and ceramics. These advantageous aspects still induce an increasing global demand for plastic materials as shown in Fig. G-7 [47–50]. Despite increasing concerns regarding the bioaccumulation of microplastics, application of the polymer-based composites is extended to wide fields such as packaging, automobile, light structures, civil engineering, aviation, sports, biomedicines, thermomechanical components and aerospace [46,51,52]. For automobiles and airplanes, the present metal materials are expected to be replaced by polymer-based composites for a reduction in weight of their bodies, resulting in contribution to a lower fuel consumption to gain fuel mileage [46].

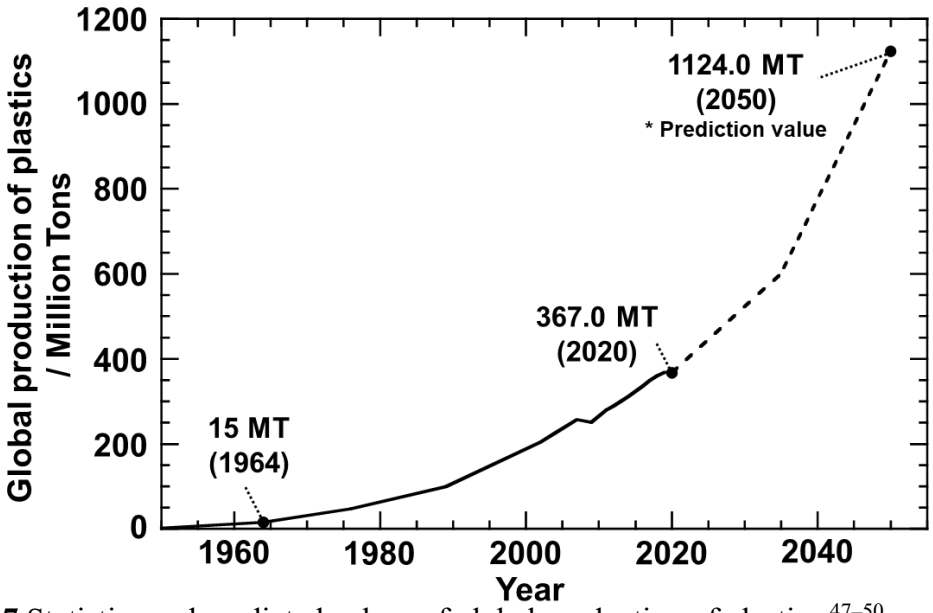

Fig. G-7 Statistics and predicted values of global production of plastics [47–50].

For polymer-based materials, addition of fillers is often critical to improve the mechanical, electrical or thermal properties and/or to reduce the price of the transformed materials [46]. Inorganic fillers such as glass fibers and carbon fibers/materials have been widely used due to their excellent mechanical strength, for providing mechanical strength. Nevertheless, production of the inorganic fillers need a large energy and it is difficult to dispose their composite due to their flame resistance [46]. In contrast, natural fibers have drawn an attention to be used as reinforcement fillers to replace synthetic fillers or inorganic fillers due to their abundant sustainable resources and biodegradability [53]. Especially, cellulosic materials as the most abundant biomass are most advantageous, because they possess excellent mechanical properties, such as tensile and flexural strength and their moduli, thermal resistance, its availability from different resource and degradability unlike synthetic fillers [1,53].

In the last three decades, nanosized materials (= nanomaterials) have been developed with the advancing nanotechnologies [10,11,51]. Usage of the nanomaterials as

fillers in polymeric matrices is expected to be effectively functionalized because they can create a large volume of total interface due to their large specific surface area. The nanoscale interphases in such composites can determine the extent of the compatibility and so affect the mechanical properties of the composite [54]. In contrast, nanomaterials are favorably to form aggregations in matrices due to their own large specific surface area. Therefore, attempts have been made to control composite interfaces on the nanoscale for improvement of their compatibility and/or control of its dispersion state. Since the aggregation of nanomaterials often prevents their improvement in mechanical properties and/or functionalization, homogeneous dispersion state of nanomaterials is regarded as a critical requirement [27]. When formation of a continuous or connected structure of fillers is established, it may allow to cause an effective improvement in their mechanical properties and/or functionalization, as a so-called percolation effect [5,26].

4. Concept of "plant cell walls"-like frameworks based on the percolation effect

ACC-CNF adsorbs readily to hydrophobic iPP and the interface between ACC-CNFs and iPP exhibits thermodynamic affinity. That is indicated the iPP microsphere coated with ACC-CNFs can be used as starting materials of their nanocomposite materials without chemical pre-modifications and additives. When the ACC-CNFs-coated iPP microspheres are provided for injection molding, ACC-CNFs exposed on the surface of each iPP microsphere may interact with each other to form a three-dimensional continuous structure in molten iPP in a furnace. The molten iPP containing the continuous structure of ACC-CNFs is injected into the mold, and the continuous structure is elongated by injection force.

Plant cells have a high axial anisotropy and connect each other with their cell walls whose main component is a bundle of cellulose microfibrils, forming a three-dimensional structure [55]. The characteristics of structure ACC-CNFs embedded in injection-molded iPP products are described as follows: (1) anisotropy toward one direction, (2) being consisted of component units (= iPP microspheres coated with ACC-CNFs), and (3) formation of a three-dimensional continuous structure. Because these characteristics are similar to plant cell walls, the three-dimensional structure of ACC-CNFs can be regarded as "plant cell walls" (=PCW)-like structure. The PCW-like structure consisted of ACC-CNFs is expected to emerge functions based on percolation effects. These are a starting idea for the material design throughout the study in this thesis. Then, the connected 3D-skelton with highly crystallinity ACC-CNFs in the nanocomposite would play a role in energy transfer pathway through the connected PCW-like frameworks.

5. Objective and outline in this dissertation

This dissertation attempts the functionalization of ACC-CNFs/iPP composite by embedding the PCW-like framework based on the described concept.

Chapter 1 deals with fabrication of nanocomposite materials embedding PCW-mimicked frameworks from the ACC-CNFs-coated iPP microspheres by injection molding. The nanocomposite has successfully contained PCW-mimicked frameworks composed of ACC-CNFs and achieved to improve in the impact resistance regardless of addition with an ultra-trace amount of ACC-CNFs. The PCW-like frameworks have been provided to contribute to its impact resistance by acting as an energy transfer pathway.

Furthermore, it has been implied that ACC-CNFs affected crystallization of iPP as a scaffold.

Chapter 2 deals with formation mechanism of the PCW-mimicked frameworks. Thermal analyses have revealed that the PCW-like frameworks of ACC-CNFs are formed spontaneously under thermal treatment without shear stress and they act as scaffolds of crystallization of iPP to form complex PCW-like ACC-CNFs/iPP framework with a core of ACC-CNFs. α-crystal of iPP crystal was promoted to form and the relative ratio was dependent on the kinds of raw materials for ACC-CNFs.

Chapter 3 deals with examination for relationship between their impact-resistance and tensile properties of the iPP composite products with the ACC-CNFs honeycomb-skeleton with different sources. Namely, it has been focused on the trade-off relationship between increase in tensile properties and decrease in the impact-resistance or vice versa in the ACC-CNF/iPP composite products. From results of tensile test, PCW-like frameworks composed of ACC-CNF derived from bamboo bleached kraft pulp (= ACC-BBKP) have contributed to improvement both elastic modulus without decreasing elongation. This suggests that the nanocomposite has achieved to overcome a trade-off relationship of the elastic modulus and elongation. In contrast, addition of ACC-CNF derived from microcrystalline cellulose (= ACC-MCC) has improved only the elastic modulus with decreasing in the elongation and addition of ACC-CNF derived from BNC (= ACC-BNC) has improved only the elongation without improvement in the elastic modulus. These results indicate that the source of raw materials for ACC-CNFs also influence the final composite products.

Here this study, it is indicated that a new concept is proposed via embedding a continuous PCW-like frameworks promoting a percolation effect to energy dissipation, leading to an advanced design of CNFs-nanocomposite plastic materials.

References

(1) Omran, A. A. B.; Mohammed, A. A. B. A.; Sapuan, S. M.; Ilyas, R. A.; Asyraf, M. R. M.; Koloor, S. S. R.; Petrů, M. Micro-and Nanocellulose in Polymer Composite Materials: A Review. *Polymers (Basel)*, **2021**, *13* (2), 1–30. https://doi.org/10.3390/polym13020231.

(2) Etale, A.; Onyianta, A. J.; Turner, S. R.; Eichhorn, S. J. Cellulose: A Review of Water Interactions, Applications in Composites, and Water Treatment. *Chemical Reviews*, **2023**, *123* (5), 2016–2048. https://doi.org/10.1021/acs.chemrev.2c00477.

(3) Klemm, D.; Cranston, E. D.; Fischer, D.; Gama, M.; Kedzior, S. A.; Kralisch, D.; Kramer, F.; Kondo, T.; Lindström, T.; Nietzsche, S.; Petzold-Welcke, K.; Rauchfuß, F. Nanocellulose as a Natural Source for Groundbreaking Applications in Materials Science: Today's State. *Materials Today*, **2018**, *21* (7), 720–748. https://doi.org/10.1016/j.mattod.2018.02.001.

(4) Tsuji, T.; Tsuboi, K.; Yokota, S.; Tagawa, S.; Kondo, T. Characterization of an Amphiphilic Janus-Type Surface in the Cellulose Nanofibril Prepared by Aqueous Counter Collision. *Biomacromolecules*, **2021**, *22* (2), 620–628. https://doi.org/10.1021/acs.biomac.0c01464.

(5) Moon, R. J.; Martini, A.; Nairn, J.; Simonsen, J.; Youngblood, J. Cellulose Nanomaterials Review: Structure, Properties and Nanocomposites. *Chemical Society Reviews*, **2011**, *40* (7), 3941–3994. https://doi.org/10.1039/c0cs00108b.

(6) Newman, R. H.; Hill, S. J.; Harris, P. J. Wide-Angle x-Ray Scattering and Solid-State Nuclear Magnetic Resonance Data Combined to Test Models for Cellulose Microfibrils in Mung Bean Cell Walls. *Plant Physiology*, **2013**, *163* (4), 1558–1567. https://doi.org/10.1104/pp.113.228262.

(7) Oehme, D. P.; Downton, M. T.; Doblin, M. S.; Wagner, J.; Gidley, M. J.; Bacic, A. Unique Aspects of the Structure and Dynamics of Elementary Iβ Cellulose Microfibrils Revealed by Computational Simulations. *Plant Physiology*, **2015**, *168* (1), 3–17. https://doi.org/10.1104/pp.114.254664.

(8) Daicho, K.; Saito, T.; Fujisawa, S.; Isogai, A. The Crystallinity of Nanocellulose: Dispersion-Induced Disordering of the Grain Boundary in Biologically Structured

Cellulose. *ACS Applied Nano Materials*, **2018**, *1* (10), 5774–5785. https://doi.org/10.1021/acsanm.8b01438.

(9) Isogai, A. Wood Nanocelluloses: Fundamentals and Applications as New Bio-Based Nanomaterials. *Journal of Wood Science*, **2013**, *59* (6), 449–459. https://doi.org/10.1007/s10086-013-1365-z.

(10) Kondo, T. Cellulose Nanofibrils Pulverized from Biomass Resources: Past, Present, and Future Perspectives. *KONA Powder and Particle Journal*, **2023**, *40*, 109–123. https://doi.org/10.14356/kona.2023003.

(11) Isogai, A. Review Development of Completely Dispersed Cellulose Nano Fibers. *Proceedings of the Japan Academy, Ser. B, Physical and Biological Sciences*, **2018**, *94* (4), 161–179.

(12) Isogai, A. TEMPO-Catalyzed Oxidation of Polysaccharides. *Polymer Journal*, **2022**, *54* (4), 387–402. https://doi.org/10.1038/s41428-021-00580-1.

(13) Saito, T.; Isogai, A. TEMPO-Mediated Oxidation of Native Cellulose. The Effect of Oxidation Conditions on Chemical and Crystal Structures of the Water-Insoluble Fractions. *Biomacromolecules*, **2004**, *5* (5), 1983–1989. https://doi.org/10.1021/bm0497769.

(14) Saito, T.; Isogai, A. Introduction of Aldehyde Groups on Surfaces of Native Cellulose Fibers by TEMPO-Mediated Oxidation. *Colloids and Surfaces A: Physicochemical and Engineering Aspects*, **2006**, *289* (1–3), 219–225. https://doi.org/10.1016/j.colsurfa.2006.04.038.

(15) Uetani, K.; Yano, H. Nanofibrillation of Wood Pulp Using a High-Speed Blender. *Biomacromolecules*, **2011**, *12* (2), 348–353. https://doi.org/10.1021/bm101103p.

(16) Nakagaito, A. N.; Yano, H. Novel High-Strength Biocomposites Based on Microfibrillated Cellulose Having Nano-Order-Unit Web-like Network Structure. *Applied Physics A: Materials Science & Processing*, **2005**, *80* (1), 155–159. https://doi.org/10.1007/s00339-003-2225-2.

(17) Albin F. Turbak; Fred W. Snyder; Karen R. Sandberg. Microfibrillated Cellulose, a New Cellulose Product: Properties, Uses, and Commercial Potential. *Journal of Applied Polymer Science: Applied Polymer Symposium*, **1983**, *37*, 815–827.

(18) Spence, K. L.; Venditti, R. A.; Habibi, Y.; Rojas, O. J.; Pawlak, J. J. The Effect of Chemical Composition on Microfibrillar Cellulose Films from Wood Pulps: Mechanical Processing and Physical Properties. *Bioresource Technology*, **2010**, *101* (15), 5961–5968. https://doi.org/10.1016/j.biortech.2010.02.104.

(19) Kondo, T.; Morita, M.; Hayakawa, K.; Onda, Y. Polysaccharide Wet Pulverization Method., US Patent, US 7 357 339 B2, 2008.

(20) Kose, R.; Mitani, I.; Kasai, W.; Kondo, T. "Nanocellulose" as a Single Nanofiber Prepared from Pellicle Secreted by Gluconacetobacter Xylinus Using Aqueous Counter Collision. *Biomacromolecules*, **2011**, *12* (3), 716–720. https://doi.org/10.1021/bm1013469.

(21) Kondo, T.; Kose, R.; Naito, H.; Kasai, W. Aqueous Counter Collision Using Paired Water Jets as a Novel Means of Preparing Bio-Nanofibers. *Carbohydrate Polymers*, **2014**, *112*, 284–290. https://doi.org/10.1016/j.carbpol.2014.05.064.

(22) Saito, T.; Kuramae, R.; Wohlert, J.; Berglund, L. A.; Isogai, A. An Ultrastrong Nanofibrillar Biomaterial: The Strength of Single Cellulose Nanofibrils Revealed via Sonication-Induced Fragmentation. *Biomacromolecules*, **2013**, *14* (1), 248–253. https://doi.org/10.1021/bm301674e.

(23) Matsuo, M.; Sawatari, C.; Iwai, Y.; Ozaki, F. Effect of Orientation Distribution and Crystallinity on the Measurement by X-Ray Diffraction of the Crystal Lattice Moduli of Cellulose I and II. *Macromolecules*, **1990**, *23* (13), 3266–3275. https://doi.org/10.1021/ma00215a012.

(24) Hori, R.; Wada, M. The Thermal Expansion of Wood Cellulose Crystals. *Cellulose*, **2005**, *12* (5), 479–484. https://doi.org/10.1007/s10570-005-5967-5.

(25) Siró, I.; Plackett, D. Microfibrillated Cellulose and New Nanocomposite Materials: A Review. *Cellulose*, **2010**, *17* (3), 459–494. https://doi.org/10.1007/s10570-010-9405-y.

(26) Lee, K. Y.; Aitomäki, Y.; Berglund, L. A.; Oksman, K.; Bismarck, A. On the Use of Nanocellulose as Reinforcement in Polymer Matrix Composites. *Composite Science and Technology*, **2014**, *105*, 15–27. https://doi.org/10.1016/j.compscitech.2014.08.032.

(27) Kargarzadeh, H.; Mariano, M.; Huang, J.; Lin, N.; Ahmad, I.; Dufresne, A.; Thomas, S. Recent Developments on Nanocellulose Reinforced Polymer Nanocomposites: A Review. *Polymer (Guildf)*, **2017**, *132*, 368–393. https://doi.org/10.1016/j.polymer.2017.09.043.

(28) Wang, L.; Roach, A. W.; Gardner, D. J.; Han, Y. Mechanisms Contributing to Mechanical Property Changes in Composites of Polypropylene Reinforced with Spray-Dried Cellulose Nanofibrils. *Cellulose*, **2018**, *25* (1), 439–448. https://doi.org/10.1007/s10570-017-1556-7.

(29) Raji, M.; Essabir, H.; ElAchaby, M.; Bouhfid, R.; Qaiss, A. E. K. Morphology Control of Poly(Lactic) Acid/Polypropylene Blend Composite by Using Silanized Cellulose Fibers Extracted from Coir Fibers. *Cellulose*, **2022**, *29* (12), 6759–6782. https://doi.org/10.1007/s10570-022-04675-7.

(30) Igarashi, Y.; Sato, A.; Okumura, H.; Nakatsubo, F.; Yano, H. Manufacturing Process Centered on Dry-Pulp Direct Kneading Method Opens a Door for Commercialization of Cellulose Nanofiber Reinforced Composites. *Chemical Engineering Journal*, **2018**, *354*, 563–568. https://doi.org/10.1016/j.cej.2018.08.020.

(31) Ljungberg, N.; Cavaillé, J. Y.; Heux, L. Nanocomposites of Isotactic Polypropylene Reinforced with Rod-like Cellulose Whiskers. *Polymer (Guildf)*, **2006**, *47* (18), 6285–6292. https://doi.org/10.1016/j.polymer.2006.07.013.

(32) Ifuku, S.; Nogi, M.; Abe, K.; Handa, K.; Nakatsubo, F.; Yano, H. Surface Modification of Bacterial Cellulose Nanofibers for Property Enhancement of Optically Transparent Composites: Dependence on Acetyl-Group DS. *Biomacromolecules*, **2007**, *8* (6), 1973–1978. https://doi.org/10.1021/bm070113b.

(33) Kim, D.-Y.; Nishiyama, Y.; Kuga, S. Surface Acetylation of Bacterial Cellulose. *Cellulose*, **2002**, *9*, 361–367.

(34) Soeta, H.; Fujisawa, S.; Saito, T.; Isogai, A. Interfacial Layer Thickness Design for Exploiting the Reinforcement Potential of Nanocellulose in Cellulose Triacetate Matrix. *Composite Science and Technology*, **2017**, *147*, 100–106. https://doi.org/10.1016/j.compscitech.2017.05.010.

(35) de la Orden, M. U.; González Sánchez, C.; González Quesada, M.; Martínez Urreaga, J. Effect of Different Coupling Agents on the Browning of Cellulose-Polypropylene Composites during Melt Processing. *Polymer Degradation and Stability*, **2010**, *95* (2), 201–206. https://doi.org/10.1016/j.polymdegradstab.2009.11.024.

(36) Tsuboi, K.; Yokota, S.; Kondo, T. Difference between Bamboo- and Wood-Derived Cellulose Nanofibers Prepared by the Aqueous Counter Collision Method. *Nordic Pulp & Paper Research Journal*, **2014**, *29* (1), 69–76. https://doi.org/10.3183/npprj-2014-29-01-p069-076.

(37) Yokota, S.; Kamada, K.; Sugiyama, A.; Kondo, T. Pickering Emulsion Stabilization by Using Amphiphilic Cellulose Nanofibrils Prepared by Aqueous Counter Collision. *Carbohydrate Polymers*, **2019**, *226*, 115293. https://doi.org/10.1016/j.carbpol.2019.115293.

(38) Tagawa, S.; Ishida, K.; Tsuji, T.; Kondo, T. Facile Size Evaluation of Cellulose Nanofibrils Adsorbed on Polypropylene Substrates Using Fluorescence Microscopy. *Cellulose*, **2021**, *28* (5), 2917–2929. https://doi.org/10.1007/s10570-021-03759-0.

(39) Utsunomiya, H.; Tsujita, Y.; Kondo, T. Cellulose Nanoanemone: An Asymmetric Form of Nanocellulose. *Cellulose*, **2022**, *29* (5), 2899–2916. https://doi.org/10.1007/s10570-021-04231-9.

(40) Ishikawa, G.; Kondo, T. Thermodynamic Effect on Interaction between Crystalline Phases in Size-Controlled ACC-Bacterial Nanocellulose and Poly(Vinyl Alcohol). *Cellulose*, **2017**, *24* (12), 5495–5503. https://doi.org/10.1007/s10570-017-1532-2.

(41) Kose, R.; Kondo, T. Size Effects of Cellulose Nanofibers for Enhancing the Crystallization of Poly(Lactic Acid). *Journal of Applied Polymer Science*, **2013**, *128* (2), 1200–1205. https://doi.org/10.1002/app.38308.

(42) Ishikawa, G.; Kondo, T. Characterization of Dual Nano-Size Effects of ACC-Cellulose Nanofibrils on Crystallization Behavior of Hydrophilic Poly(Vinyl Alcohol). *Journal of Wood Science*, **2021**, *67*, 25. https://doi.org/10.1186/s10086-021-01957-9.

(43) Ishikawa, G.; Tsuji, T.; Tagawa, S.; Kondo, T. Adsorption of Janus-Type Amphiphilic Cellulose Nanofibrils onto Microspheres of Semicrystalline Polymers. *Macromolecules*, **2021**, *54* (20), 9393–9400. https://doi.org/10.1021/acs.macromol.1c01163.

(44) Kondo, T.; Yokota, S.; Tanaka, H. Nanocomposite and Method for Producing Nanocomposite. WO 2019/112010 A1, https://patents.google.com/patent/JP6979083B2/en.

(45) Ishida, K.; Kondo, T. Evaluation of Surface Free Energy Inducing Interfacial Adhesion of Amphiphilic Cellulose Nanofibrils. *Biomacromolecules*, **2023**, *24*, 3786–3793. https://doi.org/10.1021/acs.biomac.3c00443.

(46) Hsissou, R.; Seghiri, R.; Benzekri, Z.; Hilali, M.; Rafik, M.; Elharfi, A. Polymer Composite Materials: A Comprehensive Review. *Composite Structure*, **2021**, *262*. https://doi.org/10.1016/j.compstruct.2021.113640.

(47) Plastics Europe. *Plastics-the Facts 2021 An Analysis of European Plastics Production, Demand and Waste Data*; 2021.

(48) Plastics Europe. *Plastics-the Facts 2013 An Analysis of European Latest Plastics Production, Demand and Waste Data*; 2013.

(49) Plastics Europe. *Plastics-the Facts 2015 An Analysis of European Plastics Production, Demand and Waste Data*; 2015.

(50) Ellen Macarthur Foundation. *The New Plastics Economy Rethinking the Future of Plastics*; 2016. https://www3.weforum.org/docs/WEF_The_New_Plastics_Economy.pdf.

(51) Paul, D. R.; Robeson, L. M. Polymer Nanotechnology: Nanocomposites. *Polymer (Guildf)*, **2008**, *49* (15), 3187–3204. https://doi.org/10.1016/j.polymer.2008.04.017.

(52) Crosby, A. J.; Lee, J. Y. Polymer Nanocomposites: The “Nano” Effect on Mechanical Properties. *Polymer Reviews*, **2007**, *47* (2), 217–229. https://doi.org/10.1080/15583720701271278.

(53) Sanjay, M. R.; Madhu, P.; Jawaid, M.; Senthamaraikannan, P.; Senthil, S.; Pradeep, S. Characterization and Properties of Natural Fiber Polymer Composites: A Comprehensive Review. *Journal of Cleaner Production,* **2018**, *172*, 566–581. https://doi.org/10.1016/j.jclepro.2017.10.101.

(54) Schadler, L. S.; Kumar, S. K.; Benicewicz, B. C.; Lewis, S. L.; Harton, S. E. Designed Interfaces in Polymer Nanocomposites: A Fundamental Viewpoint. *MRS Bull*, **2007**, *32* (4), 335–340. https://doi.org/10.1557/mrs2007.232.

(55) Chen, C.; Kuang, Y.; Zhu, S.; Burgert, I.; Keplinger, T.; Gong, A.; Li, T.; Berglund, L.; Eichhorn, S. J.; Hu, L. Structure–Property–Function Relationships of Natural and Engineered Wood. *Nature Reviews Materials*, **2020**, *5* (9), 642–666. https://doi.org/10.1038/s41578-020-0195-z.

Chapter 1

Impact-resistant nanocomposite plastics embedding “plant cell wall”-mimicked frameworks with ultratrace amounts of amphiphilic cellulose nanofibrils

Abstract

This chapter deals with fabrication of nanocomposite materials embedding “plant cell wall” (= PCW)-mimicked framework from the iPP microspheres coated with ACC-CNF derived from bamboo bleached kraft pulp by injection-molding. Prior to injection-molding, the ACC-CNF-coated iPP microspheres were fabricated by vibrational mixing ACC-CNF aqueous suspension and iPP microspheres under ambient conditions. The injection-molded nanocomposite has successfully contained PCW-mimicked frameworks composed of ACC-CNF and achieved to improvement in the impact resistance regardless of an ultra-trace amount of ACC-CNF approximately 0.03 wt%/iPP. It was revealed that the PCW-like frameworks have been provided to contribute to its impact resistance by acting as an energy transfer pathway. Furthermore, it has been implied that ACC-CNFs affected crystallization of iPP as a scaffold.

1.1. Introduction

Isotactic polypropylene (iPP), one of the semi-crystalline polymers, exhibits hydrophobic properties due to non-polarity molecular structure. iPP is the most available commodity plastics due to advantages such as light weight, excellent molding processability, corrosion resistance, low cost and less toxicity [1–5]. Due to its molding processability and low cost, iPP-based composite materials have been developed to improve mechanical and/or functional properties [5–10] . Reinforced iPP-based composite materials are expected to be used as structural materials replacing metallic materials, while they regularly decrease impact resistance, that is their disadvantages.

The reinforcing fillers for the composite materials require good mechanical strength and low-thermal expansion. Cellulose nanofibrils (CNFs), with excellent mechanical properties such as mechanical strength (2 – 6 GPa) and elastic modulus (160 GPa), are expected to be used as reinforcement fillers for iPP [11–14]. However, many types of CNFs exhibit hydrophilicity due to surface OH groups and have incompatibility to hydrophobic iPP. Due to their incompatibility, it is difficult to fabricate functional CNFs/iPP nanocomposites without chemical modification of CNFs or additives such as compatibilizers [9,11,12,15].

In contrast, cellulose nanofibrils (= ACC-CNFs) with highly crystallinity, prepared by aqueous counter collision (ACC) method [16–19] exhibit amphiphilic surface properties. ACC-CNFs can easily coat surface on iPP microspheres favorably by shaking in water and interfacial affinity between ACC-CNFs and iPP was found by thermodynamic analyses [20]. The iPP microsphere coated with ACC-CNFs, produced by such easy method, is expected to be used as a starting material of nanocomposites.

During melt-molding process in furnace, iPP microspheres are melted to result in forming continuous phase. Then, highly crystalline ACC-CNFs exposed onto the microspheres surface are supposed to contact each other to engage in three-dimensional continuous network frames structure in the resultant molten iPP matrix. The continuous network frames of highly crystalline ACC-CNFs embedded in molded nanocomposite are expected to readily propagate stress wave generated by an impact stress together. Hence, the nanocomposite embedding ACC-CNFs network frames comes to exhibit an improvement in impact resistance. This chapter attempts in this way to fabricate an impact-resistant nanocomposite embedding plant cell wall-mimicked framework from iPP microspheres coated with ACC-CNFs and to deal with the emergence mechanism of the improvement of the character.

1.2. Experimental Section

1.2.1. Materials

Commercial-grade homopolymer iPP microparticles (Prime Polypro™) whose an average diameter of approximately 500 μm (n = 50) were purchased from Prime Polymer Co., Ltd. (Tokyo, Japan). ACC-BBKP aqueous dispersion (nanoforest-S/B-S) was provided from Chuetsu Pulp & Paper Co., Ltd. (Toyama, Japan) [20]. Bacterial nanocellulose (= BNC) pellicle was cultured, isolated and then purified to previous papers [18]. Prior ACC treatments for BNC, purified BNC pellicle was cut into approximately 1 cm square cube and pre-fibrillated with a conventional food mixer for 1 min [21]. The pre-fibrillated BNC was provided for ACC treatments at the ejection pressure of 200 MPa with the treatment repeating cycles (= Pass) of 60 Pass, obtaining ACC-BNC. Calcofluor

White M2R (CFW) which is a fluorescent specific dye for CNFs was purchased from Sigma-Aldrich Corp. (Tokyo, Japan) [20,22,23].

1.2.2. Preparation of iPP microspheres coated with amphiphilic ACC-CNFs as starting materials of their nanocomposite

Coating process of iPP microspheres with ACC-CNFs was based on a previous study [20]. ACC-CNFs aqueous dispersion was diluted with deionized water to 0.01 wt% and to stir overnight by a magnetic stirrer for uniform dispersing state of ACC-CNFs. 120 Grams of 0.01 wt% ACC-CNFs aqueous dispersion and 30 grams of iPP microspheres were mixed homogeneously in a 250 ml polyethylene terephthalate (PET) bottle for 30 minutes at 150 rpm on a shaker (MIR-S100 ®, Panasonic Healthcare Co., Ltd., Gunma, Japan). The iPP coated with ACC-CNFs was isolated by filtration using a steel mesh with 180 μm pores and then washed with deionized water to remove excess ACC-CNFs. The coated microspheres were dried in an oven at 50 °C.

1.2.3. Surface properties analysis

Surface area measurements: For measurements of surface area of neat iPP microspheres and iPP microspheres coated with ACC-CNFs, a surface area analyzer (Monosorb, Quantachrome Instruments Co., Ltd.) was used to monitor the adsorption of N_2 gas by the ACC-CNFs at -196 °C. The surface area of each sample was estimated by fitting the resulting adsorption data to the Brunauer, Emmett and Teller (BET) equation. The specific surface areas (SSAs) of the CNFs were obtained by dividing the surface areas by the total sample masses. The SSAs both neat and ACC-CNFs-coated iPP

microspheres were instead determined based on the adsorption of octane using the BET method.

Qualitative changes of surface wettability of iPP microsphere for water after ACC-CNFs adsorption: iPP microspheres coated with ACC-CNFs derived from BNC are prepared by the described method. In glass vessel, iPP microparticles and ultrapure water mixed to place and the floating state of particles were observed.

1.2.4. Quantitation of the amounts of ACC-CNFs adsorbing onto iPP microspheres.

Direct measurements by weight: Prior to coating process, the weight of complete dried neat iPP microspheres was measured by electronic balance. After coating and washing process described above, iPP microspheres coated with ACC-CNFs were dried completely and the weight of the coated iPP microspheres was measured. The change in weight before and after ACC-CNFs coating process meant the weight of adsorbed ACC-CNFs.

Indirect measurements from viscosity of ACC-CNFs aqueous dispersion: ACC-CNFs aqueous dispersions with any concentration were prepared by dilution with deionized water. After mixing with iPP microspheres and ACC-CNFs aqueous dispersion, the filtrated aqueous dispersion with residual ACC-CNFs (non-adsorbed) was collected. The calibration curve between viscosity of the aqueous dispersion and concentration of ACC-CNFs were created by tuning fork vibration viscometer (SV-1A; A&D Co., Ltd., Tokyo, Japan). For estimation of the amounts of adsorbed ACC-CNFs, the viscosity of collected aqueous dispersion after coating was measured.

1.2.5. Prepressing

iPP microspheres coated with the ACC-CNFs were placed between two polyimide films and the films put between two stainless boards. The boards pressed at a pressure of 20 MPa for 5 min at 155 °C (Table Type Test Press SA-303, Tester Sangyo Co., Ltd., Saitama, Japan). This temperature was lower than the peak of melting point of neat iPP, providing the surface of iPP melting or softening. Thus, only promoted fusion of the surface of coated microspheres, which interacted to adsorbed ACC-CNFs. The aim of this additional prepressing is formation of the desired ACC-CNF framework to form PCW prior to the standard injection molding process.

1.2.6. Melt flow rate measurements

The melt mass-flow rates of iPP microspheres were determined using a G-02 melt flow indexer (Toyo Seiki Seisaku-sho, Ltd., Tokyo, Japan). iPP microspheres were placed and pressed into a furnace of the instrument and heated at 190, 200, or 230 °C. After heating for over 5 min, completely molten material was ejected from furnace with a loading of 2.16 kgf. The procedure was provided in the JIS K 7210-1 standard.

1.2.7. Injection molding of iPP microspheres coated with ACC-CNFs

A 10.0 grams of iPP microspheres was placed in a cylindrical furnace, whose temperature is kept at 200 °C, of manual uniaxial injection-molding instruments (Handtruder M-1, Toyo Seiki Seisakusho, Ltd., Nagano, Japan). Prior to injection molding, microspheres were heated over 5 mins, resulting completely melt and the molten iPP was compressed using a piston to be degassed. During this melting process, exit of the furnace was blocked. The molten material was uniaxially extruded from the cylinder

furnace into a mold whose temperature was kept at 80 °C and then subjected to manual pressurization for 15 s. The mold was subsequently cooled to 60 °C on a stainless bar surrounded to ice. This molded iPP based products whose shape is a dumbbell-type test piece was taken out of the mold. After 1 week of standing under air at room temperature, these specimens were subjected to mechanical testing.

1.2.8. Charpy impact test

In preparation for Charpy impact testing, these dumbbell test pieces were cut to provide rectangular specimens whose dimensions is 80 ± 2 mm × 4.0 ± 0.2 mm × 10.0 ± 0.2 mm. V-Shaped notch whose depth is a 2.0 mm was produced in specimens intended for edge-wise Charpy test based on the JIS K 7111 standard. Prior to the Charpy test, the specimens were subjected to annealing treatment for 3 h, whose temperature in the range of 25 – 130 °C. These tests used a lift angle of 140.0 ° and an impact energy of 0.5 kJ, imparted by a pendulum-style hammer. Each specimen was held at the desired temperature in the chamber of the test apparatus s (No. 195-R, Yasuda Seiki Seisakusho, Ltd., Hyogo, Japan) for 30 min in preparation for analysis, after which the Charpy impact test was carried out to determine the energy absorption capacity of the material. A minimum of five samples were assessed for each trial. The resulting data were compared statistically using t-test, compared to injection-molded products from neat iPP microspheres.

1.2.9. Confocal laser scanning microscopy observation

Confocal laser scanning microscopy (CLSM) was used to visualize the embedded ACC-CNFs in the extrusion-molded composites. Calcofluor white (CW), a

fluorescent stain adsorbed onto the hydrophilic sites of the cellulose, was used to specific dye to the ACC-CNFs [22]. Prior to these analysis, iPP microspheres coated with ACC-CNFs were dried and then mixed with a 0.001 wt% aqueous solution of CW for 10 min. The material was subsequently rinsed with water and then in an oven overnight at 50 °C. Following this, the dumbbell shaped specimen was produced by described method. The obtained specimens were cut and placed on a glass-bottomed petri dish. The observation was performed using a TCS SP8 instrument (Leica Microsystems Inc., Germany) employing a 10× dry objective lens. Fluorescence-microscopic images for a dispersion state of the stained CNFs in the iPP matrix and the differential interference contrast polarized (DIC-Pol) images for their crystalline morphology of iPP were acquired by CLSM (TCS SP8: Leica Microsystems, Wetzlar, Germany). In fluorescence microscopic observation, excitation wavelength was 405 nm and emitting fluorescence was detected between 430 to 470 nm, whereas DIC-Pol observation was performed with an attachment of a DIC-Pol filter [20,22,23]. The CLSM images were then manipulated and analyzed with Leica Application Suite X (= LAS X) software.

1.2.10. Surface properties of injection-molded products

Atomic Force Microscopy: The surface roughness and actual surface area of each sample were determined from topographical images obtained by atomic force microscopy (AFM). The AFM observations were performed using an Asylum MFP-3D Origin system (Oxford Instruments, Abingdon-on-Thames, United Kingdom) with a silicon cantilever (OMCL-AC240TS-R3; Olympus Corp., Tokyo, Japan) in the tapping mode at 25 °C. The root mean square surface roughness (R_q), arithmetic average roughness (R_a) and actual

surface area values of each sample were estimated based on 10 × 10 μm images and were the averaged values obtained from at least five measurements.

Contact Angle Measurement: The apparent contact angle values of water droplets (1 μL) were measured at 25 ± 1 °C using a Drop Master DMs401 contact angle meter (Kyowa Interface Science Co., Ltd, Saitama, Japan) with a polytetrafluoroethylene-coated needle. Contact angles were also recorded over specific time intervals beginning at droplet contact based on 5-10 measurements.

1.2.11. Visualization of heat transfer using temperature-controlled copper board

A temperature-controlled (-20 or 100 °C) copper board was placed onto injection-molded specimens. The thermal transfer behaviors with cooling or heating between the copper board and specimens were visualized with handy type thermographic camera.

1.2.12. Wide angle X-ray diffraction using synchrotron

Crystalline structure analysis of injection-molded iPP based specimens was performed by wide angle X-ray diffraction (WAXD) using synchrotron beam at SAGA Light Source BL06 (Saga, Japan). The wavelength and camera length were 1.38 Å and 159 mm, respectively. Beam size was 1 mm (width) × 0.5 mm (height). Prior to WAXD measurements, the specimens were sliced, obtaining small pieces of samples. 1D integrated intensity function was obtained from 2D diffraction images detected by imaging plate by employing the Fit2D software. All WAXD profiles were baseline-corrected in the range of 8 – 30 ° and normalized with each ratio of maximum intensity from the same baseline. Crystallinity of molded samples prepared from iPP and iPP

coated with ACC-CNFs was calculated based on the area ratio of crystalline peaks to the whole diffraction peaks as follows [24]:

$$Crystallnity\ (\chi_c)\ [\%] = \frac{(total\ crystalline\ areas\ of\ diffraction\ peaks)}{(whole\ area\ of\ diffraction\ patterns)} \times 100$$

1.3. Results and Discussion

1.3.1. Surface properties analysis

The BET SSAs of neat and coated iPP microspheres generated in this work were determined to be 1.63 and 1.32 $m^2 \cdot g^{-1}$, respectively. Hence, the BET SSA of the iPP was decreased by approximately 20 % after coating.

Surface properties of iPP changed by adsorption of ACC-CNFs according to previous report [25]. The surface properties of ACC-CNFs-coated iPP microspheres coated is expected to exhibit hydrophilicity. Fig. 1-1 shows floating behavior of iPP microspheres changed by coating with ACC-CNFs. Katoh et al. demonstrated that small hydrophilic particles floating on water surface near a glass vessel wall tend to spontaneously approach the wall by moving along the liquid meniscus, conversely, hydrophobic particles move towards the center of the glass vessel [26]. Therefore, Fig. 1-1 showed qualitatively that the surface properties of iPP microspheres changes hydrophobic to hydrophilic due to coating with ACC-CNFs. The driving force of adsorption is estimated to be replacement of unstable iPP/water interface to stable iPP/CNFs interface [27]. The hydrophobic portions of the ACC-CNFs are believed to directly adsorb onto the hydrophobic surfaces of the iPP microspheres in aqueous systems.

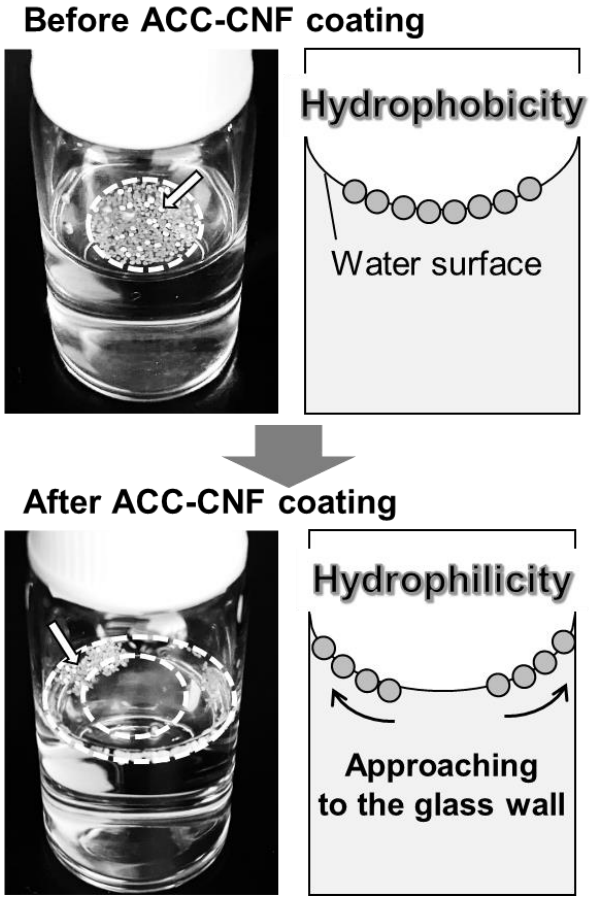

Fig. 1-1 Changing of floatation state of iPP microspheres before and after coating with ACC-CNFs.

1.3.2. The amounts of ACC-CNFs adsorbed onto the iPP microspheres surface

The amounts of ACC-CNFs contained in composite materials are an important factor because this determines the properties of the nanocomposite. A less amount of ACC-CNFs cannot emerge reinforcement effect to their composite materials. In contrast, excess amounts of ACC-CNFs in composite materials are supposed to form aggregations. Therefore, formation CNFs network without aggregation is supposed to be desirable. According to a previous report, the amounts of ACC-CNFs adsorbed onto iPP as a monolayer is approximate 0.02 – 0.03 wt% to iPP [20]. Direct and indirect measurements of the amounts of ACC-CNFs exhibited 0.029 wt% and 0.027 wt%, respectively. Namely,

the ACC-CNFs coating on iPP microspheres is estimated to form a monolayer of ACC-CNFs.

1.3.3. Melt flow rate of molten iPP

Melt flow rate, which is an indicator of viscosity of molten polymer, is a critical factor contributing to the efficiency of the injection molding process in industrial applications. Table 1-1 shows the summary of the melt flow rates determined for the neat iPP, ACC-CNFs-coated iPP and prepressed ACC-CNFs-coated iPP. The ACC-CNFs-coated iPPs evidently had higher melt flow rate values that indicates the coating with the ACC-CNFs improved the viscoelastic properties of the iPP. That is, proposed that ACC-CNFs can provide beneficial to production efficiency. The molten iPP ejected perpendicularly from the furnace of the melt flow rate instruments, then anisotropic ACC-CNFs are likely to align to perpendicular direction in molten iPP. As iPP molecular chain due to affinity interaction with ACC-CNFs [20], entanglements of iPP molecular chain may be resolved by the alignments. Namely, it is possible that the molten iPP became thixotropic as a result of addition of ACC-CNFs. In addition, prepress treatments below the melting point of neat iPP allowed the surface melting or softening to resolving entanglements, and then the melt flow rate of prepressed coated iPP microspheres was highly increased.

Table 1-1 Melt flow rates of the neat, ACC-CNFs-coated and prepressed ACC-CNFs-coated iPP microspheres.

		Neat iPP microspheres	iPP microspheres coated with ACC-CNFs	Prepressed iPP microspheres coated with ACC-CNFs
Melt flow rate / g·10 min^{-1}	190 ºC	4.70	5.00	5.10
	200 ºC	6.55	6.73	9.14
	230 ºC	16.50	17.30	28.20

1.3.4. Observation of embedded ACC-CNFs into iPP based specimen

The procedure of nanocomposite plastics embedding a PCW-like framework is summarized in Fig. 1-2 and the appearance of an injection-molded plastic specimen are showed in Fig. 1-3 (a). The specimen appears uniformly transparent without discoloration and white spots. that suggested ACC-CNFs dispersed uniformly on macroscopic scale. Fig. 1-3 (b) shows CLSM images of the cross-section (that is, the normal direction (ND) – transverse direction (TD)) of the plastic specimen. The embedded ACC-CNFs, stained with specific dye, dispersed in whole matrix. Based on the both images, the cross-section of the composite specimen was divided into three regions (skin, intermediate, and core) and schematic diagram of the divided region is showed in Fig. 1-3 (c).

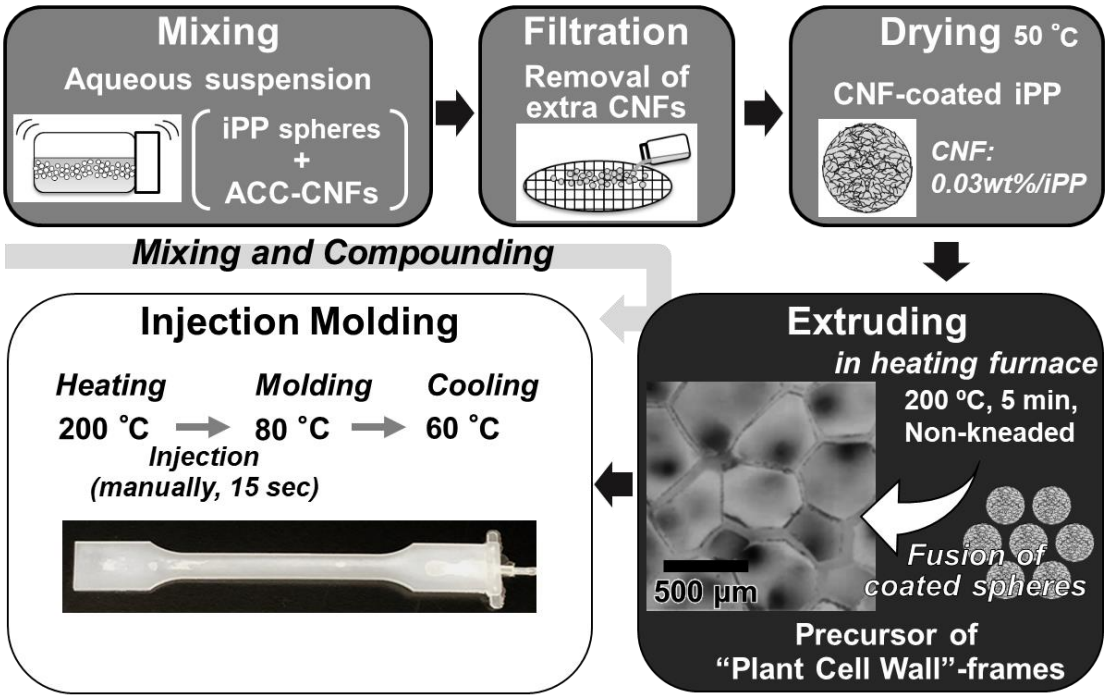

Fig. 1-2 Summary of the processes used to prepare an injection-molding ACC-CNFs/iPP plastics embedding "plant cell wall"-like frameworks.

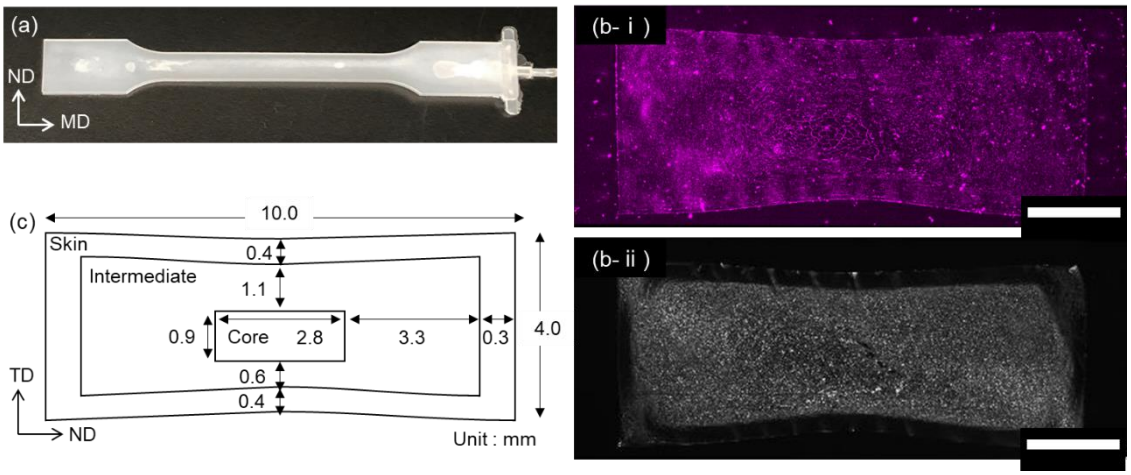

Fig. 1-3 (a) Appearance of injection-molded plastic. (b) CLSM images of injection-molded plastics TD-MD cross section; (i) dark field fluorescence image and (ii) differential interference contrast polarized (DIC-Pol) image. Bars indicate 2 mm (c) Illustration of TD-ND cross section separating skin, inter and core regions defined from both CLSM images.

Fig. 1-4 presents CLSM dark field fluorescence images of the injection-molded ACC-CNFs/iPP nanocomposite at core region and of Japanese ceder sapwood. The cellulose in both samples was stained with CFW, a fluorescent probe, and appears gray in these images. The cross section of injection-molded specimen is defined from three directions (ND, TD, and machine direction (MD)) which is indicated in Fig. 1-4. The patterns formed by the embedded ACC-CNFs in the iPP along these two directions were similar to those in the butt end and radial section of the cedar sapwood, respectively. This result confirms that a PCW-like framework was embedded in the iPP composite using the process shown in Fig. 1-4. The ND-TD projection shows pores having sizes of several hundred micrometers that are narrower compared with the initial diameter of 500 μm, or that are extended in the direction of extrusion. In addition, the ND-MD projection indicates extension of the microspheres as a consequence of the extrusion process. These changes could be associated with the thixotropic nature of the molten iPP after coating. It should also be noted that the ACC-CNFs framework was maintained in the final product. The wide-range CLSM image of the ND-MD section (Fig. 1-5) also demonstrates the presence of the ends of an individual elongated PCW-like framework embedded in the nanocomposite after injection molding. The cell seen in this image appears to have been elongated by a factor of 2.5 to 3.5.

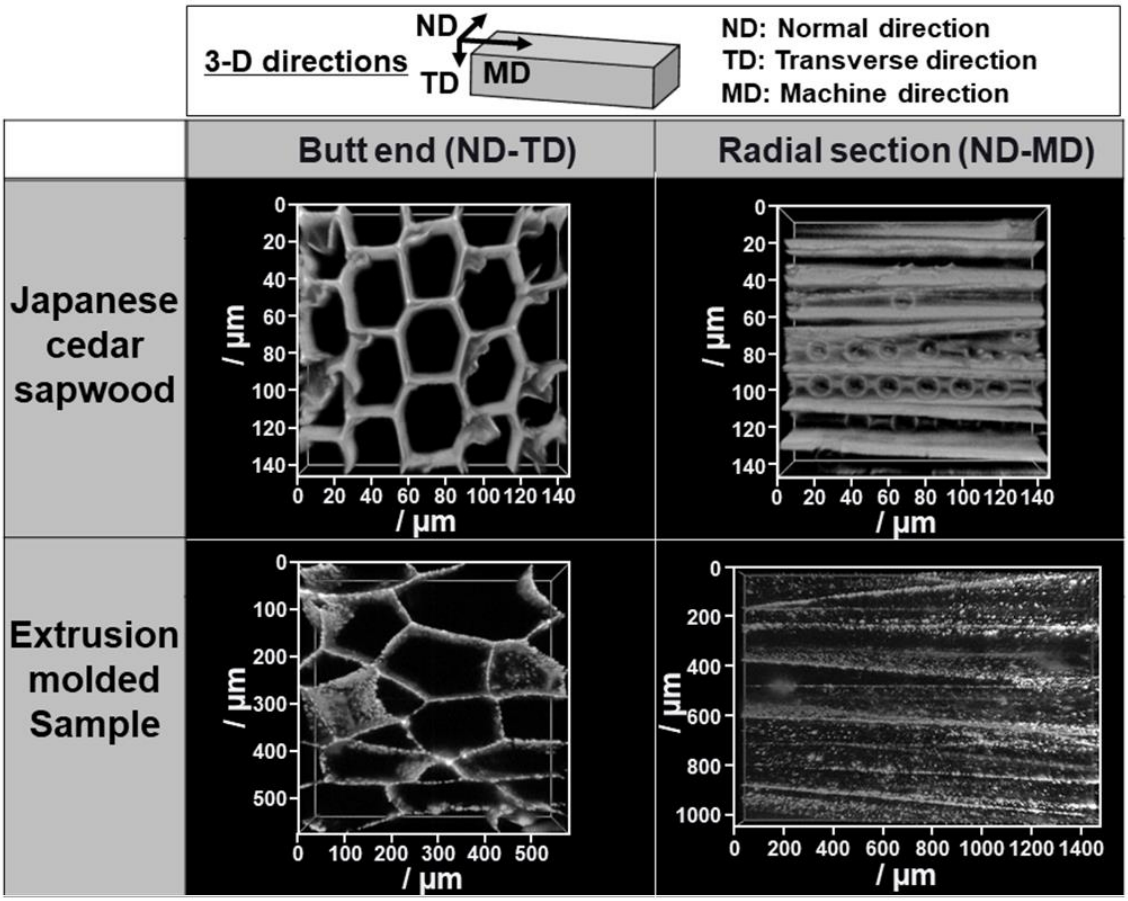

Fig. 1-4 CLSM images of a PCW-type framework embedded in an ACC-CNFs/iPP nanocomposite (lower) and of cellulose cell walls in Japanese cedar sapwood (upper) as a reference. Cellulose (gray, λex: 405 nm, λem: 415-500 nm) in the nanocomposite was stained with 0.001% Calcoflour white, whereas the cellulose cell walls were naturally fluorescent (gray, λex: 405 nm, λem: 420-600 nm). Each specimen was fabricated using a sliding microtome to expose the internal structure.

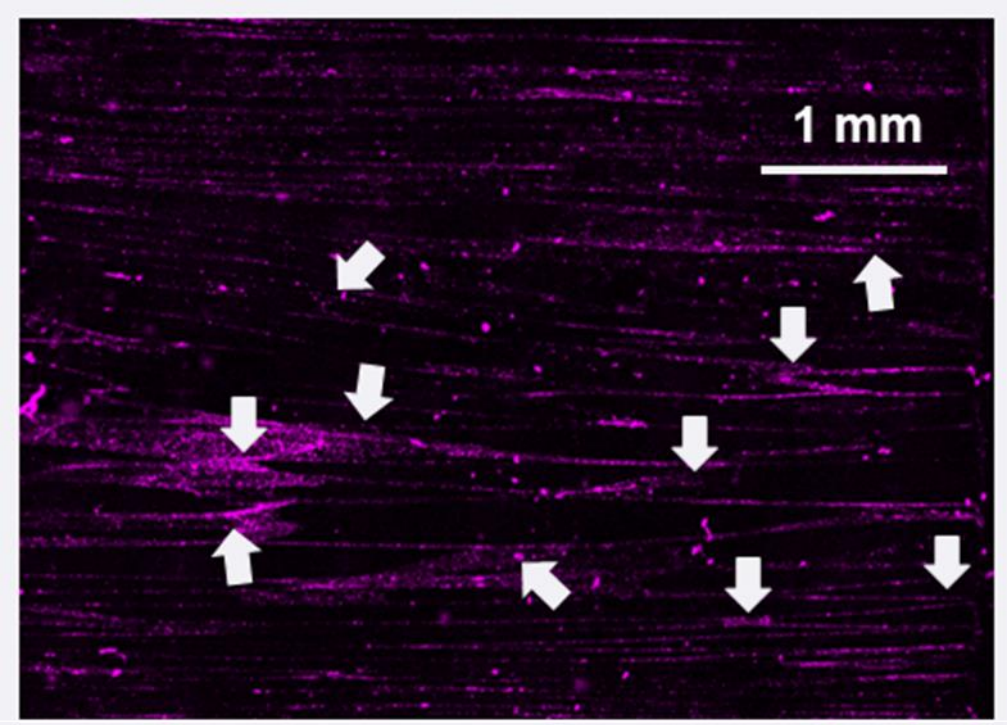

Fig. 1-5 A CLSM wide-range image of the ND-MD section of a PCW-like framework embedded in an ACC-CNFs/iPP nanocomposite. Cellulose (pink; λex: 405 nm, λem: 415-500 nm) in the molded plastics was stained with 0.001% CW. A sliding microtome was employed to expose the internal structure. The arrow heads indicate the ends of an individual elongated "plant cell wall" made of ACC-CNFs after injection-molding.

Fig. 1-6 shows TD-ND cross section CLSM merged image combined fluorescence image and differential interference polarized (DIC-Pol) image of the injection-molded nanocomposite products. Fig. 1-6 revealed PCW-framework formed in core region, while ACC-CNFs dispersed randomly in skin and intermediate region. In addition, iPP crystalline lamella formed perpendicular to the PCW framework. The merged CLSM image implied that PCW frameworks composed of ACC-CNFs promoted iPP crystallization.

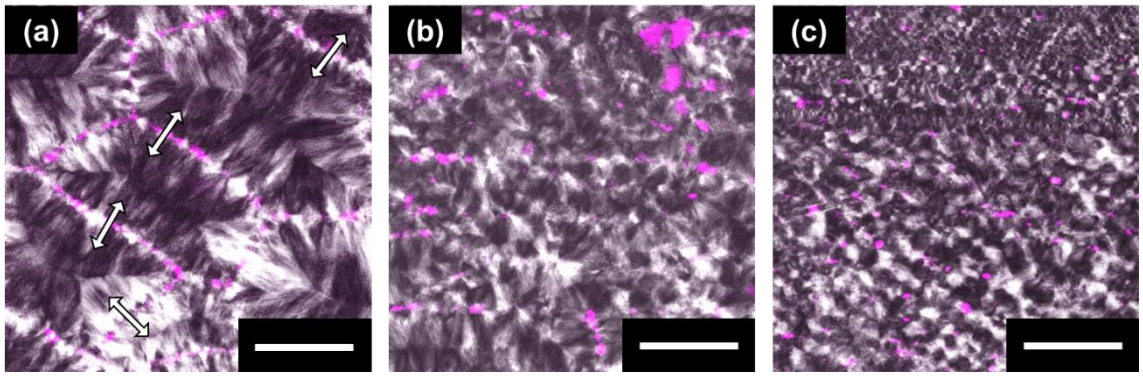

Fig. 1-6 TD-ND cross section CLSM merged image combined dark field fluorescence image and differential interference contrast polarized (DIC-Pol) image; (a) core, (b) intermediate and (c) skin region obtained from specimen made by iPP microspheres coated with ACC-CNFs. Arrows indicate direction of lamella orientation. ACC-CNFs, stained by calcofluor white, were show by pink. Bars indicate 50 μm.

1.3.5. Impact absorption energy

The impact absorption energy of the injection-molded products, determined by Charpy impact tests, was summarized in Fig. 1-7. Above 40 °C, the impact resistance of both two types of ACC-CNF/iPP specimens, especially the prepressed one, was improved. In addition, high temperature-annealing (105 and 130 °C) enhanced energy absorption property of prepressed one. Kitao and Tsuruta reported that impact resistance of semi-crystalline polymers was increased by annealing treatment [28,29]. The reason is estimated that melting of tiny crystals, whose melting temperature is lower than annealing temperature, contributes to increasing mobility of polymer chains constrained by these crystals. Generally, decreasing in size of spherulite is promoted by addition of a nucleating agent, which induces crystallization, and Fig. 1-6 (a) implied ACC-CNFs acted as a nucleating agent. Therefore, enhancement of absorbed energy by high temperature annealing was tiny crystals formed by addition of ACC-CNFs.

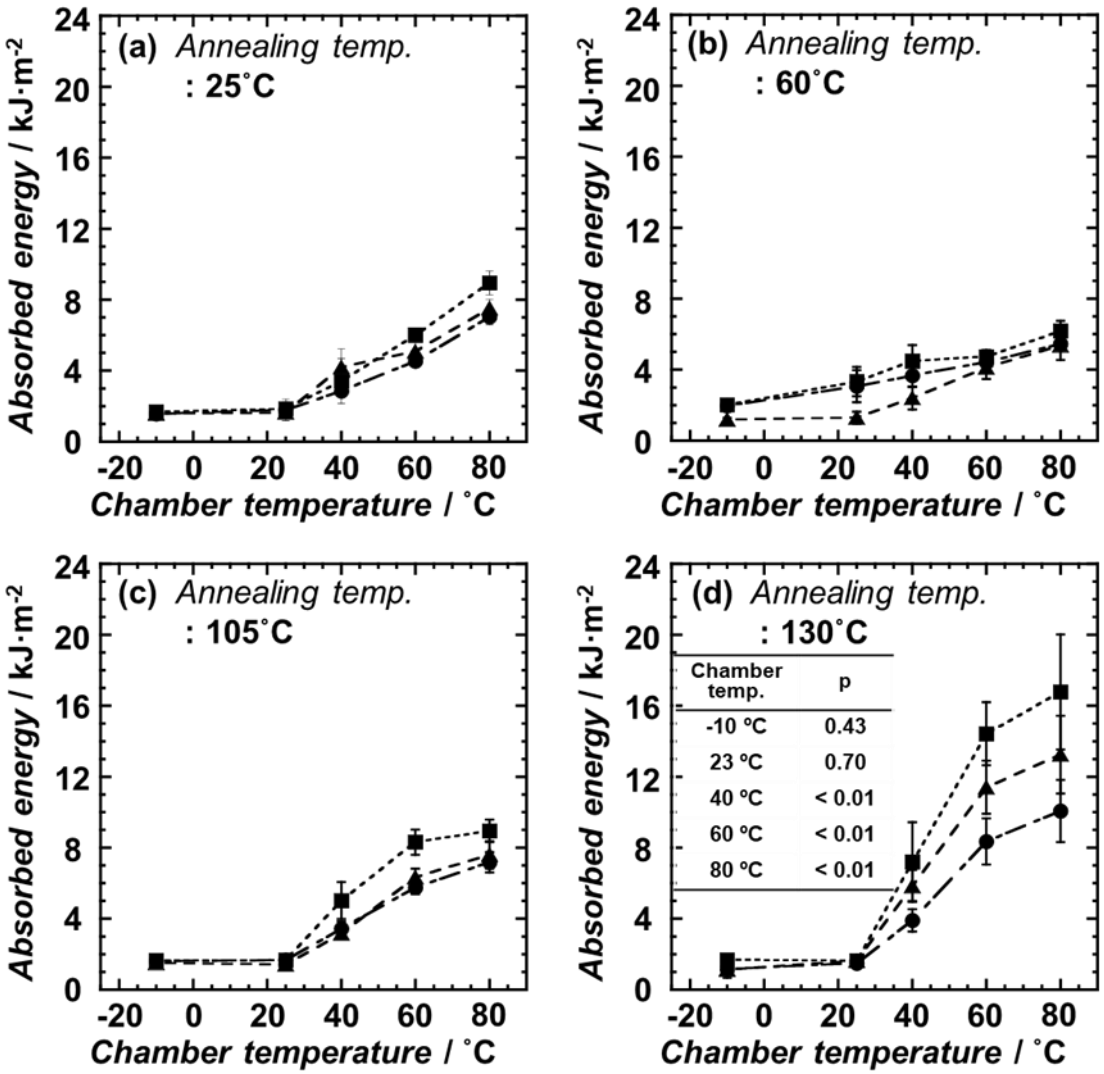

Fig. 1-7 The absorbed energy of products fabricated using various post-annealing temperatures (reflecting impact resistance) as functions of test temperature. The post-annealing for the products was conducted at (a) 25, (b) 60, (c) 105 and (d) 130 °C. All post-annealing treatments were performed for 3 h. Legend: ● = neat iPP, ▲ = 0.03 wt% ACC-CNFs/iPP, ■ = prepressed 0.03 wt% ACC-CNFs/iPP. The t-test values in (d) for comparisons between the prepressed ACC-CNFs/iPP and the neat iPP with $p < 0.05$ are considered statistically significant (*). The arrow in (a) indicates the data points corresponding to the samples in Figure 1-5. p = probability value.

Because no differences were apparent between the various products when post-annealed at 25 °C and tested at 25 °C, then additional Charpy impact tests without notches

were conducted. The results are presented in Fig. 1-8. The average values for the two samples were 55.6 kJ/m^2 in the case of the neat iPP and 73.3 kJ/m^2 for the prepressed 0.03 wt% ACC-CNFs and both values exhibited statistically difference with $p < 0.05$. These data confirm that the incorporation of the ACC-CNFs at 0.03 wt% to produce a PCW-like framework provided superior performance, even at 25 °C (at which optical impact resistant is not normally observed). It should be emphasized that the impact resistance of the molded products prepared from the prepressed ACC-CNFs-coated iPP, which contained the embedded PCW-like structure, exhibited the best performance.

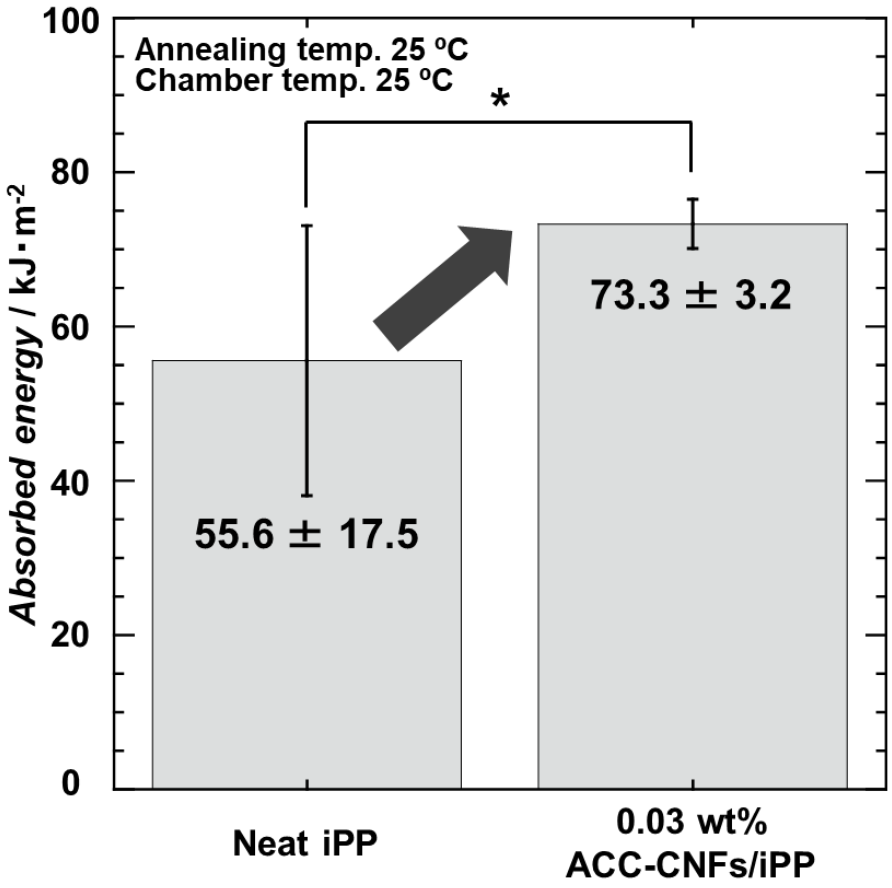

Fig. 1-8 Absorbed energy measured by Charpy impact test without notch. Values meant average ± standard derivation and were compared statistically using by the t-test, with $p < 0.05$ considered statistically significant (*)

In the following discussion, the author neglects the prepressed specimens because this process is less applicable to industrial processing. The data in Fig. 1-7 demonstrate that the impact resistance of the composite made from the ACC-CNFs-coated iPP microspheres with a post-annealing temperature of 105 °C was greater than that of the sample comprising neat iPP microspheres by the least 30 % over the same temperature range. Remarkably, the impact resistance of the ACC-CNFs-coated iPP product port-annealed 130 °C was improved by approximately 150 % (while the prepressed ACC-CNFs-coated iPP specimen was improved by approximately 200 %) compared with the neat iPP product. It should be noted that products made by injection molding with kneading from ACC-CNFs-coated iPP microspheres exhibited approximately 20% lower than that of neat iPP materials produced in the same manner (0.03 wt% ACC-CNFs/iPP: 4.09 kJ/m^2, Neat iPP: 5.22 kJ/m^2, Annealing temp. = 25 °C, Chamber temp. = 25 °C, with notch). It implies that PCW-mimicked framework contributes improvements in impact resistance of the nanocomposites.

1.3.7. Monitoring heat transfer through the PCW structure

Fig. 1-9 shows thermographic images of injection-molded products attached a temperature-controlled copper board, which indicated arrows in these images. The double headed arrows demonstrate relatively hot regions heated from copper. These images exhibited that enhancement of energy transfer occurs in the nanocomposite containing PCW-framework. Accordingly, a critical factor responsible for the improved impact resistance obtained from the ACC-CNFs was likely the formation of a PCW-like framework that promoted energy transfer.

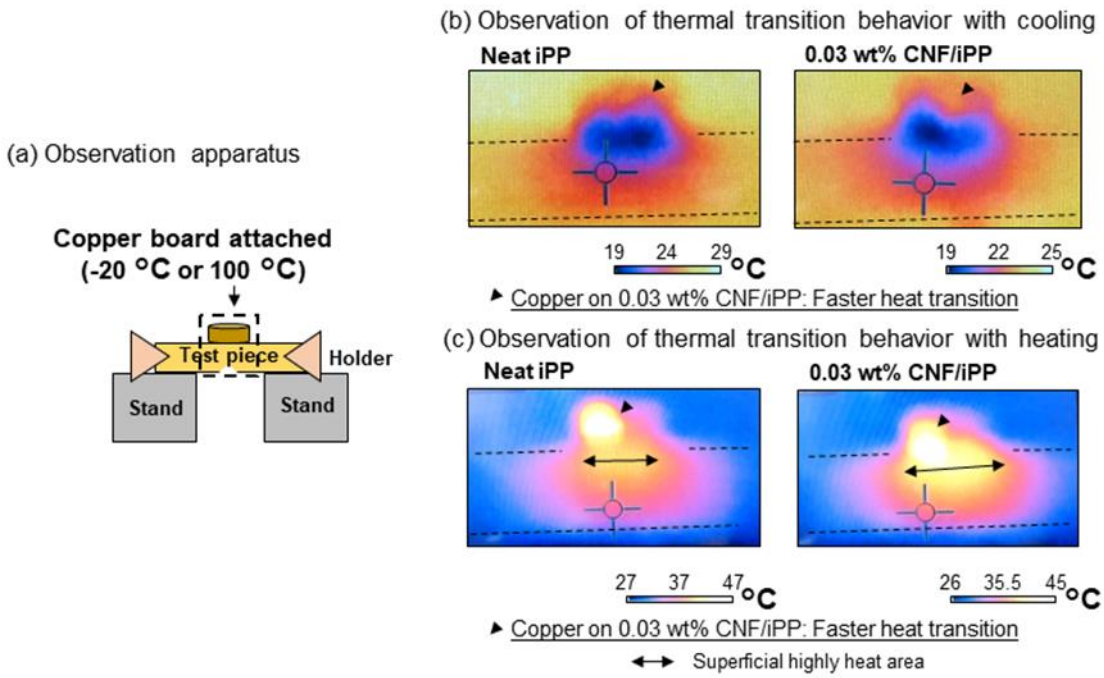

Fig. 1-9 Monitoring of heat transfer by attaching of a temperature-controlled copper board to an individual test piece comprising an extrusion-molded nanocomposite product. (a) The apparatus for monitoring thermal transfer. (b) Thermal transfer data obtained upon cooling by -20 °C copper. The arrows indicate the increased temperatures comparing neat iPP and 0.03 wt% ACC-CNFs/iPP samples. (c) Thermal transfer data obtained with heating by 100 °C copper. The arrows indicate the decreased temperatures comparing neat iPP and 0.03 wt% ACC-CNFs/iPP samples. The double headed arrows demonstrate that regions of relatively high temperature were associated with the copper. These data confirm that the 3D honeycomb-like structure of the ACC-CNFs in the extrusion-molded iPP nanocomposite contributed to the transfer of impact energy based on thermal transitions.

1.3.9. Surface properties of the injection-molded nanocomposite

As shown in Fig. 1-1, the surfaces of ACC-CNFs-coated iPP microspheres were rendered hydrophilic owing to the presence of the ACC-CNFs. Interestingly, the surface of the molded products prepared from these materials were not hydrophilic (see the contact angle values in Table 1-2). This finding suggests that the product surface comprised only iPP, that is, the amphiphilic ACC-CNFs did not appear on the surface of

the final products. However, the water contact angles on the nanocomposite in an atmosphere saturated with water vapor become significantly greater than those on neat iPP over time (Table 1-2).

Table 1-2 Melt flow rates of the neat, ACC-CNFs-coated and prepressed ACC-CNFs-coated iPP microspheres.

Starting material	Contact angle θ (Apparent contact angle θ') / °			Surface roughness (Root mean square values / nm)	Roughness factor
	0 hours	1 hours	6 hours		
Neat iPP	102.9 (110.6)	84.6 (90.9)	69.9 (75.1)	174.6 ± 69.8	1.08 ± 0.02
iPP microspheres coated with ACC-CNFs	99.2 (120.0)	89.9 (108.7)	72.3 (87.4)	229.4 ± 79.8	1.21 ± 0.11

cos θ' = r cos θ (θ: true contact angle, θ': apparent contact angle, r: roughness factor)

Fig. 1-10 (a) and (b) present cross-sectional images acquired along the mechanical direction (that is, along the TD-MD) of the extrusion-molded nanocomposite. From the fluorescence image acquired from the ACC-CNFs (Fig. 1-10 (a)) together with the intensity depth profile (Fig. 1-10 (b)) it is evident that CNFs were absent from the material surfaces. This result confirm that the surfaces would have been hydrophobic and can possibly be ascribed to the higher melt flow rate of the nanocomposite. The surface roughness value of the nanocomposite provided in Table 1-2, which was calculated based on AFM images, also exceeded that of the neat iPP. This increase in roughness may have been related to the higher contact angle of the former material. The roughened surface seen after incorporation of the ACC-CNFs could have resulted from the epitaxial growth of iPP on the ACC-CNFs.

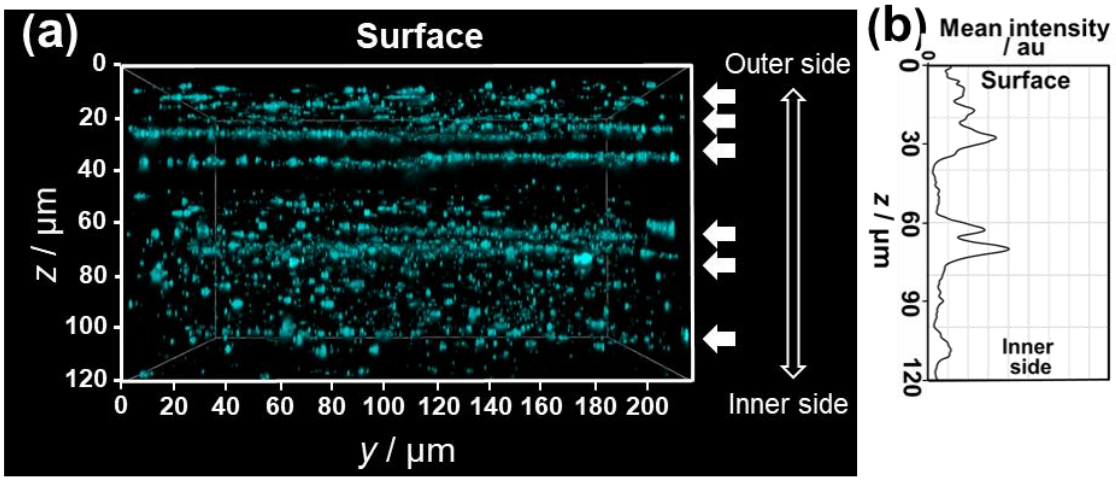

Fig. 1-10 Surface characterization of the 0.03 wt% ACC-CNFs/iPP composite. (a) A cross-sectional CLSM image of the composite along the MD. In this image, blue regions indicate the presence of cellulose. (b) The distribution of cellulose based on fluorescence intensity.

1.3.10. Crystalline structure analysis

The mechanical properties of iPP, which is a semi-crystalline polymer, are affected by their crystalline structure and crystallinity. Fig. 1-11 shows WAXD profiles of injection-molded specimens from each region (skin, intermediate and core). WAXD profiles assigned prepressed iPP microspheres coated with ACC-CNFs (b) exhibited the higher crystallinity compared to that of neat iPP (a). Moreover, nanocomposite specimen contained crystalline mixture structure (α-, and β-form) while specimen from neat iPP have α-form structure dominantly. To date, it has been reported that β-form crystal, meta-stable structure, have superior toughness [30]. However, specimen prepared from ACC-CNFs-coated iPP microspheres kneaded before molding did not improve its crystallinity and dominantly α-form structure (Fig.1-11 (c)). These results suggested that PCW-framework composed of ACC-CNFs affected crystallization of iPP β-form and dispersed ACC-CNFs did not promote crystallization of β-form. Therefore, from the points of iPP

crystalline structure, the β-crystal formation promoted by the PCW-mimicked framework also might contribute to improvement in impact resistance.

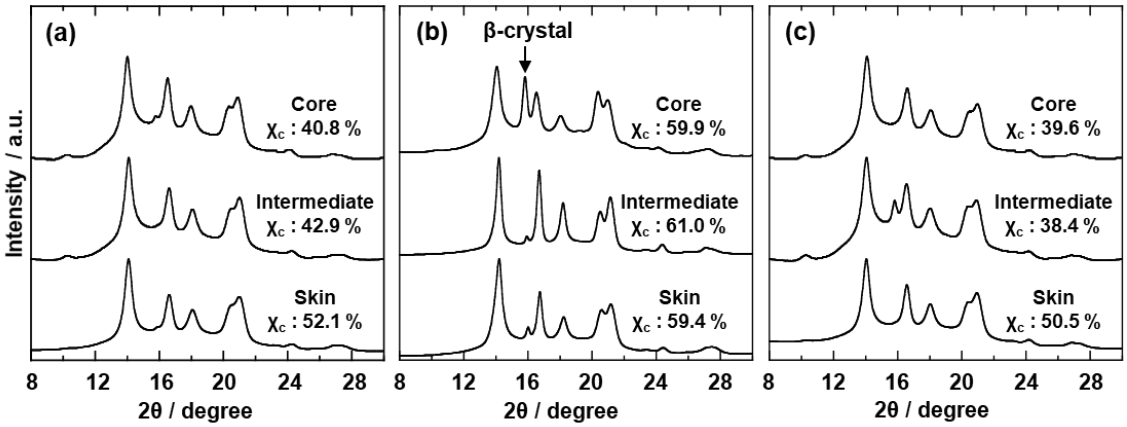

Fig. 1-11 WAXD patterns of injection-molded specimens (a) neat PP, (B) prepressed ACC-CNFs-coated iPP microspheres, and (c) prepressed ACC-CNFs-coated iPP microspheres kneaded before injection molding. All patterns were normalized at the maximum intensity.

1.3.11. Proposed mechanism for improved impact resistance

Injection-molded specimen prepared from iPP microspheres coated with ACC-CNFs exhibited higher impact resistance under Charpy test with notch above 40 °C temperature. Especially, prepressing treatment is allowed to enhance energy absorbing properties. Additionally, in Charpy impact test at 25 °C without notch, absorbed energy of the nanocomposite was approximately 30 % higher than that of neat iPP. Injection-molding with kneading decreased impact resistance approximate 30 %.

Fig. 1-12 depicts a proposed mechanism by which the impact resistance of the present molded products containing ACC-CNFs was increased. In general, it is challenging to identify a specific cause for this effect because the improvement may arise from synergetic effect. However, the highly crystalline ACC-CNFs arranged in a 3D

honeycomb-like framework in these composites would be expected to readily propagate impact energy in the form of elastic and plastic waves together with thermal dissipation.

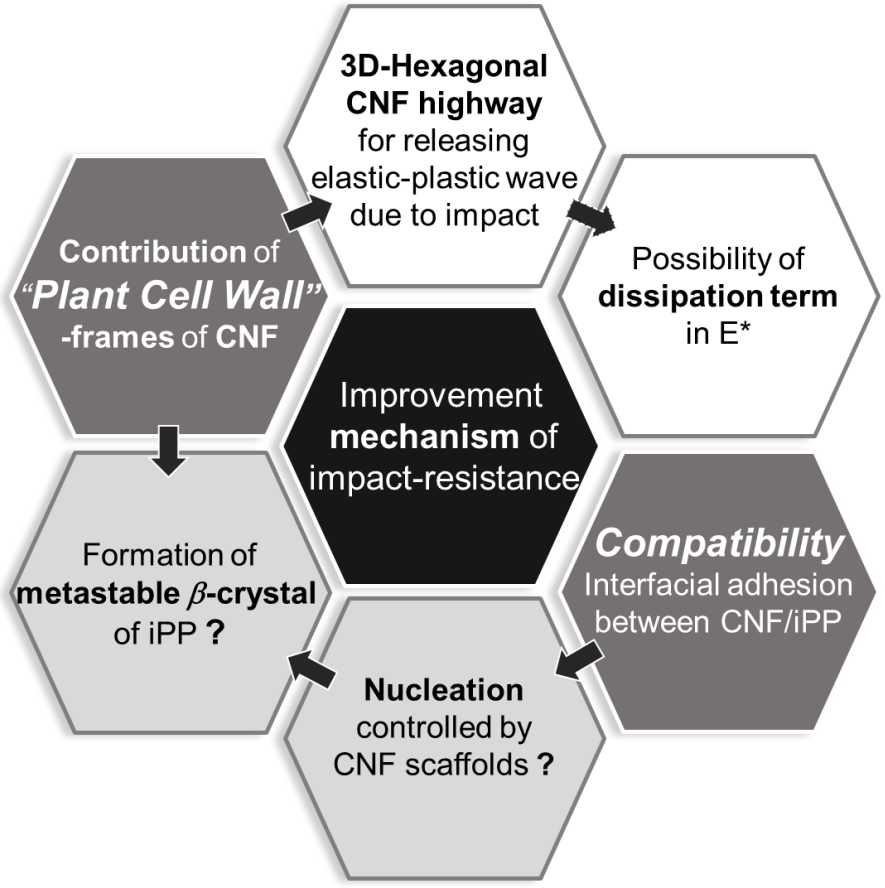

Fig. 1-12 Factors possibly contributing to the improved impact resistance of the molded products containing PCW-like structures based on ACC-CNFs.

1.4. Conclusion

This chapter achieved development of a chemical-free method using favorably adsorption properties of ACC-CNFs to produce nanocomposite plastics. The surface coating of ACC-CNFs changed surface properties of iPP microspheres from hydrophobic to hydrophilic. The adsorption of ACC-CNFs onto iPP microspheres surface contributed

increasing the melt flow rate of the iPP and so provided improved viscoelastic properties suitable for industrial processing.

Simple injection-molding process fabricated nanocomposite embedding “plant cell wall”-mimicked frameworks. The nanocomposite exhibits maximum 150 % increase in the impact strength nonetheless the amount of containing ACC-CNFs was very low (approximately 0.03 wt%/iPP). Embedded “PCW”-like framework acted as energy transfer pathway and promoted β-form crystallization during molding process. Although the improvement in impact resistance is affected by the synergic effect and it is difficult to clarify the detailed mechanism, formation of the “PCW”-like framework is an important factor of emergence of the impact resistance.

Fig. 1-13 summarizes the relationship between additive amounts of nanocellulose and improvement in impact resistance of the iPP-based nanocomposite. It is apparent that the present specimens had the lowest cellulose loading by approximately 2 orders of magnitude. In addition, there materials exhibited the greatest improvements in impact resistance and could permit tunable impact resistance values. Therefore, this chapter proposes a novel concept meant mimicry of natural structure with excellent function, and the concept can contribute to the development of composite material design.

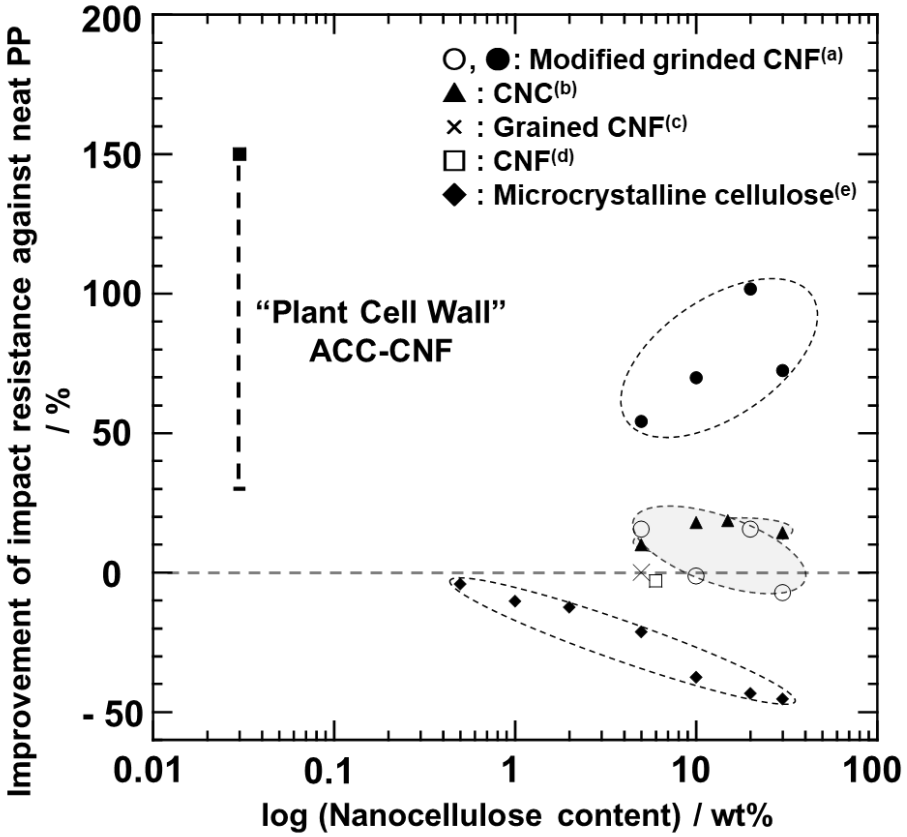

Fig. 1-13 Improvements in impact resistance as a function of the logarithm of cellulose content for various iPP/cellulose nanocomposite. (a-e) are from reference [31–35]

Reference

(1) Sauter, D. W.; Taoufik, M.; Boisson, C. Polyolefins, a Success Story. *Polymers (Basel)*, **2017**, *9* (6), 185. https://doi.org/10.3390/polym9060185.

(2) Busico, V.; Cipullo, R. Microstructure of Polypropylene. *Progress Polymer Science*, **2001**, *26*, 443–533.

(3) Libster, D.; Aserin, A.; Garti, N. Advanced Nucleating Agents for Polypropylene. *Polymers for Advanced Technologies*, **2007**, *18* (9), 685–695. https://doi.org/10.1002/pat.970.

(4) Liang, C. Y.; Pearson, F. G. Infrared Spectra of Crystalline and Stereoregular Polymers. Part I. Polypropylene. *Journal of Molecular Spectroscopy*, **1961**, *5* (1–6), 290–306. https://doi.org/10.1016/0022-2852(61)90094-7.

(5) Paszkiewicz, S.; Pypeć, K.; Irska, I.; Piesowicz, E. Functional Polymer Hybrid Nanocomposites Based on Polyolefins: A Review. *Processes*, **2020**, *8* (11), 1475. https://doi.org/10.3390/pr8111475.

(6) Schadler, L. S.; Kumar, S. K.; Benicewicz, B. C.; Lewis, S. L.; Harton, S. E. Designed Interfaces in Polymer Nanocomposites: A Fundamental Viewpoint. *MRS Bull*, **2007**, *32* (4), 335–340. https://doi.org/10.1557/mrs2007.232.

(7) Kim, D. W.; Han, S.; Lee, H.; Shin, J.; Choi, S. Q. Swelling-Based Preparation of Polypropylene Nanocomposite with Non-Functionalized Cellulose Nanofibrils. *Carbohydrate Polymers*, **2022**, *277*. https://doi.org/10.1016/j.carbpol.2021.118847.

(8) Inês Bruno Tavares, M.; Freitas Nogueira, R.; Aguiar da Silva San Gil, R.; Preto, M.; Oliveira da Silva, E.; Bruno Rocha e Silva, M.; Miguez, E. Polypropylene-Clay Nanocomposite Structure Probed by H NMR Relaxometry. *Polymer Testing*, **2007**, *26* (8), 1100–1102. https://doi.org/10.1016/j.polymertesting.2007.07.012.

(9) Wang, L.; Hikima, Y.; Ohshima, M.; Sekiguchi, T.; Yano, H. Evolution of Cellular Morphologies and Crystalline Structures in High-Expansion Isotactic Polypropylene/Cellulose Nanofiber Nanocomposite Foams. *RSC Advances*, **2018**, *8* (28), 15405–15416. https://doi.org/10.1039/c8ra01833b.

(10) Bikiaris, D. Microstructure and Properties of Polypropylene/Carbon Nanotube Nanocomposites. *Materials*, **2010**, *3* (4), 2884–2946. https://doi.org/10.3390/ma3042884.

(11) Ljungberg, N.; Cavaillé, J. Y.; Heux, L. Nanocomposites of Isotactic Polypropylene Reinforced with Rod-like Cellulose Whiskers. *Polymer (Guildf)*, **2006**, *47* (18), 6285–6292. https://doi.org/10.1016/j.polymer.2006.07.013.

(12) Peng, Y.; Gallegos, S. A.; Gardner, D. J.; Han, Y.; Cai, Z. Maleic Anhydride Polypropylene Modified Cellulose Nanofibril Polypropylene Nanocomposites with Enhanced Impact Strength. *Polymer Composite*, **2016**, *37* (3), 782–793. https://doi.org/10.1002/pc.23235.

(13) Nakagaito, A. N.; Yano, H. Toughness Enhancement of Cellulose Nanocomposites by Alkali Treatment of the Reinforcing Cellulose Nanofibers. *Cellulose*, **2008**, *15* (2), 323–331. https://doi.org/10.1007/s10570-007-9168-2.

(14) Moon, R. J.; Martini, A.; Nairn, J.; Simonsen, J.; Youngblood, J. Cellulose Nanomaterials Review: Structure, Properties and Nanocomposites. *Chemical Society Reviews*, **2011**, *40* (7), 3941–3994. https://doi.org/10.1039/c0cs00108b.

(15) Kargarzadeh, H.; Mariano, M.; Huang, J.; Lin, N.; Ahmad, I.; Dufresne, A.; Thomas, S. Recent Developments on Nanocellulose Reinforced Polymer Nanocomposites: A Review. *Polymer (Guildf)*, **2017**, *132*, 368–393. https://doi.org/10.1016/j.polymer.2017.09.043.

(16) Kondo, T. Cellulose Nanofibrils Pulverized from Biomass Resources: Past, Present, and Future Perspectives. *KONA Powder and Particle Journal*, **2023**, *40*, 109–123. https://doi.org/10.14356/kona.2023003.

(17) Kondo, T.; Morita, M.; Hayakawa, K.; Onda, Y. Polysaccharide Wet Pulverization Method., US Patent, US 7 357 339 B2, 2008.

(18) Kose, R.; Mitani, I.; Kasai, W.; Kondo, T. “Nanocellulose” as a Single Nanofiber Prepared from Pellicle Secreted by Gluconacetobacter Xylinus Using Aqueous Counter Collision. *Biomacromolecules*, **2011**, *12* (3), 716–720. https://doi.org/10.1021/bm1013469.

(19) Kondo, T.; Kose, R.; Naito, H.; Kasai, W. Aqueous Counter Collision Using Paired Water Jets as a Novel Means of Preparing Bio-Nanofibers. *Carbohydrate Polymers*, **2014**, *112*, 284–290. https://doi.org/10.1016/j.carbpol.2014.05.064.

(20) Ishikawa, G.; Tsuji, T.; Tagawa, S.; Kondo, T. Adsorption of Janus-Type Amphiphilic Cellulose Nanofibrils onto Microspheres of Semicrystalline Polymers. *Macromolecules*, **2021**, *54* (20), 9393–9400. https://doi.org/10.1021/acs.macromol.1c01163.

(21) Utsunomiya, H.; Tsujita, Y.; Kondo, T. Cellulose Nanoanemone: An Asymmetric Form of Nanocellulose. *Cellulose*, **2022**, *29* (5), 2899–2916. https://doi.org/10.1007/s10570-021-04231-9.

(22) Tsuji, T.; Tsuboi, K.; Yokota, S.; Tagawa, S.; Kondo, T. Characterization of an Amphiphilic Janus-Type Surface in the Cellulose Nanofibril Prepared by Aqueous Counter Collision. *Biomacromolecules*, **2021**, *22* (2), 620–628. https://doi.org/10.1021/acs.biomac.0c01464.

(23) Tagawa, S.; Ishida, K.; Tsuji, T.; Kondo, T. Facile Size Evaluation of Cellulose Nanofibrils Adsorbed on Polypropylene Substrates Using Fluorescence Microscopy. *Cellulose*, **2021**, *28* (5), 2917–2929. https://doi.org/10.1007/s10570-021-03759-0.

(24) Farrow, G. The Measurement of Crystallinity in Polypropylene Fibres by X-Ray Diffraction. *Polymer (Guildf)*, **1961**, *2* (4), 409–417. https://doi.org/10.1016/0032-3861(61)90046-5.

(25) Kose, R.; Kasai, W.; Kondo, T. Switching Surface Properties of Substrates by Coating with a Cellulose Nanofiber Having a High Adsorbability. *Sen'i Gakkaishi* **2011**, *67* (7), 163–168. https://doi.org/10.2115/fiber.67.163.

(26) Kato, K.; Hideomi, F.; Eiichiro, I. メニスカス液面状の浮遊粒子の運動 Behavior of a Small Particle on a Liquid Meniscus Surface. *Transactions of the Japan Society of Mechanical Engineers. B*, **1991**, *57* (536), 1203–1209.

(27) Ishida, K.; Kondo, T. Evaluation of Surface Free Energy Inducing Interfacial Adhesion of Amphiphilic Cellulose Nanofibrils. *Biomacromolecules*, **2023**, *24*, 3786–3793. https://doi.org/10.1021/acs.biomac.3c00443.

(28) Kitao, K.; Tsuruta, H. ポリエチレンの衝撃特性に及ぼすアニーリングの影響. *Koubunshi Rombunshu*, **1995**, *52* (3), 181–186.

(29) Kitao, koichi; Tsuruta, hidekazu. ポリプロピレンの衝撃特性に及ぼすアニーリングの影響. *Koubunshi Ronbunshu*, **1995**, *52* (8), 497–503.

(30) Chen, H. B.; Karger-Kocsis, J.; Wu, J. S.; Varga, J. Fracture Toughness of α- and β-Phase Polypropylene Homopolymers and Random- and Block-Copolymers. *Polymer (Guildf)*, **2002**, *43* (24), 6505–6514. https://doi.org/10.1016/S0032-3861(02)00590-6.

(31) Liang, D.; Liu, W.; Zhong, T.; Liu, H.; Dhandapani, R.; Li, H.; Wang, J.; Wolcott, M. Nanocellulose Reinforced Lightweight Composites Produced from Cotton Waste via Integrated Nanofibrillation and Compounding. *Scientific Reports*, **2023**, *13* (1). https://doi.org/10.1038/s41598-023-29335-z.

(32) Wang, X.; Wang, P.; Liu, S.; Crouse, J.; Gardner, D. J.; Via, B.; Gallagher, T.; Elder, T.; Peng, Y. Material Properties of Spray-dried Cellulose Nanocrystal Reinforced Homopolymer Polypropylene Composites. *Polymer Composite*, **2023**. https://doi.org/10.1002/pc.27806.

(33) Iwamoto, S.; Yamamoto, S.; Lee, S. H.; Endo, T. Solid-State Shear Pulverization as Effective Treatment for Dispersing Lignocellulose Nanofibers in Polypropylene Composites. *Cellulose*, **2014**, *21* (3), 1573–1580. https://doi.org/10.1007/s10570-014-0195-5.

(34) Peng, Y.; Gallegos, S. A.; Gardner, D. J.; Han, Y.; Cai, Z. Maleic Anhydride Polypropylene Modified Cellulose Nanofibril Polypropylene Nanocomposites with Enhanced Impact Strength. *Polymer Composite*, **2016**, *37* (3), 782–793. https://doi.org/10.1002/pc.23235.

(35) Mubarak, Y. A. Tensile and Impact Properties of Microcrystalline Cellulose Nanoclay Polypropylene Composites. *International Journal of Polymer Science*, **2018**, *2018*, Article ID 1708695. https://doi.org/10.1155/2018/1708695.

Chapter 2

Transcrystalline polypropylene-based honeycomb structures spontaneously induced on “plant cell wall”-like frameworks of amphiphilic cellulose nanofibrils by aqueous counter collision

Abstract

This chapter deals with formation mechanism of the PCW-like frameworks. In chapter 1, an impact-tolerant nanocomposite embedding PCW-like framework of ACC-CNF was fabricated from the iPP microsphere coated with ACC-CNFs as a starting material. The PCW-like framework contributed to its impact resistance by acting an energy transfer pathway, formation of the PCW-like framework is an important factor of the improvement in its impact resistance. Furthermore, it was implied that the PCW-like framework affected crystallization of iPP as a scaffold during the injection-molding process. In this chapter, the ACC-CNFs-coated iPP microspheres were subjected to thermal treatment without shear stress for clarification of formation of the PCW-like framework. The PCW-like frameworks of ACC-CNFs were spontaneously formed in iPP martix. Moreover, it was revealed that the PCW-like framework acted as scaffolds of crystallization of iPP α-crystal to form complex PCW-like ACC-CNFs/iPP framework with a core of ACC-CNFs. α-crystal of iPP crystal was promoted to form and the relative ratio was dependent on the kinds of raw materials for ACC-CNFs.

2.1. Introduction

As described in general introduction, hydrophilic CNFs have a disadvantage to mix with hydrophobic plastics to yield a compatible CNF/plastic composite. For fabrication the compatible CNF-composite plastics, chemical pre-treatments providing to hydrophobic surface properties or addition of additives are often required. In contrast, chapter 1 proposed a chemical-free injection-molding process via simply mixing ACC-CNFs aqueous dispersion and iPP microspheres to fabricate CNF/iPP nanocomposite. The nanocomposite fabricated by the molding process embedded PCW-mimicked framework and exhibited improvement in impact resistance. Thermographic observation revealed that the PCW-like frameworks acted as an energy transfer pathway to contribute to improvement in impact resistance. Namely, formation of the PCW-like framework is an important factor of improvement in impact resistance of the nanocomposite.

Physical properties of iPP which is a semi-crystalline polymer with polymorphisms are dependent on the degree of crystallinity and distribution of their crystalline forms with three polymorphisms (α-, β-, and γ-form) [1,2]. In chapter 1, since it was also indicated that the PCW-like framework might affect iPP crystallization, another possibility of its improvement in impact resistance of the nanocomposite was nucleation-controlled crystal growth promoted by ACC-CNFs scaffolds. Moreover, as previous study it was elucidated that indicators of the affinity interfacial interaction between ACC-CNFs and iPP were dependent on a kind of raw materials of ACC-CNFs [3]. Then, the crystallization of iPP on the PCW-like framework could be affected by the raw materials of ACC-CNFs. Therefore, this chapter attempts to clarify both formation mechanism of the PCW-like framework and effect of the PCW-like framework, which was composed of

ACC-CNFs with different sources, on iPP crystallization under thermal treatments without shear stress.

2.2. Experimental Section

2.2.1. Preparations of ACC-CNFs aqueous dispersions

Bacterial nanocellulose (= BNC) pellicle was cultured, isolated and then purified according to previous reports [4,5]. Microcrystalline cellulose (= MCC; Funacel II®, Funakoshi Co., Ltd., Tokyo, Japan) was purified as described in a previous paper [6]. The 0.3 wt% ACC-CNFs dispersions were prepared by the ACC treatments of 200 MPa over 60 cycles (= passes) for BNC and MCC, respectively. 1.7 wt% ACC-CNFs dispersion derived from bamboo bleached kraft pulp (= BBKP) were provided from Chuetsu Pulp & Paper Cp., Ltd. (nanoforest-S®, Toyama, Japan). The aforementioned ACC-CNFs are termed as ACC-BNC, ACC-MCC, and ACC-BBKP, respectively.

2.2.2. Coating iPP microspheres with ACC-CNFs

Each ACC-CNFs dispersion was diluted with deionized water to 0.01 wt% and stirred overnight by a magnetic stirrer for uniform dispersing states of ACC-CNFs. As in chapter 1, isotactic homopolymer polypropylene (iPP) microspheres with 500 μm in diameter (Prime Polypro H-700®, Prime Polymer Co., Ltd., Tokyo) Japan were used as starting base-materials. Coating process of the iPP microspheres with ACC-CNFs was based on a previous study [3]. 120 grams of 0.01 wt% ACC-CNFs aqueous dispersions and 30 grams of iPP microspheres were shaken horizontally to be mixed in a 250 mL polyethylene terephthalate (PET) bottle for 30 min at 150 rpm on a shaker (MIR-S100®, Panasonic Healthcare Co., Ltd., Gumma, Japan). The iPP microspheres coated with ACC-

CNFs were isolated by filtration using a steel mech with 180 μm pores and then washed with deionized water to remove excess ACC-CNFs. The coated microspheres were dried in an oven at 50 ºC.

2.2.3. Crystallization temperature of iPP coated with ACC-CNFs

To estimate crystallization temperature of iPP, differential scanning calorimetry (DSC) measurements were performed on 5.00 ± 0.05 mg of samples under nitrogen atmosphere using X-DSC 7000 (Hitachi High-Tech Corp., Tokyo, Japan). The sample particles placed in an aluminum samples pan were heated to 200 ºC and the temperature was maintained for 10 min to be completely melted without any iPP crystalline residues. The samples were then cooled to 50 ºC at -10 ºC/min to monitor crystallization behavior of iPP and kept at the temperature for 10 min, before re-heated to 200 ºC at 10 ºC/min to measure the melting temperature. All data were analyzed with the software attached to the instrument.

iPP microspheres coated with ACC-BBKP, which had the largest affinity to iPP among ACC-CNFs [3], was subjected to further cooling scans with different rates to estimate the growth type of crystallization using DSC (Diamond DSC7, PerkinElmer Japan Co., Ltd., Kanagawa, Japan). 5.0 ± 0.1 mg of iPP microspheres coated with ACC-BBKP were sealed in aluminum pans. Samples were first heated to 200 ºC and at this temperature was kept for 10 min. Then, samples were cooled to 50 ºC at rates of -5, -10, -15 and -20 ºC/min, so that the heat flow due to crystallization of iPP were monitored.

2.2.4. Wide-angle X-ray diffraction (WAXD) measurements

45 mL of a 0.3 wt% ACC-CNFs dispersions were freeze-dried with a freeze-dryer (Freeze-Zone 2.5, Labconco Corp., Kansan, America). The freeze-dried ACC-CNFs were subjected to wide-angle X-ray diffraction (WAXD) using SmartLab (Rigaku Corp., Tokyo, Japan). Radiation with wavelength of 0.154 nm was produced at 40 kV and 30 mA. The samples were measured by a reflection mode at a scanning rate 20 º/min in the diffraction angle range of 5 – 40 º. After removing the amorphous halos due to the glass substrate from the entire diffraction image, crystallinity index (C.I.) of ACC-CNFs was calculated with Segal method [7].

$$C.I. = \frac{I_{(200)} - I_{18.5}}{I_{(200)}} \times 100$$

$I_{(200)}$ and $I_{18.5}$ are the X-ray diffraction intensities due to (200) plane in cellulose I and amorphous region at 18.5 º, respectively.

iPP samples containing ACC-CNFs after crystallization in DSC pans were subjected to WAXD measurements to determine the crystalline form of iPP and to calculate their crystallinity. The WAXD measurements was carried out under the same condition described above. Crystallinity of samples prepared from iPP and iPP coated with ACC-CNFs were calculated based on the area ratio of the total crystalline peaks in the whole diffraction pattern as follows [8]:

$$Crystallnity\ [\%] = \frac{(total\ crystalline\ areas\ of\ diffraction\ peaks)}{(whole\ area\ of\ diffraction\ patterns)} \times 100$$

2.2.5. Microscopic observation

Polarized optical microscopy: After cooling process in DSC measurements, neat iPP microspheres and iPP microspheres coated with ACC-CNFs were picked out from

DSC aluminum pans for polarized optical microscopic observation (POM; BH, Olympus Corp., Tokyo, Japan).

Confocal laser scanning microscopy (CLSM): Prior to observation, iPP microspheres coated with ACC-CNFs were stained with a CNF-specific fluorescent agent as follow [3,9]: 10 mg of the coated iPP microspheres and 1.0 mL of 0.001 wt% calcofluor white (CFW; Sigma-Aldrich Japan Co., LLC, Tokyo, Japan) aqueous solution were mixed in a microtube with shaking for 30 min at room temperature. Then, the treated iPP microspheres were isolated and rinsed with ultrapure water 3 times and dried. 5.00 ± 0.05 mg of the iPP samples with the stained ACC-CNFs was placed in an aluminum pan, and heated up in a DSC chamber to be completely melted followed by cooling under the same thermal scanning conditions of the aforementioned DSC measurements.

Samples of both neat iPP and iPP coated with the stained ACC-CNFs were provided for CLSM observations. Fluorescence-microscopic images for a dispersion state of the stained CNFs in the iPP matrix and the differential interference polarized (DIC-Pol) images for their crystalline morphology of iPP were acquired by CLSM (TCS SP8: Leica Microsystems, Wetzlar, Germany). In fluorescence microscopic observation, an excitation wavelength was 405 nm and emitting fluorescence was detected between 430 – 470, whereas DCI-Pol observation was performed with an attachment of a DIC-Pol filter. The CLSM images were then manipulated and analyzed with Leica Application Suite X (LAS X) software.

2.3. Results and Discussion

2.3.1. Crystalline structure and crystallinity index of ACC-CNFs

Prior to examination of crystallization of iPP affected by ACC-CNFs, the freeze-dried ACC-CNFs derived from different raw materials were characterized by wide-angle X-rat diffraction (WAXD). Diffraction patterns of three ACC-CNFs indicated all of the crystalline domains are composed of cellulose I having a typical reflection due to (200) plane. Table 2-1 also listed crystallinity index (C.I.) calculated by the Segal method based on the profiles. The results indicated that the C.I. values were in the order of ACC-BNC > ACC-MCC > ACC-BBKP with the same trend as reported previously [3,6].

Table 2-1 ACC-CNFs crystal form and crystallinity index (C.I.) calculated by Segal method.

Sample	Crystal form	C.I. (%)
ACC-BNC	Cellulose I	92.2 ± 0.1
ACC-BBKP	Cellulose I	77.1 ± 1.6
ACC-MCC	Cellulose I	84.4 ± 0.1

2.3.2. Crystallization temperature of iPP and ACC-CNFs/iPP

Fig. 2-1 shows the crystallization exothermic peaks of the three ACC-CNFs/iPP samples together with neat iPP in their cooling scan from 200 ºC to 50 ºC at -10 ºC/min. On-set crystallization temperature (= T_c) and off-set T_c were indicated as an intersection of baselines with tangent having positive and negative slopes, respectively. On-set T_c, peak T_c and off-set T_c of samples were listed in Table 2-2. On-set T_c of iPP coated with

ACC-CNFs significantly higher than that of neat iPP. For heterogeneous interface between crystalline polymers and crystalline fillers, crystallization from melt states of polymers on the interface were often promoted by the surface of fillers [1,10–16]. In previous studies, iPP crystals were likely to grow on a fiber surface with cellulose I crystals to form transcrystalline structure [10,11,13]. In the present case, ACC-CNFs are also supposed to work as a nucleating agent, since ACC-CNFs own a high crystallinity of cellulose I.

Next, the ACC-CNFs having different of C.I. (see Table 2-1) were investigated in terms of the relationship to the induced crystalline morphology of iPP. On-set T_c became higher in order of ACC-BNC/iPP > ACC-BBKP/iPP > ACC-MCC/iPP, corresponding the order in the degree of hydrophobicity among ACC-CNFs as reported previously [17]. The broadening of the exothermic crystallization peaks for iPP crystallization in the presence of ACC-CNFs may be due to formation of iPP crystals on the surface of the CNFs.

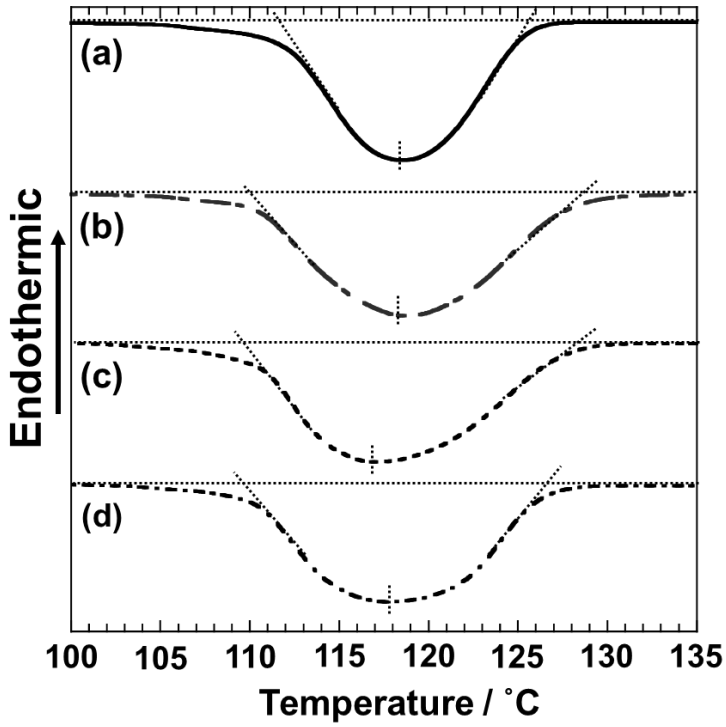

Fig. 2-1 Differential scanning calorimetric thermograms of three samples corresponding to Fig. 2-1 with neat iPP in their cooling scan at the rate of 10 ºC/min: (a) Neat iPP, (b) ACC-BNC/iPP, (c) ACC-BBKP/iPP and (d) ACC-MCC/iPP.

Table 2-2 On-set, peak and off-set T_c of neat iPP and iPPs coated with various ACC-CNFs based on their exothermic DSC curves corresponding to Fig. 2-1.

Sample	T_c (℃)		
	On-set	Peak	Off-set
Neat iPP	124.0 ± 1.0	118.2 ± 0.1	111.9 ± 0.1
ACC-BNC/iPP	128.1 ± 0.1	118.4 ± 0.6	110.2 ± 0.1
ACC-BBKP/iPP	127.1 ± 0.5	117.2 ± 0.5	110.4 ± 0.3
ACC-MCC/iPP	126.5 ± 0.1	117.9 ± 0.2	110.0 ± 0.2

2.3.3. iPP crystalline form and its crystallinity induced by ACC-CNFs

Neat iPP and ACC-CNFs/iPP after thermally treated in the DSC chamber were picked up from DSC aluminum pans. The treated samples transformed to disk shape which had 7 mm in diameter and 300 μm in thickness, and they were subjected to WAXD measurements. Fig 2-2 showed WAXD profile of each sample with the intensity as a function of scanning angle, 2θ. The obtained diffraction patterns exhibited four typical diffraction peaks due to iPP crystal lattices assigned to its α- and β-forms. No diffractions due to cellulose crystalline domains of ACC-CNFs appeared. It is not detectable presumably because ACC-CNFs were contained as the ultra-trace amounts to iPP (0.03 wt% of iPP weight). In iPP crystals, five peak patterns portraying the α-form given by the planes (110), (040), (130), (111) and (-131) were detected at the scattering angles of 14 º, 17 º, 18.5 º, 21 º, and 22 º, respectively [2,18]. In contrast, two peaks due to the β-form of iPP were assigned at the angles of 16 º and 21 º. Taking these into accounts, the diffraction pattern in Fig. 2-2 revealed under a stress-free condition that neat iPP formed crystalline β-form dominantly, whereas ACC-CNFs assisted to induce crystallization of the mixture of α-form and β-form. In conjunction with the DSC results, the broader crystallization exothermic peak in the ACC-CNFs/iPP as shown in Fig. 2-1 (b) is likely due to formation of the mixed crystals with the two forms.

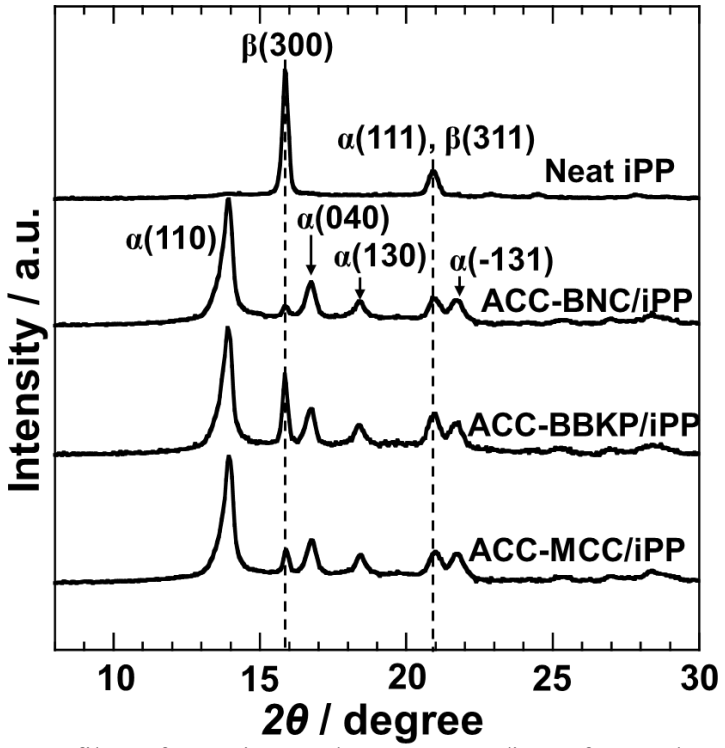

Fig. 2-2 WAXD profiles of neat iPP and ACC-CNFs/iPP after melt-crystallization in DSC pans.

Here, relative ratio of β-form in crystalline region is represented as K_β, which is calculated by the following formula [2]:

$$K_\beta = I_{(110)\beta}/(I_{(110)\alpha} + I_{(040)\alpha} + I_{(130)\alpha} + I_{(110)\beta})$$

I is a diffraction intensity and its subscripts indicate lattice planes. Then, relative ratio of α-form in crystalline region was indicated as 1-K_β. The values in Table 2-3 suggests that ACC-CNFs favorably induced crystallization of iPP α-form in the order of ACC-BNC/iPP, ACC-MCC/iPP and ACC-BBKP/iPP. Namely, α-form formation of iPP was dependent on the ACC-CNFs sources. In chapter 1, for the injection-molded products, ACC-BBKP/iPP products contained of a mixture of α-form and β-form, while neat iPP products was composed mostly of α-form. Then, it was assumed that the formation was possibly induced by shear stresses for the melt state [1]. However, this chapter indicated

that the similar crystallization of iPP occurred in the presence of ACC-CNFs without shear force. Namely, the crystallization of a mixture of α- and β-forms occurs spontaneously on the ACC-CNFs, particularly on ACC-BBKP.

Table 2-3. Crystallinity and relative ratio of α-form for each sample after melt crystallization in the DSC system.

Sample	Crystallinity (%)	relative ratio of α-form ($1\text{-}K_\beta$)
Neat iPP	43.5 ± 0.3	0.04
ACC-BNC/iPP	48.0 ± 0.8	0.90
ACC-BBKP/iPP	51.2 ± 1.1	0.72
ACC-MCC/iPP	47.3 ± 1.1	0.85

Crystallization inducing its epitaxial growth is usually affected by the scaffold having the structural similarity [1]. Therefore, iPP molecular chains are supposed to adhere to hydrophobic faces on the amphiphilic ACC-CNFs like ACC-BNC and ACC-MCC to result in formation of α-crystals. In contrast, ACC-BBKP exhibiting the similar hydrophobicity induced crystallization of a mixture of α- and β-crystals. This may be influenced by the residual hemicellulose contained more in BBKP to play a role as natural compatibilizer with regard to iPP [3]. Then, surfaces of ACC-BBKP containing hemicellulose may prevent formation of crystal nuclei as seen in other ACC-CNFs. In this way, the difference in the α-form ratio may depend on the contamination on the surface of the raw materials.

Fig. 2-3 shows melting endothermic peaks of the iPP coated with ACC-CNFs and neat iPP samples corresponding to those in Fig. 2-2 and Table 2-2 on 2nd heating scans to 200 ºC at 10 ºC/min. The neat iPP, which was consisted of β-form crystal as shown in Fig. 2-2, exhibited two typical melting endothermic peaks. In general, the β-form crystals were melted at a lower temperature than of α-form crystals [19,20] and the melting peaks sometimes appear as a few peaks without overlapping depending on the relative stability of the β-form crystals [12,13]. In fact, the lower endothermic peal (= 147.1 ºC) and its shoulder at 152.9 ºC appeared to indicate melting of β-form crystals. The highest endothermic peak at 166.4 ºC indicated melting of α-form. It is noted that ACC-BBKP/iPP having the largest K_β values among ACC-CNFs/iPP exhibited two detectable endothermic peaks due to melting β-form at 145.4 ºC and at 152.9 ºC and an endothermic peak due to melting α-form at 160.7 ºC. The single endothermic peak due to melting β-form of ACC-MCC/iPP was slightly detected at 145.8 ºC and an endothermic peak due to melting α-form at 161.3 ºC was detected. In contrast, an endothermic peak due to β-form in ACC-BNC/iPP was not significantly detected and an endothermic peak due to melting α-form was only detected at 161.1 ºC. Additionally, the endothermic peak temperature due to melting of α-form was the lowest in ACC-BBKP/iPP. The phenomenon was indicative the possibility that residual hemicellulose in ACC-BBKP acted as a compatibilizer, as shown in a previous study [3].

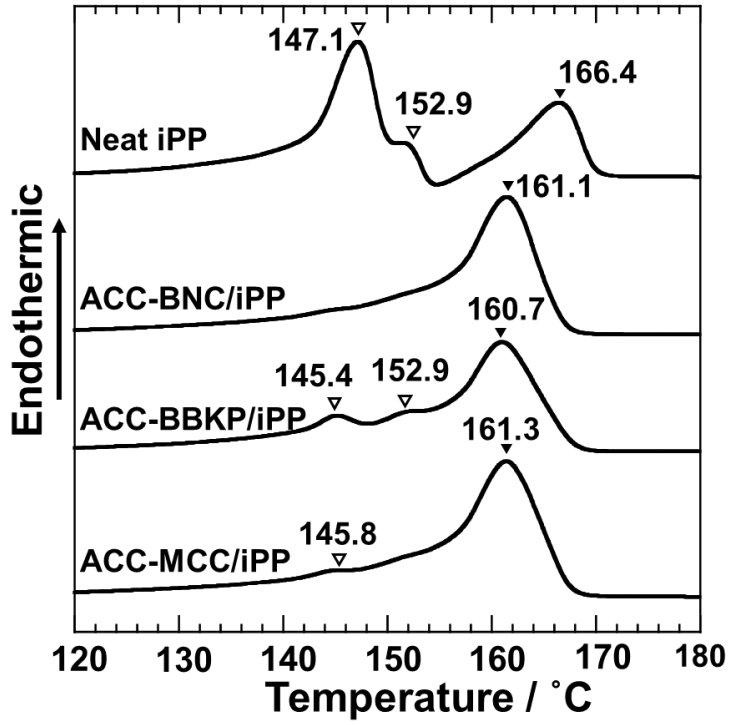

Fig. 2-3 Melting endothermic peaks of samples on 2nd heating at the rate of 10 ºC/min to 200 ºC. Hollowed and filled triangles indicate peak temperature due to melting β-form and α-form, respectively.

2.3.4. Crystalline morphology induced spontaneously from melted iPP/ACC-CNFs

iPP crystalline morphology in sheet samples prepared in DSC pans was observed by using polarized optical microscopy (POM). In POM, crystalline regions are closed up to be observed without amorphous regions as dark under transmitted polarized light. The crystalline morphologies of neat iPP (a) and iPP coated with ACC-CNFs (ACC-BNC/iPP (b), ACC-BBKP/iPP (c) and ACC-MCC/iPP (d)) are shown in Fig. 2-4. All samples of ACC-CNFs/iPP exhibited formation of honeycomb-like frames. As already described in chapter 1, regularly aligned iPP lamella appeared to attach perpendicular to the honeycomb-frames of amphiphilic ACC-CNFs based on the cross-section images of the thermally treated ACC-CNFs/iPP samples (see Fig. 1-6 (a)). The lamella growth

directions were likely to occur along the width direction of the honeycomb frameworks. The POM images also indicated that the areas surrounded by the crystalline honeycomb-frames exhibited amorphous regions. In contrast, POM images of neat iPP did not exhibit such crystalline honeycomb-like frame morphologies, indicating that the crystalline honeycomb-like frame morphologies can be induced spontaneously by the coating ACC-CNFs on iPP.

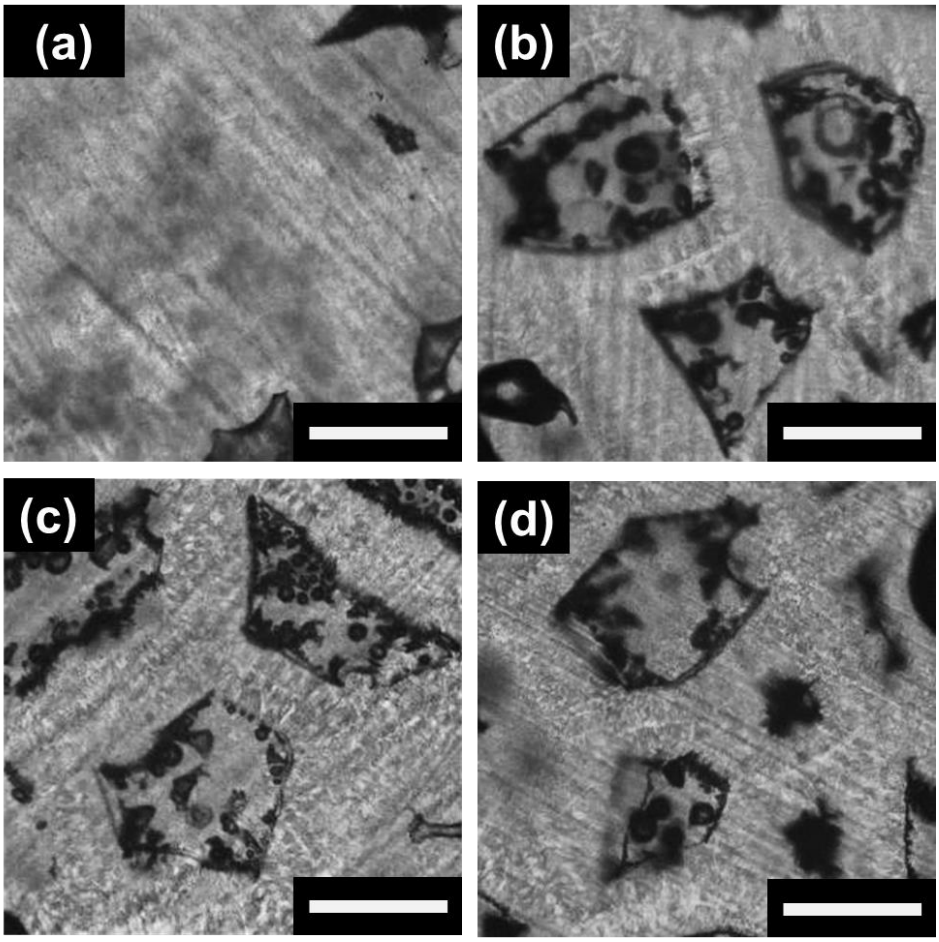

Fig. 2-4 POM images of the crystalline morphologies of iPP crystals after melt-crystallization in DSC pan: (a) neat iPP, (b) ACC-BNC/iPP, (c) ACC-BBKP/iPP, and (d) ACC-MCC/iPP. The bars indicate 200 μm.

In order to visualize dispersion of ACC-CNFs in iPP crystalline matrices, the samples sheets were prepared in DSC pans using iPP microspheres coated with ACC-CNFs with CFW staining for CLSM observation [3]. DIC-Pol images (1), fluorescence images (2) and their merge images (3) of each sample were displayed in Fig 2-5. Similarly to Fig. 2-4 (b-d), the DIC-Pol images of ACC-CNFs/iPP (b-1, c-1, and d-1) showed the honeycomb-like crystalline regions in the sample sheet, and their inner center areas were indicated to be lower crystalline. Conversely, the honeycomb-like frame crystalline morphologies were not observed for the neat iPP sample (a-1).

The DIC-Pol images together with fluorescence-merged images of the ACC-CNFs/iPP sheets confirmed that the ACC-CNFs were connected to form the honeycomb-like structure inducing iPP crystallization, which allows presence of amorphous areas of iPP at the center of the frames surrounded by the iPP crystals. Since the DSC measurements had already indicated that the individual ACC-CNFs played a role of the nucleating agents for iPP crystals, the honeycomb-like frameworks of ACC-CNFs were most likely to encourage the growth of the transcrystallization of iPP to establish a symmetric crystalline domain [21].

As previous reported [12,13,16,22], it was suggested that fiber-reinforced plastic composites tend to form columnar crystalline regions, namely formation of transcrystalline layers between the fiber and plastic interface. The columnar structure in the transcrystals is supposed to be symmetrical to the fiber axis. In the present study, ACC-CNFs as a nucleating agent allow to form the honeycomb-like frameworks, and simultaneously to induce the honeycomb-like transcrystalline structure. The mean width values of honeycomb-like transcrystalline structure, were 137.0 ± 16.3, 128.6 ± 14.3, and 132.6 ± 13.9 μm, for ACC-BNC/iPP, ACC-MCC/iPP, and ACC-BBKP/iPP, respectively.

These values depend on the ACC-CNFs from various sources, and the order of the width values corresponded to the same order of on-set T_c (see Table 2-2), indicating that the width values were dependent on crystal nucleation ability of ACC-CNFs.

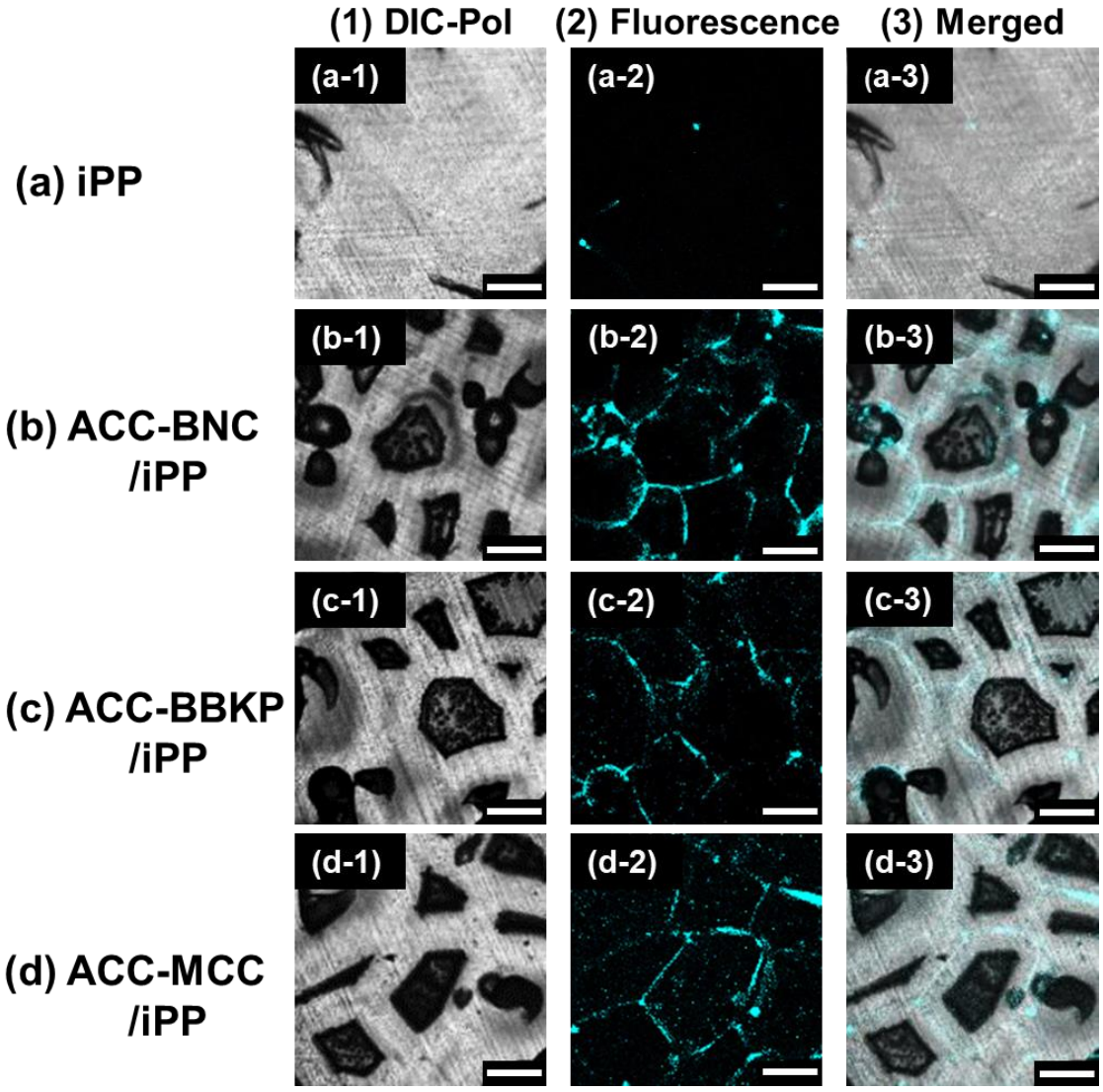

Fig. 2-5 CLSM images of each sample sheet: (a) Neat iPP, (b) ACC-BNC/iPP, (c) ACC-BBKP/iPP, and (d) ACC-MCC/iPP. (1) DIC-Pol image, (2) fluorescence image, and (3) their merge image. The bars indicate 250 μm.

2.3.5. The epitaxial growth in crystallization of iPP coated with ACC-CNFs

Through melting and cooling process, the iPP microspheres coated with ACC-CNFs spontaneously formed heterogeneous structure having a transcrystalline honeycomb-frame structure with its inner low crystalline regions. Due to heterogeneous structure, the dimension of crystallization could not be calculated by so-called Avrami plots under isothermal crystallization. For calculating the dimension of iPP crystallization in the presence of ACC-CNFs, iPP microspheres coated with ACC-BBKP were provided for non-isothermal crystallization in a cooling process at a constant rate. The growth type of crystallization can be estimated under some cooling rates by the following equation [23]:

$$X_c(T) = 1 - exp(\frac{K}{\varphi^n}) \quad (1)$$

where $X_c(T)$ is relative degree of crystallinity as a function of temperature, φ is the constant cooling rate (-5, -10, -15, and -20 ºC/min), n is a constant depending on the mechanism of crystal growth with nucleation, and K is the crystallization rate constant. Equation (1) can be transformed to equation (2):

$$log\{-ln(1 - X_c(T)\} = -n\, log\, \varphi + log\, K \quad (2)$$

When log {- ln (1-$X_c(T)$} was plotted as a function of log φ as shown in Fig. 2-6 (b), the n value obtained by the slope were in the range of 1.7 – 1.9, suggesting a two-dimensional crystallization growth under a heterogeneous nucleation mechanism. Generally, the formation mechanism of transcrystalline structure is controlled based on many crystal nuclei formed onto single fiber axis, and the growth form the nuclei were hindered in the lateral extension and forced the growth in one direction with single fiber as axis. Although ACC-CNFs honeycomb-like frames consisted of many CNFs connected each other, not single fiber, the crystal growth direction estimated by the resultant n values can be allowed to regard as a kind of transcrystalline structure.

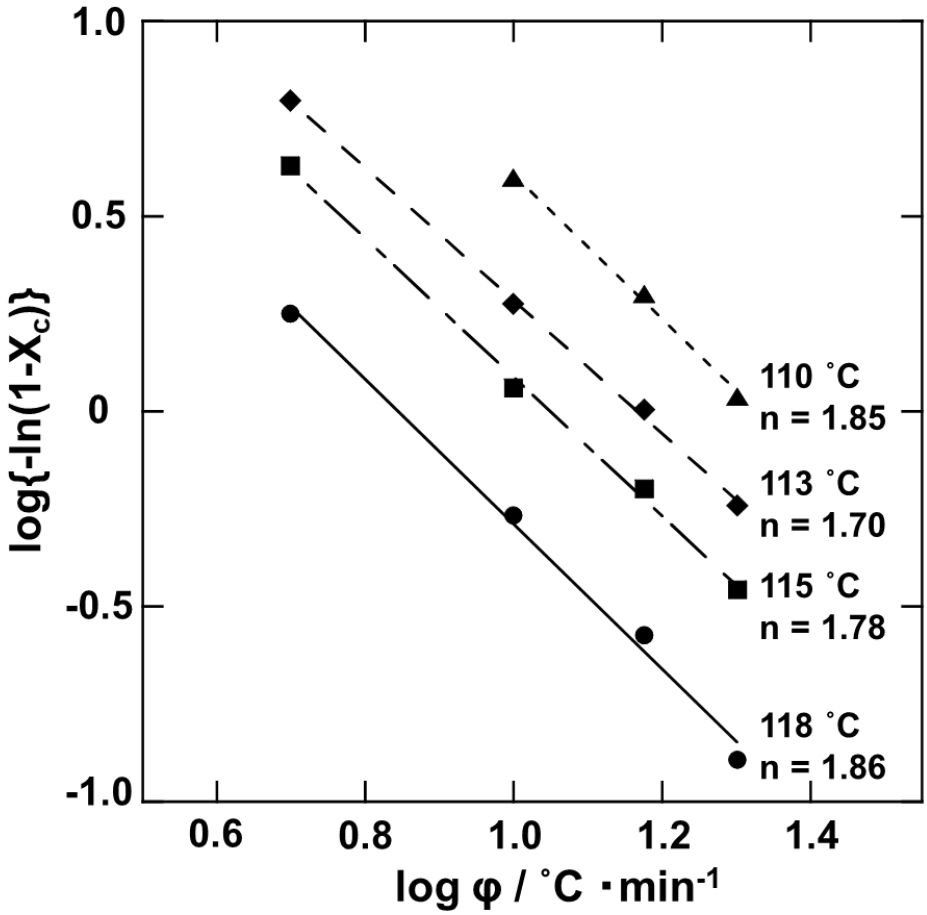

Fig. 2-6 Plots of log {- ln(1-X_c(T))} versus log φ obtained from the differential scanning calorimetric thermograms under constant cooling rates.

The formation mechanism of the transcrystalline honeycomb-iPP frames with ACC-CNFs in this study is summarized schematically in Fig. 2-7. From DSC analyses and CLSM optical observations, melted ACC-CNFs/iPP microspheres allow spontaneous formation of shish of CNFs and kebab of iPP crystals on the fiber surface to result in connected honeycomb super structures. Namely, ACC-CNFs were arranged to be honeycomb-like frameworks spontaneously involving a shish-kebab structure on melt-crystallization of ACC-CNFs/iPP.

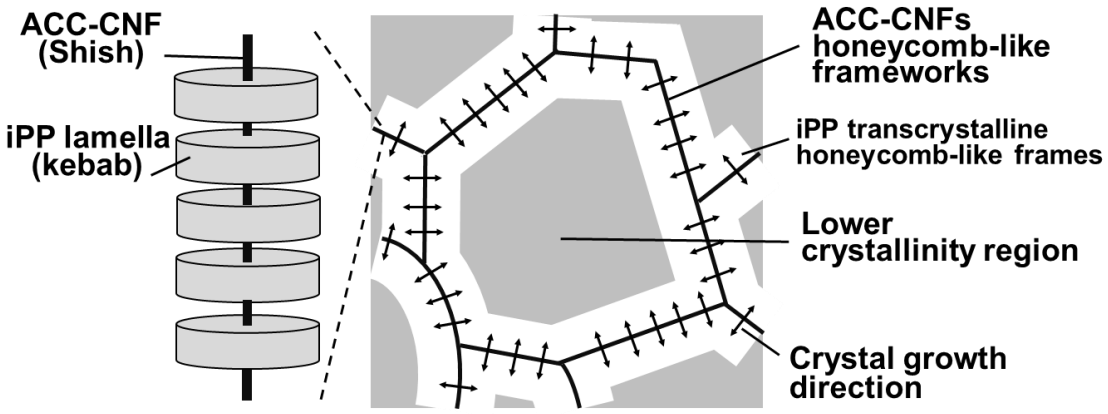

Fig. 2-7 Schematic image of transcrystalline honeycomb-frame formation of iPP on ACC-CNFs scaffolds to achieve accumulation of two-dimensional disk shape crystals.

2.4. Conclusion

In this chapter, it was revealed that the PCW-like framework was formed spontaneously in iPP matrices when the ACC-CNFs-coated iPP microspheres were subjected to thermal treatment. The PCW-like framework induced on transcrystalline structure of iPP α-form, resulting formation of complex PCW-like ACC-CNFs/iPP frameworks strucrure with a core of ACC-CNFs. Furthermore, optical observations suggested that surrounded region by the transcrystalline structure was amorphous. The width of transcrystalline structure was 130 – 140 μm, not depending on a type of ACC-CNFs. In contrast, both starting temperature of crystallization and relative ratio of α-form were dependent on a kind of raw materials of ACC-CNFs. Thermal analyses indicated the crystalline growth type from melted iPP on ACC-CNFs scaffolds was likely to an accumulation of two-dimensional disk shape crystals.

Reference

(1) Libster, D.; Aserin, A.; Garti, N. Advanced Nucleating Agents for Polypropylene. *Polymers for Advanced Technologies*, **2007**, *18* (9), 685–695. https://doi.org/10.1002/pat.970.

(2) Jones, A. T.; Aizlewood, J. M.; Beckett, D. R. Crystalline Forms of Isotactic Polypropylene. *Die Makromolekulare Chemie*, **1964**, *75*, 134–158.

(3) Ishikawa, G.; Tsuji, T.; Tagawa, S.; Kondo, T. Adsorption of Janus-Type Amphiphilic Cellulose Nanofibrils onto Microspheres of Semicrystalline Polymers. *Macromolecules*, **2021**, *54* (20), 9393–9400. https://doi.org/10.1021/acs.macromol.1c01163.

(4) Kose, R.; Mitani, I.; Kasai, W.; Kondo, T. "Nanocellulose" as a Single Nanofiber Prepared from Pellicle Secreted by Gluconacetobacter Xylinus Using Aqueous Counter Collision. *Biomacromolecules*, **2011**, *12* (3), 716–720. https://doi.org/10.1021/bm1013469.

(5) Utsunomiya, H.; Tsujita, Y.; Kondo, T. Cellulose Nanoanemone: An Asymmetric Form of Nanocellulose. *Cellulose*, **2022**, *29* (5), 2899–2916. https://doi.org/10.1007/s10570-021-04231-9.

(6) Kondo, T.; Kose, R.; Naito, H.; Kasai, W. Aqueous Counter Collision Using Paired Water Jets as a Novel Means of Preparing Bio-Nanofibers. *Carbohydrate Polymers*, **2014**, *112*, 284–290. https://doi.org/10.1016/j.carbpol.2014.05.064.

(7) Isogai, A.; Usuda, M. Crystallinity Indexes of Cellulosic Materials. *Sen'i Gakkaish*,*i* **1990**, *46* (8), 324–329. https://doi.org/10.2115/fiber.46.8_324.

(8) Farrow, G. The Measurement of Crystallinity in Polypropylene Fibres by X-Ray Diffraction. *Polymer (Guildf)*, **1961**, *2* (4), 409–417. https://doi.org/10.1016/0032-3861(61)90046-5.

(9) Tagawa, S.; Ishida, K.; Tsuji, T.; Kondo, T. Facile Size Evaluation of Cellulose Nanofibrils Adsorbed on Polypropylene Substrates Using Fluorescence Microscopy. *Cellulose*, **2021**, *28* (5), 2917–2929. https://doi.org/10.1007/s10570-021-03759-0.

(10) Gray, D. G. Polypropylene Transcrystallization at the Surface of Cellulose Fibres. *Journal of Polymer Science Part C: Polymer Letters*, **1974**, *12* (9), 509–515. https://doi.org/10.1002/pol.1974.130120903.

(11) Quillin, D. T.; Caulfield, D. F.; Koutsky, J. A. Crystallinity in the Polypropylene/ Cellulose System. I. Nucleation and Crystalline Morphology. *Journal of Applied Polymer Science*, **1993**, *50* (7), 1187–1194.

(12) Jenekel, E.; Teege, E.; Hinrich, W. Transkristallisation in Hochmolekularen Stoffen. *Colloid and Polymer Science*, **1952**, *129*, 19–24.

(13) Hata, T.; Ohsaka, K.; Yamada, T.; Nakamae, K.; Shibata, N.; Matsumoto, T. Transcrystalline Region of Polypropylene: Its Formation, Structure and Mechanical Properties. *The Journal of Adhesion*, **1994**, *45* (1–4), 125–135. https://doi.org/10.1080/00218469408026633.

(14) Varga, J.; Karger-Kocsis, J. Interfacial Morphologies in Carbon Fibre-Reinforced Polypropylene Microcomposites. *Polymer (Guildf)*, **1995**, *36* (25), 4877–4881. https://doi.org/10.1016/00323-8619(59)9305E-.

(15) Looijmans, S. F. S. P.; Spanjaards, M. M. A.; Puskar, L.; Cavallo, D.; Anderson, P. D.; van Breemen, L. C. A. Synergy of Fiber Surface Chemistry and Flow: Multi-Phase Transcrystallization in Fiber-Reinforced Thermoplastics. *Polymers (Basel)*, **2022**, *14* (22), 4850. https://doi.org/10.3390/polym14224850.

(16) Quan, H.; Li, Z. M.; Yang, M. B.; Huang, R. On Transcrystallinity in Semi-Crystalline Polymer Composites. *Composite Science and Technology*, **2005**, *65* (7–8), 999–1021. https://doi.org/10.1016/j.compscitech.2004.11.015.

(17) Tsuji, T.; Tsuboi, K.; Yokota, S.; Tagawa, S.; Kondo, T. Characterization of an Amphiphilic Janus-Type Surface in the Cellulose Nanofibril Prepared by Aqueous Counter Collision. *Biomacromolecules*, **2021**, *22* (2), 620–628. https://doi.org/10.1021/acs.biomac.0c01464.

(18) Somani, R. H.; Hsiao, B. S.; Nogales, A.; Fruitwala, H.; Srinivas, S.; Tsou, A. H. Structure Development during Shear Flow Induced Crystallization of I-PP: In Situ Wide-Angle X-Ray Diffraction Study. *Macromolecules*, **2001**, *34* (17), 5902–5909. https://doi.org/10.1021/ma0106191.

(19) Li, J. X.; Cheung, W. L.; Jia, D. A Study on the Heat of Fusion of β-Polypropylene. *Polymer (Guildf)*, **1999**, *40* (5), 1219–1222. https://doi.org/10.1016/S0032-3861(98)00345-0.

(20) Zhang, P.; Liu, X.; Li, Y. Influence of β-Nucleating Agent on the Mechanics and Crystallization Characteristics of Polypropylene. *Materials Science and Engineering*, *A* **2006**, *434* (1–2), 310–313. https://doi.org/10.1016/j.msea.2006.07.049.

(21) Gray, D. G. Transcrystallization of Polypropylene at Cellulose Nanocrystal Surfaces. *Cellulose*, **2008**, *15* (2), 297–301. https://doi.org/10.1007/s10570-007-9176-2.

(22) Fitchmun, D. R.; Newman, S. Surface Crystallization of Polypropylene. *Journal of Polymer Science: Part A-2: Polymer Physics*, **1970**, *8* (9), 1545–1564. https://doi.org/10.1002/pol.1970.160080909.

(23) Koga, N. Ozawa's Kinetic Method for Analyzing Thermoanalytical Curves: History and Theoretical Fundamentals. *Journal of Thermal Analysis and Calorimetry*, **2013**, *113* (3), 1527–1541. https://doi.org/10.1007/s10973-012-2882-5.

Chapter 3

Tensile property of nanocomposites embedding “plant cell wall”-mimicked frameworks of ultratrace amphiphilic cellulose nanofibrils derived from various raw materials

Abstract

This chapter deals with examination for relationship between impact-resistance and tensile properties of the iPP composite products with the ACC-CNFs honeycomb-skeleton with different sources. Namely, it has been focused on the trade-off relationship between increase in tensile properties and decrease in the impact-resistance or vice versa in the ACC-CNF/iPP composite products. From results of tensile test, PCW-like frameworks composed of ACC-BBKP have contributed to improvement both elastic modulus without decreasing elongation. This suggests that the nanocomposite has achieved to overcome the trade-off relationship of the elastic modulus and elongation. In contrast, addition of ACC-MCC has improved only the elastic modulus with decreasing in the elongation and addition of ACC-BNC has improved only the elongation without improvement in the elastic modulus. These results indicate that the source of raw materials for ACC-CNFs also influence the final composite products.

3.1. Introduction

As described above, ACC-CNFs favorable adsorb onto iPP microspheres simply by shaking ACC-CNFs aqueous dispersions and the interfacial affinity between ACC-CNFs and iPP was found due to a thermodynamic interaction, depending on the cellulose raw materials for preparation of ACC-CNFs [1]. In chapter 1, it was indicated that an impact-resistant composite embedding PCW-mimicked framework was fabricated from the iPP microspheres coated with ACC-CNFs derived from bamboo bleached kraft pulp (= ACC-CNFs/iPP). The embedded PCW-like framework acted as an energy transfer pathway to contribute to improvement in impact resistance of the nanocomposite. Chapter 2 indicated PCW-like framework acted as scaffolds of iPP crystallization of α-form, whose relative ratio was dependent on a kind of raw materials of ACC-CNFs.

The emergence of the mechanical properties for nanocomposite is affected by the compatibility between the interface and the total interfacial areas. The previous study reported that although ACC-BNC exhibited less specific surface areas approximately by 1/3 compared to the other two ACC-CNFs, both ACC-BBKP and ACC-BNC exhibited the similar surface properties [2]. In contrast, ACC-MCC showed the inferior value to them. In addition, tensile elastic modulus and impact resistance have a trade-off relationship each other. Impact-tolerant polymer composites may lose their tensile elastic modulus compared with the based polymer sole products. In this chapter, tensile properties of the above unique composite materials embedding PCW-type frameworks with a ultratrace quantity of CNFs are focused and their dependence of the cellulose raw materials for production ACC-CNFs on the composite properties is also examined.

3.2. Experimental Section

3.2.1. Materials

Commercial-grade homopolymer iPP microspheres with 500 μm in diameter were purchased from Prime Polymer Co., Ltd. (Tokyo, Japan) [1]. ACC-CNFs aqueous dispersion, derived from BBKP, was provided from Chuetsu Pulp & Paper Co., Ltd. (Toyama, Japan). BNC pellicle was incubated, isolated and then purified according to previous reports [3,4]. MCC power (Funacel II®) were purchased from Funakoshi Co., Ltd. (Tokyo, Japan). Phenol (≥ 99.0 %) and sulfuric acid (≥ 99.0 %), purchased from Fujifilm Wako Pure Chemical Corp. (Osaka, Japan), were used for phenol-sulfuric acid method to estimate the amounts of CNFs adsorbed onto the iPP microspheres [1].

3.2.2. Preparation ACC-BNC and ACC-MCC aqueous dispersions

Purified BNC pellicle described above was pre-fibrillated with a conventional food mixer for 1 min prior to ACC process [4]. MCC powders were washed and purified according to the previous reports [5,6]. BNC and MCC were provided for their ACC treatments at the ejection pressure of 200 MPa with the treatment repeating cycles (= Pass) of 60 Passes, respectively [3,5].

3.2.3. Preparation of iPP microspheres coated with CNFs

In chapters 1 and 2, PET bottle with 250 mL volume was used as a mixing vessel for tens of grams of iPP for coating process in CNFs aqueous dispersions. This chapter, instead, attempts to scale up the coating process by using a conventional washing machine. Typically, aqueous dispersion of CNFs and filtrated water were poured to a washing tub and mixed to prepare 7.5 L of aqueous dispersion with targeted concentrations. Then, 1.0

kg of iPP microspheres was added to the washing tub containing the ACC-CNFs aqueous dispersion. After mixing for 30 mins, the treated iPP microspheres were filtrated by steel mesh with a pore size of 150 μm in diameters and the residual particles were dried in an oven at 50 ºC. The filtrated aqueous dispersion with residual ACC-CNFs (non-adsorbed) was also collected to use for estimation of the adsorbed amounts of ACC-CNFs as described later.

3.2.4. Fluorescence microscopic (FM) observation

Prior to FM observation, adsorbed ACC-CNFs onto iPP microspheres were stained with calcofluor white M2R (CFW; Fluorescent Brightener 28®, MP Biomedicals LLC, Santa Ana, United States) in the 0.001 wt% of aqueous solution [1,2,7]. 1.0 g of the iPP microspheres coated with ACC-CNFs were mixed with 5.0 mL the CFW aqueous solution for 30 mins of staining. After mixing, the treated particles were filtrated by the same steel mech above described and dried at 50 ºC. Fluorescence observation was carried out by ECLIPSE Ts2-FL (Nikon Solutions Co., Ltd., Tokyo, Japan) under DAPI filter under excitation wavelength and emission wavelength of 361 – 389 nm and 430 – 490 nm, respectively.

3.2.5. Estimation of the amounts of adsorbed ACC-CNFs on the iPP microspheres

The total amounts of adsorbed ACC-CNFs were estimated from the change in mass concentration before and after adsorption. For estimation method phenol-sulfuric acid method was employed according to a previous study [1]. The 1.0 mL of a 5.0 wt% phenol aqueous solution and 1.0 mL of the residual CNFs aqueous dispersion after coating, were mixed in a shielded glass vial. Then, 5.0 mL of concentrated sulfuric acid (≥ 99.0

wt%) was added, and the mixture was shaken for 15 mins at room temperature. The absorbance of the mixture was measured at 490 nm using UV-vis (V-650 spectorometer, JASCO Corp., Tokyo, Japan). The concentration of non-adsorbed ACC-CNFs in the dispersion (= ρ_{after}) was determined from the absorbance based on a calibration curve for the known concentration of the ACC-CNFs dispersion. The calculation was based on the following equation.

$$The\ amouts\ of\ adsorbed\ ACC-CNFs\ per\ iPP\ [wt\%] = 100 \times W_{CNF\ sus.} \times (\rho_{before} - \rho_{after}) / W_{pp}$$

$W_{CNFs\ sus.}$ indicates weight of ACC-CNFs in the suspension and W_{PP} indicates iPP microspheres weight, and their values were 7500 g and 1000 g, respectively. ρ_{before} is the mass concentration of CNFs before adsorption.

3.2.6. Molding dumbbell shaped specimens for mechanical tests

The size of dumbbell shaped specimens prepared from iPP microspheres by injection molding was in accordance with JIS K 7139 A13 type. The injection molding was conducted with an instrument (HM7-C®, Nisseil Plastic Industrial Co., Ltd., Nagano, Japan.) with a single screw kneading. Dried iPP microspheres were put into the furnace of the molding machine to be melted and/or extruded at 190 ºC, and then injected to the molded with kept at 60 ºC to be cooled and fixed of the specimens.

Note that products made by simple injection molding with kneading with an ACC-CNFs level of 0.03 wt% exhibited an initial impact resistance approximately 20 % lower at ambient conditions than that of neat iPP materials produced in the same manner. In contrast, the current samples fabricated with a minor change following the proposed process via ACC-CNFs-coated iPP exhibited no change when compared with neat iPP

materials at ambient conditions, which has been reported in chapter 1. Therefore, the sample system in this chapter is possibly allowed to take the previous results on the impact-resistance into account in comparison of the data based on the following mechanical tests.

3.2.7. Tensile tests

The specimens obtained above were provided for uniaxial tensile test using a tensile testing machine (STA1150, A&D Co., Ltd., Tokyo, Japan) equipped with a 500 N load cell at a crosshead rate of 10 mm/min at 25 ºC under the humidity of 50 %. The upper limit of elongation was approximately 620 %. Five specimens of each sample were performed for the statistically significant data. Stress – strain curves (S-S curved) were plotted from the obtained data, and the elastic modulus and yield strength were calculated with an included software (TACT).

3.2.8. Wide-angle X-ray diffraction (WAXD)

Injection-molded specimens containing ACC-CNFs derived from different raw materials were subjected to wide-angle X-ray diffraction (WAXD) to determine their crystalline structure and crystallinity. Before WAXD measurements, the specimens were pulverized by rotter mill (Pulverisette 14™, Fritsch Japan Co., Ltd., Kanagawa, Japan) under liquid nitrogen. For obtaining ideal WAXD profiles, samples are required to be pulverized into sufficiently small particles. Note that there could be the concern on reducing the crystal size by cryogenic grinding. Pulverization at room temperature causes partial melting due to the frictional heat, which may cause manipulation of artificially too large particles and/or breaking the herein crystalline structure. Cutting with knife or

scissors is also insufficient to obtain small particles. Therefore, it is considered here that cryogenic pulverization is an optical method to prepare WAXD samples. The pulverized specimens were subjected to WAXD using SmartLab (Rigaku Corp., Tokyo, Japan). Radiation with wavelength of 0.154 nm was produced at 40 kV and 30 mA. The samples were measured by a reflection mode with a scanning rate of 20 º/min in the range of 5 – 40 º of the diffraction angle. After removing the amorphous halos due to the glass substrate from the entire diffraction of iPP-based specimens, the crystalline from contained in the specimens was determined based on the obtained diffraction patterns. Crystallinity of molded samples prepared from iPP and iPP coated with ACC-CNFs were calculated based on the area ratio of crystalline peaks to the whole diffraction peaks as follows [8]:

$$Crystallnity\ (\chi_c)\ [\%] = \frac{(total\ crystalline\ areas\ of\ diffraction\ peaks)}{(whole\ area\ of\ diffraction\ patterns)} \times 100$$

3.3. Results and Discussion

3.3.1. Dependence of ACC-BBKP adsorbed on iPP upon concentration of its aqueous dispersion for initial mixing

Non-adsorbed or excess CNFs in iPP matrix of ACC-CNFs/iPP composites are supposed to act as a structural defect to cause decrease in toughness of the composite. Therefore, the coating behaviors of ACC-CNFs on iPP microspheres was a critical issue, prior to examination of the structure-property relationship in their composite products. ACC-BBKP which is commercially-produced ACC-CNFs and had the largest specific surface areas and the largest affinity interaction to iPP surface, was employed for the investigation [1].

Fig. 3-1 shows fluorescent microscopic images of iPP microspheres prepared by mixing with ACC-BBKP aqueous dispersion with different concentrations (0.005, 0.01, and 0.04 wt%) after stained with the cellulose specific dye of CFW. Note that the subscript number in the sample name for ACC-BBKP$_{0.005}$, ACC-BBKP$_{0.01}$, and ACC-BBKP$_{0.04}$ indicates concentration of their aqueous dispersions. In dark-field fluorescence images, neat iPP microspheres did not emit fluorescence (Fig. 3-1 (a)). On the country, all ACC-BBKP/iPP coated under different concentration of the aqueous dispersions (Fig. 3-1 (b-d)) exhibited fluorescent emission due to the cellulose specific dye. This indicated that ACC-BBKP covered the surface of iPP microspheres. The fluorescence brightness of ACC-BBKP$_{0.04}$/iPP was higher than those of the other two samples, indicating its higher density of ACC-BBKP adsorbed. The higher concentration of ACC-BBKP were adsorbed, the higher fluorescent intensity appeared (see Fig. 3-1 and Table 3-1).

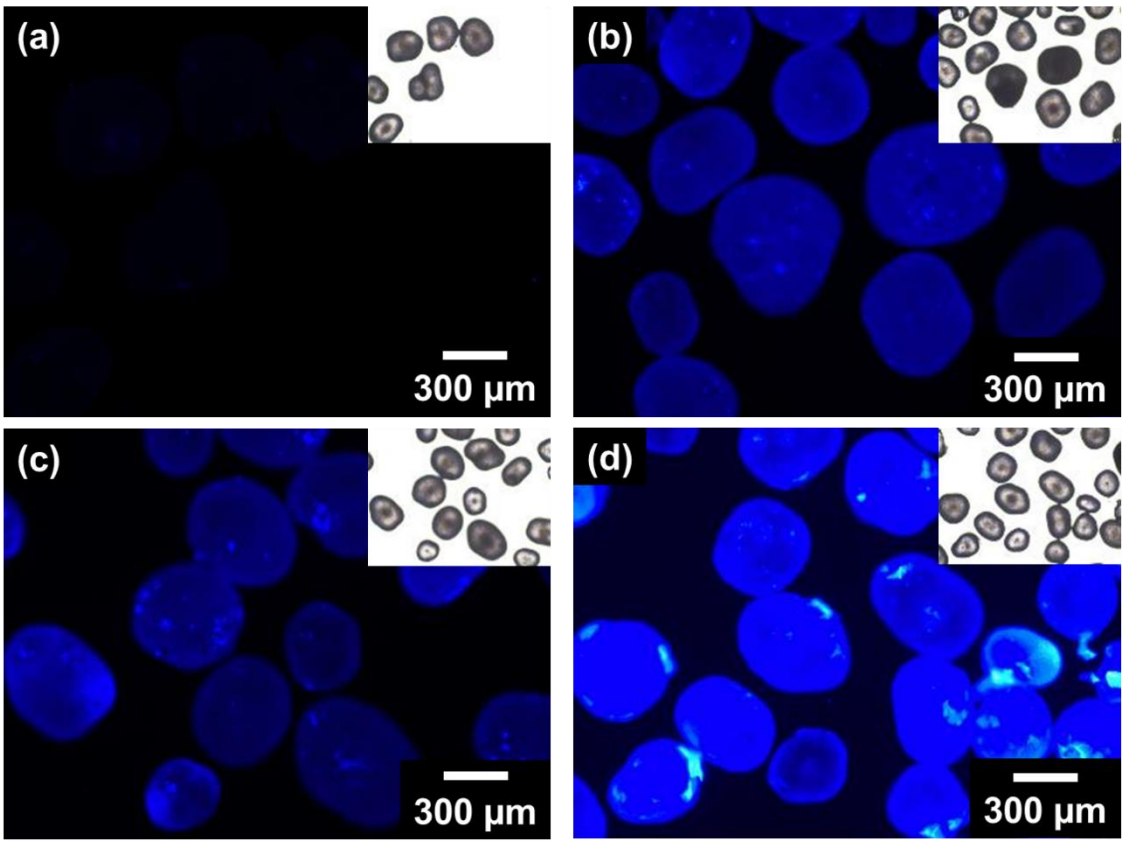

Fig. 3-1 Dark-field fluorescent images of iPP microspheres stained with CFW and the insets are bright-field images of the same microspheres: (a) Neat iPP, (b) ACC-BBKP$_{0.005}$/iPP, (c) ACC-BBKP$_{0.01}$/iPP, and (d) ACC-BBKP$_{0.04}$/iPP. The subscript number indicates concentration of the ACC-BBKP aqueous suspension for coating.

Table 3-1 The amounts of ACC-BBKP (per iPP weight) adsorbed onto iPP microspheres estimated by phenol-sulfuric acid method. ±: standard deviation.

Sample	The amounts of CNFs per PP / %
ACC-BBKP$_{0.005}$/iPP	0.020 ± 0.04
ACC-BBKP$_{0.01}$/iPP	0.045 ± 0.03
ACC-BBKP$_{0.04}$/iPP	0.103 ± 0.91

The concentration of the adsorbed ACC-BBKP in the individual coated samples was determined by phenol-sulfuric acid method as listed in Table 3-1. According to the previous reports [1,9], the adsorption amount ca 0.03 wt% of ACC-BBKP corresponds to a monolayer coating on iPP microspheres with 500 μm in diameter when the surface roughness was ignored. Taking it into accounts, Table 3-1 indicates that the monolayer coverage of ACC-BBKP on iPP surfaces is assumed to be conducted by shaking in the concentration range of 0.005 – 0.01 wt% of the aqueous dispersions.

3.2.2. Tensile properties

Fig. 3-2 displays appearance of the specimens prepared from each of ACC-BBKP/iPP as listed in Table 3-1. Specimens of neat iPP, ACC-BBKP$_{0.005}$/iPP and ACC-BBKP$_{0.01}$/iPP were all transparent, indicating that ACC-BBKP were well dispersed in the iPP matrix. In contrast, white spots were observed in a specimen from ACC-BBKP$_{0.04}$/iPP. As already shown in Fig 3-1 (d) and Table 3-1, the white spots would be aggregation of the excess nanofibrils, and presumably they were further adsorbed over the ACC-BBKP monolayer on iPP. In addition, a streak as a white line due to micro-air appeared in the center of the specimen. The aggregation of the excess ACC-BBKP possibly prevented from degassing iPP matrix or caused formation voids among fibers by uniaxial elongation in injection-molding process.

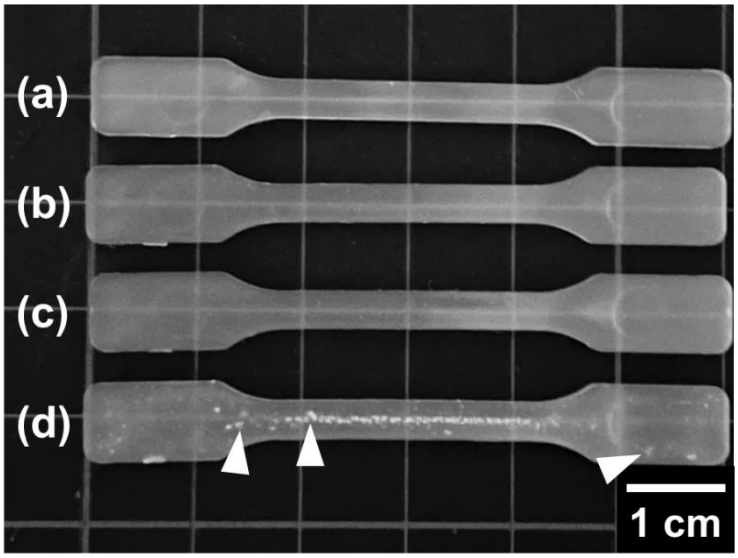

Fig. 3-2 Appearance of dumbbell-shaped specimens: (a) Neat iPP, (b) ACC-BBKP$_{0.005}$/iPP, (c) ACC-BBKP$_{0.01}$/iPP and (d) ACC-BBKP$_{0.04}$/iPP. White spots in (d) appeared as aggregations of ACC-CNFs, as indicated by a white triangle head.

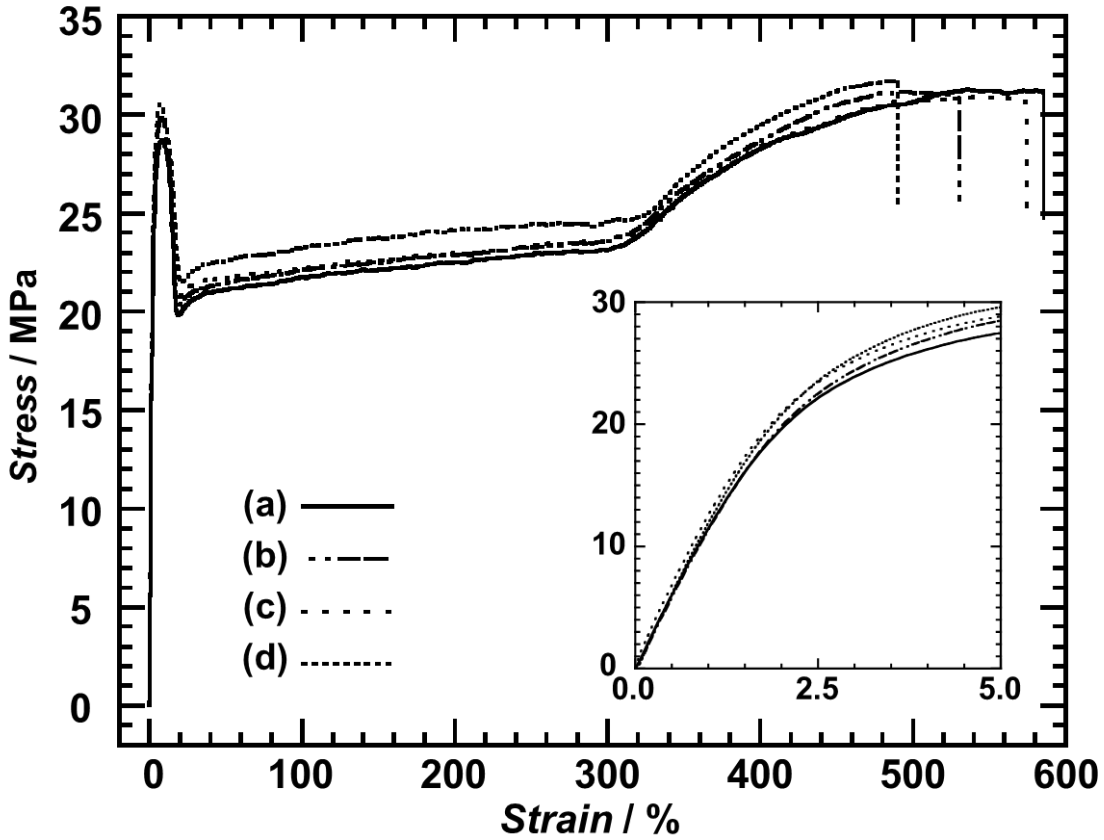

Fig. 3-3 Stress-Strain curve of each sample prepared from (a) Neat iPP, (b) ACC-BBKP$_{0.005}$/iPP, (c) ACC-BBKP$_{0.01}$/iPP, and (d) ACC-BBKP$_{0.04}$/iPP.

A shown in Fig. 3-3, stress-strain (S-S) curves of injection-molded specimens from ACC-BBKP/iPP indicated that all specimens were well elongated presumably attractive interfaces between ACC-BBKP and iPP matrix adsorbed. The average values of the elastic modulus, yield stress and stain at break were listed in Table 3-2. The elastic moduli of products from ACC-BBKP$_{0.01}$/iPP and ACC-BBKP$_{0.04}$/iPP were superior to that of neat iPP. In contrast, ACC-BBKP$_{0.005}$/iPP products, containing ACC-BBKP 0.020 wt% per iPP (see Table 3-1), did not exhibit improvement in the elastic modulus compared to neat iPP. As reported chapter 1, iPP coated with coverage of 0.030 wt% ACC-CNFs provides nanocomposite plastics embedding "PCW"-type frameworks by a usual injection-molding. The embedded PCW-frameworks were found to work for improvement of impact-resistance of the product, because of being an energy-transferring path. In this chapter, although the minimum coverage of 0.020 wt% ACC-BBKP$_{0.005}$ for iPP may not be enough to form the frameworks, the yield stress of all the composite products exhibited higher values than that of neat iPP. The improvement in the yield stress achieved at least approximately 5%. Considering the ultratrace amounts of ACC-BBKPs addition (0.03 wt%), the values of 5% appeared to be a significant value as the Student's *t*-test was suggested. It should be added that at the yield point, crystalline lamella of iPP as folding molecular chains is supposed to start transforming to fiber structure due to elongation of the molecular chains by tensile stresses [10]. This may be a reason that ACC-BBKP might prevent transformation of crystalline lamella.

Table 3-2 Tensile properties of each sample. Values were average ± standard deviation. Values were compared statistically with Neat iPP using the T-test. * meant statistically significant with $p < 0.05$.

Starting sample	Elastic modulus / GPa	Yield strength / MPa	Strain at break / %
Neat PP	1.23 ± 0.04	28.57 ± 0.60	595.8 ±17.8
ACC-BBKP$_{0.005}$/iPP	1.22 ± 0.04	30.02 ± 0.17*	573.5 ± 30.3
ACC-BBKP$_{0.01}$/iPP	1.32 ± 0.03*	29.87 ± 0.19*	596.5 ± 20.9
ACC-BBKP$_{0.04}$/iPP	1.30 ± 0.04*	30.72 ± 0.29*	526.3 ± 32.5*

Elongation at break of the product from ACC-BBKP$_{0.04}$/iPP with the coverage of 0.10 wt% decreased by over 10 % when compared with neat iPP. It is presumably because the aggregations of ACC-BBKP, which were indicated by white triangle heads in Fig. 3-2, worked as stress-concentrated points in the plastic region. Therefore, ACC-BBKP$_{0.01}$/iPP, which was less covered with 0.045 wt%, exhibited some improvement in both stiffness and toughness, and therefore the amounts of ACC-BBKP contained ACC-BBKP$_{0.01}$/iPP (= 0.045 wt% in Table 3-1) is an appropriate amount at present.

3.3.3. Dependence of tensile properties on ACC-CNFs raw materials

The morphologies and surface properties of ACC-CNFs depend on their origins [1,2,7]. The reinforcement effect for iPP may also be affected by ACC-CNFs from different origins. Here, iPP microspheres coated with ACC-BNC and ACC-MCC were prepared using their 0.01 wt% aqueous dispersion to yield the injection-molded products embedding PCW-type frameworks. In Fig. 3-4, bright field and fluorescence images for

the above iPP microspheres stained with the cellulose specific dye of CFW (a, b), together with appearance of their products (c) are shown. These confirmed that both ACC-BNC and ACC-MCC were also favorably adsorbed on surface of iPP microspheres, and their injection-molded products were transparent with embedding PCW-like frameworks of CNFs in the iPP matrix, as reported in chapter 1.

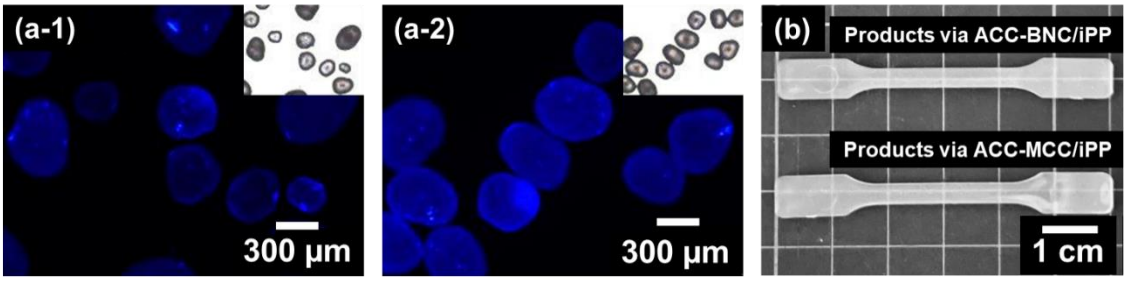

Fig. 3-4 (a) Dark-field fluorescent images of iPP microspheres coated with ACC-BNC (a-1: ACC-BNC/iPP) and ACC-MCC (a-2: ACC-MCC/iPP) stained with CFW (b) Their dumbbell shaped specimens prepared via their injection-molding.

Table 3-3 based on the S-S curves of all molded products as shown in Fig. 3-5 lists tensile properties in the injection-molded products of iPP microspheres coated with various CNFs derived from different raw materials. The amounts of CNFs per iPP were almost the same values as ca. 0.04 wt% among the listed ACC-CNFs. When compared with neat iPP, ACC-MCC/iPP, as well as ACC-BBKP, the molded products exhibited improvement in both elastic modulus and yield strength. The value of strain at break was more than 500 % until the ductile fracture. In contrast, ACC-BNC/iPP products did not exhibited improvement in their elastic modulus and yield strength, except performing a larger elongation. This may be attributed to degree of formation PCW-like frameworks, due to the smaller specific surface area of ACC-BNC compared to the other two ACC-CNFs [2]. This requires further investigation concerning the relationship between the

property-embedded PCW-frameworks. Note that the mechanism of improvement in mechanical properties attributed to synergetic effects due to the frame-engaged structure.

Mechanical properties of iPP as crystalline polymer are usually dependent on its crystalline structure including the distribution and crystallinity. As shown in WAXD diffraction patterns of Fig. 3-6, crystalline structure of the injection-molded products from neat iPP and ACC-MCC/iPP with the comparable crystallinity of 54 % was dominated by α-form that is a stable structure of iPP crystal. On the contrary, products derived from both ACC-BBKP/iPP and ACC-BNC/iPP were composed of a mixture of α-form and β-form of iPP. Their crystallinity was almost identical to be 45 – 47 %, which was less than that for products from neat iPP and ACC-MCC/iPP. Here, the relative ratio of β-form in crystalline region as K_β is calculated by the following formula [11]:

$$K_\beta = I_{(110)\beta}/(I_{(110)\alpha} + I_{(040)\alpha} + I_{(130)\alpha} + I_{(110)\beta})$$

I is a diffraction intensity and its subscripts indicate lattice planes. The K_β of ACC-BBKP/iPP and ACC-BNC/iPP were 0.18 and 0.15, respectively. In contrast, the corresponding values of neat iPP and ACC-MCC/iPP was 0.10. Neat iPP with β-form has usually less elastic modulus and larger elongation at break under a tensile stress in comparison to neat iPP products with α-form [12]. As both crystallinity and comparison ratio of the crystal form of ACC-MCC/iPP are the same those of neat iPP, the improvement of elastic modulus of ACC-MCC/iPP is due to the PCW-type frameworks composed of ACC-MCC. In addition, the lower crystallinity and high K_β values of composites prepared from ACC-BBKP and ACC-BNC might prevent decrease in strain break when compared with neat iPP products. Concerning β-form formation of iPP crystals, shear stress to molten iPP was reported to enhance the formation of β-form [13]. A previous paper reported that the strength in the affinity interaction between ACC-CNFs

and iPP is dependent on raw materials for ACC-CNFs, and in particular ACC-BBKP and ACC-BNC yield a greater affinity to iPP when compared with ACC-MCC [1]. Therefore, iPP interacted strongly with ACC-BBKP and ACC-BNC in the injection-molding process could receive a larger shear force to induce formation of β-crystals of iPP. Conversely, such a crystalline transformation of iPP might not occur in the case of ACC-MCC/iPP having less mutual affinity.

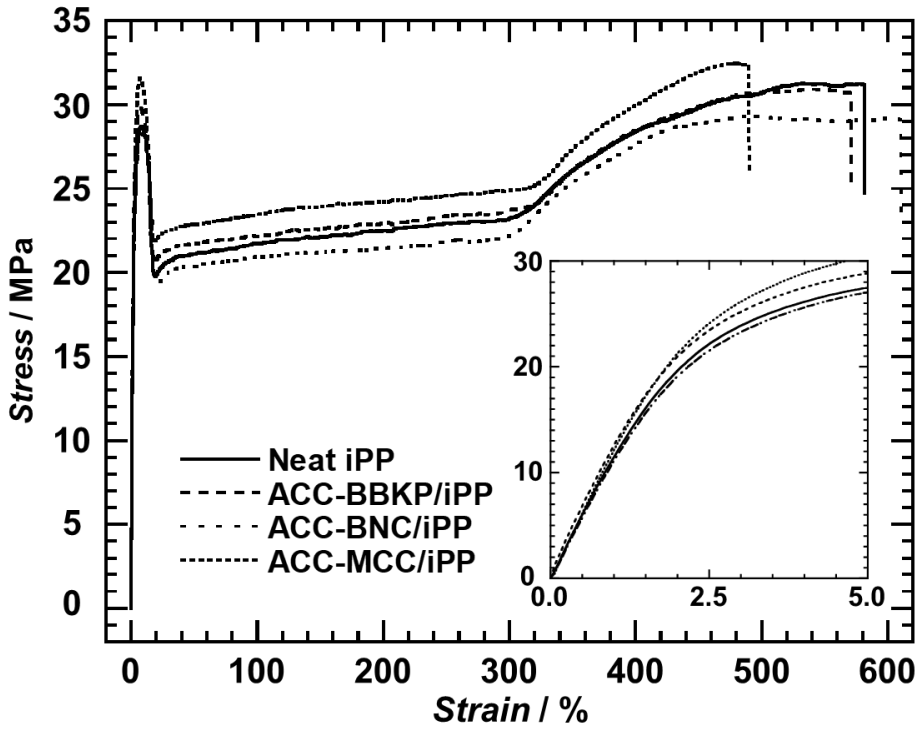

Fig. 3-5 Stress – Strain curves of injection-molded products from Neat iPP and various ACC-CNFs/iPP.

Table 3-3 Tensile properties of injection-molded products prepared from various ACC-CNFs/iPP. All values were average ± standard deviation.

Starting sample	The amounts of CNFs per PP / %	Elastic modulus / GPa	Yield strength / MPa	Strain at break / %
Neat iPP	-	1.23 ± 0.04	28.57 ± 0.60	595.8 ± 17.8
ACC-BBKP/iPP	0.045 ± 0.03	1.32 ± 0.03*	29.87 ± 0.19*	596.5 ± 20.9
ACC-BNC/iPP	0.041 ± 0.01	1.19 ± 0.04	28.59 ± 0.60	All samples did not fracture
ACC-MCC/iPP	0.044 ± 0.05	1.29 ± 0.02*	31.75 ± 0.40*	503.6 ± 9.2*

Values were compared statistically with neat iPP using the T-test. * indicates statistical significance with $p < 0.05$ vs Neat iPP.

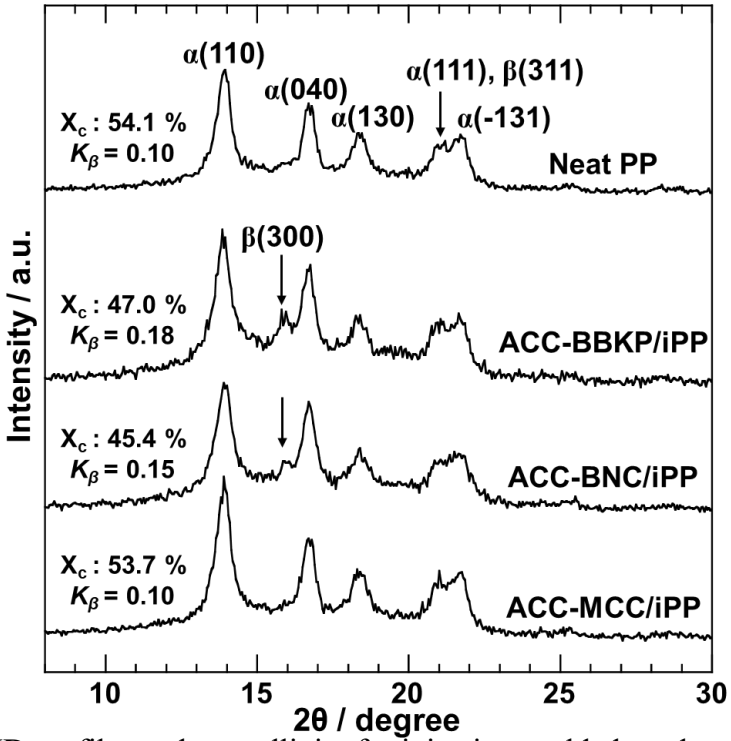

Fig. 3-6 WAXD profiles and crystallinity for injection-molded products derived from neat iPP and various ACC-CNFs/iPP.

3.4. Conclusion

In this chapter, it was focused to reveal tensile properties of ACC-CNFs/iPP products containing the frameworks with various ACC-CNFs. The composite materials from ACC-BBKP/iPP and ACC-MCC/iPP exhibited their enhanced mechanical strength, despite the extremally small addition of CNFs with 0.04 wt% to iPP. In contrast, ACC-BNC did not emerge such a reinforcement effect, despite significant improvement in the elongation. Taking the above into accounts, ACC-MCC and ACC-BNC are likely to contribute to improvement in stiffness and toughness, respectively. Accordingly, products via iPP covered with ACC-BBKP has achieved enhancement for both properties, although the contribution of PCW-mimicked frameworks of ACC-BBKP in iPP matrix is still unclear and further investigation is required. Furthermore, the injection-molding products fabricated from neat iPP and ACC-MCC/iPP were composed of iPP α-crystals while those of fabricated from ACC-BBKP/iPP and ACC-BNC/iPP were composed of a mixture of iPP crystals α-form and β-form. It was implied that the formation of β-form was promoted by shear stress caused by the stronger affinity interaction of these ACC-CNFs.

Reference

(1) Ishikawa, G.; Tsuji, T.; Tagawa, S.; Kondo, T. Adsorption of Janus-Type Amphiphilic Cellulose Nanofibrils onto Microspheres of Semicrystalline Polymers. *Macromolecules*, **2021**, *54* (20), 9393–9400. https://doi.org/10.1021/acs.macromol.1c01163.

(2) Tsuji, T.; Tsuboi, K.; Yokota, S.; Tagawa, S.; Kondo, T. Characterization of an Amphiphilic Janus-Type Surface in the Cellulose Nanofibril Prepared by Aqueous Counter Collision. *Biomacromolecules*, **2021**, *22* (2), 620–628. https://doi.org/10.1021/acs.biomac.0c01464.

(3) Kose, R.; Mitani, I.; Kasai, W.; Kondo, T. "Nanocellulose" as a Single Nanofiber Prepared from Pellicle Secreted by Gluconacetobacter Xylinus Using Aqueous Counter Collision. *Biomacromolecules*, **2011**, *12* (3), 716–720. https://doi.org/10.1021/bm1013469.

(4) Utsunomiya, H.; Tsujita, Y.; Kondo, T. Cellulose Nanoanemone: An Asymmetric Form of Nanocellulose. *Cellulose*, **2022**, *29* (5), 2899–2916. https://doi.org/10.1007/s10570-021-04231-9.

(5) Kondo, T.; Kose, R.; Naito, H.; Kasai, W. Aqueous Counter Collision Using Paired Water Jets as a Novel Means of Preparing Bio-Nanofibers. *Carbohydrate Polymers*, **2014**, *112*, 284–290. https://doi.org/10.1016/j.carbpol.2014.05.064.

(6) Kose, R.; Kasai, W.; Kondo, T. Switching Surface Properties of Substrates by Coating with a Cellulose Nanofiber Having a High Adsorbability. *Sen'i Gakkaishi*, **2011**, *67* (7), 163–168. https://doi.org/10.2115/fiber.67.163.

(7) Tagawa, S.; Ishida, K.; Tsuji, T.; Kondo, T. Facile Size Evaluation of Cellulose Nanofibrils Adsorbed on Polypropylene Substrates Using Fluorescence Microscopy. *Cellulose*, **2021**, *28* (5), 2917–2929. https://doi.org/10.1007/s10570-021-03759-0.

(8) Farrow, G. The Measurement of Crystallinity in Polypropylene Fibres by X-Ray Diffraction. *Polymer (Guildf)*, **1961**, *2* (4), 409–417. https://doi.org/10.1016/0032-3861(61)90046-5.

(9) Kondo, T.; Tanaka, H.; Yokota, S. Nanocomposite and Manufacturing Method of Nanocomposite. JP6979083B2, 2021. https://patents.google.com/patent/JP6979083B2/en.

(10) Peterlin, A. Molecular Model of Drawing Polyethylene and Polypropylene. *Journal of Materials Science*, **1971**, *6*, 490–508.

(11) Jones, A. T.; Aizlewood, J. M.; Beckett, D. R. Crystalline Forms of Isotactic Polypropylene. *Die Makromolekulare Chemie* **1964**, *75*, 134–158.

(12) Karger-Kocsis, J.; Varga, J. Effects of β-α Transformation on the Static and Dynamic Tensile Behavior of Isotactic Polypropylene. *Journal of Applied Polymer Science*, **1996**, *62* (2), 291–300. https://doi.org/10.1002/(sici)1097-4628(19961010)62:2<291::aid-app4>3.0.co;2-s.

(13) Libster, D.; Aserin, A.; Garti, N. Advanced Nucleating Agents for Polypropylene. *Polymers for Advanced Technologies*, **2007**, *18* (9), 685–695. https://doi.org/10.1002/pat.970.

Summary

ACC-CNFs, which favorably adsorb to iPP microspheres, are available as reinforcing fillers without chemical modifications and additives. In this dissertation, the author attempts to fabricate a nanocomposite plastic from iPP microspheres coated with ACC-CNFs as starting materials of their nanocomposite.

Chapter 1 attempted to fabricate the nanocomposite plastic from the iPP microspheres coated with ACC-CNFs derived from BBKP by injection-molding. Macroscopic aggregations of ACC-CNFs were not observed in the nanocomposite and the nanocomposite achieved improvement in impact resistance up to a maximum of 150 % regardless an ultratrace amount of ACC-CNFs approximately 0.03 wt%/iPP. It was revealed that a PCW-like continuous framework of ACC-CNFs was formed in the nanocomposite and contributed to its impact resistance by acting as an energy transfer pathway. Moreover, it was implied that crystallization of iPP was affected by the PCW-like framework.

Chapter 2 revealed the formation mechanism of the PCW-like framework. The ACC-CNFs-coated iPP microspheres were subjected to thermal treatment without shear stress, then the PCW-like framework was spontaneously formed in iPP matrix. The PCW-like framework acted as scaffolds of iPP α-form crystallization, resulting formation of the complex PCW-like ACC-CNFs/iPP framework with a core of ACC-CNFs. The relative ratio of α-crystals was dependent on the kinds of raw materials for ACC-CNFs.

Chapter 3 indicated to examine tensile properties of the nanocomposite embedding the PCW-like frameworks. The nanocomposite containing ACC-BBKP exhibited improvement in tensile elastic modulus without decreasing in elongation, that meant the nanocomposite achieved to overcome a trade-off relationship between tensile

modulus and elongation. In contrast, addition of ACC-MCC improved only tensile elastic modulus and addition of ACC-BNC improved only elongation. These results indicate that the source of raw materials of ACC-CNFs also influences the final composite products. Furthermore, the white spots due to aggregations of ACC-CNFs were observed in the nanocomposite fabricated from iPP microspheres coated with 0.10 wt% ACC-BBKP and the nanocomposite exhibited to decrease in elongation at break approximately 10 % compared with neat iPP product.

As described above, it was revealed that the injection-molding applied to the ACC-CNFs-coated iPP microspheres as starting materials can induce a three-dimensional continuous PCW-like framework of ACC-CNFs in the nanocomposite. The nanocomposite exhibited an improvement in both impact-resistance and tensile strength, even though the addition of ACC-CNFs was with an ultra-trace amount. Namely, this dissertation achieved that embedding PCW-like framework of an ultratrace amount of ACC-CNFs in iPP matrix can improvement in impact resistance of the nanocomposite plastics.

In traditional designs for nanocomposite, homogenous dispersion state of nanomaterials has been considered appropriate for improvement of material properties. Here this study, it is indicated that a new concept is proposed via embedding a continuous PCW-like frameworks promoting percolation effect dissipation, leading to an advanced design of CNFs-nanocomposite plastic materials.

List of publications

1) Impact-resistant nanocomposite plastics embedding “plant cell walls”-mimicked frameworks with ultratrace amounts of amphiphilic cellulose nanofibrils

Tetsuo Kondo, Gento Ishikawa, Masato Kamogawa, Yutaro Tsujita, Shingo Yokota, Tsubasa Tsuji and Daisuke Tatsumi

ACS Applied Polymer Materials, **2024**, *6*, 1276-1285.

(https://pubs.acs.org/doi/10.1021/acsapm.3c02278)

(Chapter 1)

2) Transcrystalline polypropylene-based honeycomb structures spontaneously induced on amphiphilic cellulose nanofibrils prepared by aqueous counter collision

Masato Kamogawa, Yutaro Tsujita and Tetsuo Kondo

Journal of Fiber Science and Technology (accepted)

(Chapter 2)

3) Tensile property of iPP based composites embedding “plant cell wall”-mimicked frameworks of ultratrace amphiphilic cellulose nanofibrils derived from various raw materials

Masato Kamogawa and Tetsuo Kondo

Journal of Fiber Science and Technology (accepted)

(Chapter 3)

Acknowledgements

The work described in this dissertation has been carried out from 2019 to 2024 at the Graduate School of Bioresource and Bioenvironmental Science, Kyushu University under supervision of Professor Tetsuo Kondo.

The author would like to express the deepest appreciation to Professor Tetsuo Kondo, Graduate School of Bioresource and Bioenvironmental Science, Kyushu University and Faculty of Agriculture, and Tokyo University of Agriculture and Technology. Without Professor Kondo's guidance, discussions, and supervision, the achievement of this research would not have been possible.

The author would like to express the deepest appreciation to Associate Professor Daisuke Tatsumi, Graduate School of Bioresource and Bioenvironmental Science, Kyushu University, for his helpful advices and discussions.

The author would like to express the deepest appreciation to Professor Takuya Kitaoka, Graduate School of Bioresource and Bioenvironmental Science, Kyushu University, and Professor Yoshinobu Tsujii, Institute for Chemical Research, Kyoto University, for their reviewing this work.

The author deeply thanks Associate Professor Shingo Yokota, Graduate School of Bioresource and Bioenvironmental Science, Kyushu University, for his helpful advices and suggestions.

The author deeply thanks Professor Ryo Funada, Faculty of Agriculture, Tokyo University of Agriculture and Technology, for his greatest support.

The author deeply thanks to Mrs. Runa Watanabe, a secretary of Biomaterial Design Laboratory, Graduate School of Bioresource and Bioenvironmental Science, Kyushu University, for her greatest and kindest support.

The author deeply thanks Associate Professor Mariko Ago, Institute of Agriculture, Tokyo University of Agriculture and Technology, and Assistant Professor Yutaro Tsujita, Institute of Agriculture, Tokyo University of Agriculture and Technology, for their helpful advices and discussions.

The author would like to thank Chuetsu Pulp & Paper Co., Ltd., Toyama, Japan for kindly providing ACC-BBKP.

The author expresses gratitude for Assistant Professor Gento Ishikawa, Ariake National College of Technology, Assistant Professor Satomi Tagawa, Faculty of Engineering, Shinshu University, Dr. Hikari Utsunomiya, Japan Bio Science Laboratory Co. Ltd., Dr. Suresh Rao, Mitsubishi Chemical Corp., Dr. Tsubasa Tsuji, Chuetsu Pulp & Paper Co., Ltd., Dr. Ryo Takahama, Faculty of Engineering, Hokkaido University, Dr. Koichiro Ishida, Institute for Chemical Research, Kyoto University, and Dr. Go Takayama, Faculty of Engineering, Hokkaido University, for their helpful advices and discussions.

The author would like to thank members in Biomaterial Design Laboratory and Biomacromolecular Materials Laboratory, Graduate School of Bioresource and Bioenvironmental Science, Kyushu University, for their helpful advices.

Last but not least, the author wishes to express the sincerest appreciation to his father and sister for their warmest support, understanding and patience. The author dedicates the execution of this study to his the late mother.

March, 4, 2024
At Tokyo

Masato Kamogawa